NATIONAL ADVISORY COMMITTEE FOR AERONAUTICS

NACA-UNIVERSITY CONFERENCE ON AERODYNAMICS, CONSTRUCTION, AND PROPULSION

VOLUME I
AIRCRAFT STRUCTURES AND MATERIALS

Lewis Flight Propulsion Laboratory
Cleveland, Ohio.

October 20, 21, and 22, 1954

NACA

NACA-UNIVERSITY CONFERENCE ON AERODYNAMICS, CONSTRUCTION, AND PROPULSION

VOLUME I
AIRCRAFT STRUCTURES AND MATERIALS

Lewis Flight Propulsion Laboratory
Cleveland, Ohio.

October 20, 21, and 22, 1954

INTRODUCTION

The NACA-University Conference was held to acquaint university personnel with recent developments in aeronautical research. Wherever possible, each paper reviews the status of the field under consideration, points out recent significant advances, and suggests promising avenues for future research.

The papers presented are considered to supplement, rather than substitute for, the reports in which the NACA customarily releases its work. Information regarding the NACA's regular reports may be obtained from the Division of Research Information, NACA, 1512 H Street N. W., Washington 25, D. C.

This volume (Volume I of three) contains the papers presented at the conference that deal with aircraft structures and materials. Volume II of the series contains the papers on aerodynamics, and Volume III contains the papers on aircraft propulsion.

CONFERENCE PROGRAM

VOLUME I

AIRCRAFT STRUCTURES

AERONAUTICAL MATERIALS

VOLUME II

AERODYNAMICS

VOLUME III

PROPULSION

NACA-UNIVERSITY CONFERENCE

October 20-21-22, 1954

*Attendance List

Name	School
Abbott, I. H.	NACA-Washington
Abramson, H. N.	Texas Agricultural & Mining College
Albright, L. F.	University of Oklahoma
Ambrose, H.	University of Tennessee
Anderson, E. W.	Iowa State University
Andes, A. S.	University of Kansas
Archer, D. H.	Carnegie Institute of Technology
Ault, G. M.	NACA-Lewis
Bailey, N. P.	Renssalaer Polytechnic Institute
Baker, R. D.	University of Utah
Barzelay, M. E.	Syracuse University
Bates, G.	NACA-Washington
Beane, J.	University of Buffalo
Berlad, A.	NACA-Lewis
Bicknell, J.	Massachusetts Institute of Technology
Birkenhauer, Rev. H. F.	John Carroll University
Bisplinghoff, R. L.	Massachusetts Institute of Technology
Bisson, E. E.	NACA-Lewis
Bleich, H.	Columbia University
Bloom, M.	Polytechnic Institute of Brooklyn
Bogdanoff, J. L.	Purdue University
Bogdonoff, S. M.	Princeton University
Bolz, R. E.	Case Institute of Technology
Breuer, D. W.	U. S. Air Force Institute of Technology
Broadwell, J. E.	University of Michigan
Brull, M. A.	University of Michigan
Bryson, A. E.	Harvard University
Burggraf, Lt. O. R.	U. S. Air Force Institute of Technology
Burlage, H.	Case Institute of Technology
Calhoun, Maj. J. D.	U. S. Air Force Institute of Technology
Campbell, G.	Renssalaer Polytechnic Institute
Carter, W. M.	University of Kentucky
Choppesky, Rev. J. C.	St. Louis University
Chi Chou, P.	Drexel Institute of Technology
Chu, S. T.	Ohio State University

*Attended one or more days of the conference.

Name	School
Cocanougher, J. E.	Miami University (Ohio)
Cohen, H.	Carnegie Institute of Technology
Comp, L. A.	University of Oklahoma
Cook, W. L.	NACA-Ames
Corning, G.	University of Maryland
Cronk, A. E.	University of Minnesota
Crossley, F. R. E.	Yale University
Daley, Maj. D. H.	U. S. Air Force Institute of Technology
Dancy, Maj. A. G.	U. S. Military Academy
Dean, R. C.	Massachusetts Institute of Technology
Deissler, R. G.	NACA-Lewis
Dingeldein, R. C.	NACA-Langley
Dow, N. F.	NACA-Langley
Draper, C. S.	Massachusetts Institute of Technology
Dryden, H. L. .	NACA-Washington
Dubois, G.	Cornell University
Durham, F. P.	University of Colorado
Dutton, D. W.	Georgia Institute of Technology
Eckert, E. R. G.	University of Minnesota
Erdoss, B.	Stevens Institute of Technology
Eringen, J.	Purdue University
Farmer, A.	Renssalaer Polytechnic Institute
Farrar, D. F.	Vanderbilt University
Ferrell, W. L.	Ohio University
Fleming, W.	University of Buffalo
Fogel, C.	University of Buffalo
Folsom, R. G.	University of Michigan
Forstall, W.	Carnegie Institute of Technology
Frankel, S. J.	Illinois Institute of Technology
Galowin, L.	Polytechnic Institute of Brooklyn
Gardiner, R. A.	NACA-Langley
Garrick, I. E.	NACA-Langley
Gatewood, B. E.	U. S. Air Force Institute of Technology
Gawain, T H.	U. S. N. Postgraduate School-Calif.
Gessow, A.	NACA-Langley
Gilruth, R R.	NACA-Langley
Ginsburg, A.	NACA-Lewis

Name	School
Graham, P. F.	Ohio State University
Greiner, H.	Renssalaer Polytechnic Institute
Grove, C. S.	Syracuse University
Grummann, H.	St. Louis University
Hakkinen, R. J.	Massachusetts Institute of Technology
Halfman, R. L.	Massachusetts Institute of Technology
Harper, J. H.	Georgia Institute of Technology
Harrington, R. P.	Renssalaer Polytechnic Institute
Hawthorne, Q. J.	Tri-State College
Hazen, D. C.	Princeton University
Head, R. M.	U. S. N. Postgraduate School-Calif.
Heaslet, M.	NACA-Ames
Heimerl, G.	NACA-Langley
Heldenfels, R.	NACA-Langley
Hertler, E. G.	University of Maryland
Hooper, I. P.	Rose Polytechnic Institute
Houbolt, J. C.	NACA-Langley
Hubbard, H. H.	NACA-Langley
Humble, L. V.	NACA-Lewis
Ingard, K. U.	Massachusetts Institute of Technology
Jackson, T. W.	Georgia Institute of Technology
Jennings, B. H.	Northwestern University
Johnsen, I. A.	NACA-Lewis
Johnson, H. A.	University of California
Jones, B.	University of Cincinnati
Kahr, C. H.	U. S. N. Postgraduate School-Calif.
Kaplan, C.	NACA-Langley
Kawamura, R.	Cornell University
Keister, P. H.	U. S. Air Force Institute of Technology
Kestin, J.	Brown University
King, W. J.	University of California at Los Angeles
Kochendorfer, F.	NACA-Lewis
Korkegi, R.	University of Southern California
Korst, H. H.	University of Illinois
Kuerti, G.	Case Institute of Technology
Lairabee, E. E.	Massachusetts Institute of Technology
Landon, R. D.	University of Akron

Name	School
Lane, F.	New York University
Langhaar, H. L.	University of Illinois
Lee, E. H.	Brown University
Lee, J. D.	Ohio State University
Lesher, E. J.	University of Michigan
Lessen, M.	University of Pennsylvania
Lew, H. G.	Pennsylvania State College
Lo, H.	Purdue University
Lopez, H.	Renssalaer Polytechnic Institute
Love, E. S.	NACA-Langley
Ludewig, J. W.	Carnegie Institute of Technology
Martin, H. C.	University of Washington
Martinuzzi, F.	Stevens Institute of Technology
Mathauser, E. E.	NACA-Langley
Mattica, H. C.	Renssalaer Polytechnic Institute
McCloy, R. W.	University of Illinois
McKay, W.	Massachusetts Institute of Technology
Meyerhoff, L.	Brooklyn Polytechnic Institute
Miller, R. H.	Massachusetts Institute of Technology
Miller, W. H.	Catholic University
Morgan, G. W.	Brown University
Morkovin, M. V.	Johns Hopkins University
Murphy, G.	Iowa State University
Myers, P. S.	University of Wisconsin
Nelson, W. J.	NACA-Langley
Nichols, M. N.	NACA-Langley
Niedenfuhr, F. W.	Ohio State University
Nielsen, J. N.	NACA-Ames
O'Brien, M. P.	University of California
Osterle, J. F.	Carnegie Institute of Technology
Pai, S. I.	University of Maryland
Painter, N.	University of Chicago
Palmer, C.	NACA-Washington
Pangborn, D.	Renssalaer Polytechnic Institute
Pasqua, P. F.	University of Tennessee
Paxton, H. W.	Carnegie Institute of Technology
Peery, D. J.	University of Michigan

Name	School
Pell, W. H.	Brown University
Pinkerton, R. M.	North Carolina State University
Polhamus, E. C.	NACA-Langley
Poulson, Capt. J. A.	U. S. Air Force Institute of Technology
Press, H.	NACA-Langley
Prior, J. A.	University of Pennsylvania
Probstein, R. F.	Brown University
Purser, P. E.	NACA-Langley
Ranov, T.	University of Buffalo
Raspet, A.	Mississippi State College
Reid, E. G.	Stanford University
Regier, A. A.	NACA-Langley
Reinath, F.	Ohio University
Rex, Maj. E. M.	U. S. Air Force Institute of Technology
Rhines, F. N.	Carnegie Institute of Technology
Rhode, R.	NACA-Washington
Richardson, A. S.	Massachusetts Institute of Technology
Riparbelli, C.	Cornell University
Robinson, R. G.	NACA-Ames
Roshko, A.	California Institute of Technology
Rott, N.	Cornell University
Rouleau, W. T.	Carnegie Institute of Technology
Rubesin, M.	NACA-Ames
Ruptash, J.	University of Wichita
Rutkowski, J.	Wayne University
Saltzer, C.	Case Institute of Technology
Sandorff, D. E.	Massachusetts Institute of Technology
Saxon, D.	University of Chicago
Schmitt, A. F.	Purdue University
Schwartz, F. L.	University of Michigan
Seiff, A.	NACA-Ames
Sellars, J. R.	University of Michigan
Seltzer, L. Z.	West Virginia University
Sevin, E.	Illinois Institute of Technology
Shen, S. F.	University of Maryland
Sherling, W. G.	Alabama Polytechnic Institute
Sherwood, A. W.	University of Maryland
Smith, K. E.	University of Detroit
Smull, T. L. K.	NACA-Washington

Name	School
Spreiter, J. R.	NACA-Ames
Stanley, P.	Purdue University
Stenning, A. H.	Massachusetts Institute of Technology
Stewart, O. W.	University of Kentucky
Stillwell, H. S.	University of Illinois
Stolworthy, E. H.	University of New Hampshire
Sutton, J. F.	Clemson University
Sutton, M. A.	Ohio State University
Swanson, W. M.	Case Institute of Technology
Syvertson, C. A.	NACA-Ames
Taylor, E. J.	Ohio University
Teichman, F. K.	New York University
Thompson, F. L.	NACA-Langley
Tifford, A.	Ohio State University
Trangott, S. C.	Johns Hopkins University
Truitt, R. W.	Virginia Polytechnic Institute
Upson, R. H.	University of Minnesota
Uyehara, O. A.	University of Wisconsin
Veletsos, A. S.	University of Illinois
Vincent, E. T.	University of Michigan
Von Eschen, G. L.	Ohio State University
Vopat, W. A.	Cooper Union Institute of Technology
Vuilleumier, R.	Stevens Institute of Technology
Walsh, E. T.	Case Institute of Technology
Ward, V. G.	Ohio State University
Watkins, C.	NACA-Langley
Waxer, L. J.	Boston University
West, C. T.	Ohio State University
Winternitz, P. F.	New York University
Wright, R. H.	NACA-Langley
Wulff, J.	Massachusetts Institute of Technology
Yates, C. C.	University of Pittsburgh
Yeh, H.	Johns Hopkins University
Yen, K. T.	Renssalaer Polytechnic Institute
Yuan, S. W.	Polytechnic Institute of Brooklyn
Zimmerman, R. H.	Ohio State University

1. SOME APPLICATIONS OF GENERALIZED HARMONIC ANALYSIS TO PROBLEMS IN AIRPLANE DYNAMICS

By Harry Press, John C. Houbolt, and Franklin W. Diederich
Langley Aeronautical Laboratory

INTRODUCTION

Many aeronautical problems are concerned with the response of an aircraft to an erratic or random disturbance. The randomness in the disturbance introduces complications in the analysis of such problems and necessitates the use of specialized statistical techniques. The recent development of the theory of random processes and particularly the development of the techniques of generalized harmonic analysis have provided methods suitable for the analysis of many of these problems. The basic mathematical developments have been evolved largely by Norbert Wiener (ref. 1). The earliest applications of these techniques appear to have been made in communications engineering. Recently, Clementson and Liepmann have pioneered their application to aeronautical problems (refs. 2 and 3, respectively). Inasmuch as these techniques should find increasing usefulness in aeronautics, it appears appropriate to present a paper outlining some of the fundamental elements of these techniques and reviewing some of the results obtained at the NACA in their applications to gust load and runway roughness problems. Some of the results to be presented have recently been published in references 4 to 8; others are new.

Figure 1 shows some typical random-type disturbances that occur in aeronautical problems. The first sketch represents an airplane encountering rough air, where the curve represents the variations in vertical gust velocity. The second sketch represents a buffeting wing, where the curve shows the lift fluctuations. The last sketch represents taxiing over a rough runway. The runway height variations have, of course, been exaggerated for illustrative purposes. In all cases, the disturbances are erratic or random and cannot be defined in explicit form. However, in order to determine the airplane response, a mathematical representation and a technique for performing response calculations for such disturbances are needed. The technique of generalized harmonic analysis appears suited for these purposes and, as a background for the applications to be described, the first part of the paper will briefly review four of the fundamental aspects of this approach. These aspects cover the representation of a random function by means of a power spectrum and the use of the spectrum for response calculations.

FUNDAMENTAL ASPECTS OF GENERALIZED HARMONIC ANALYSIS

Representation of random disturbance. - The first aspect of the theory to be considered is that of the analytical representation of a random disturbance, and is covered on the left half of figure 2. A typical random disturbance $y(t)$ is shown on the top of the figure. The conventional approach to the analysis of erratic functions, such as $y(t)$, is to obtain a frequency representation by making use of Fourier series or Fourier integrals. However, since these random disturbances are aperiodic and do not subside in time, conventional Fourier techniques cannot be used. Instead, a frequency representation may be obtained in some cases in the following manner: For the disturbance $y(t)$, an overall measure of disturbance intensity is given by the mean square value $\overline{y^2(t)}$. This quantity usually exists and has been termed the "power." By considering the contributions to this power of the various frequencies present in the disturbance $y(t)$, one arrives at the concept of a density function. The power spectral density function $\Phi(\omega)$ is illustrated by the sketch, and describes the contributions to the total power of the sinusoidal components of the disturbance at the various frequencies. It follows from this definition that the total area under the spectral curve equals the power.

The mathematical expression for the power spectrum $\Phi(\omega)$ is shown on the lower part of the figure and is given by

$$\Phi(\omega) = \lim_{T\to\infty} \frac{1}{2\pi T}\left|\int_{-T}^{T} y(t)e^{-i\omega t}\,dt\right|^2$$

where the bars designate the absolute value of the complex quantity. It is of interest to note that this integral, which is the Fourier transform of $y(t)$, does not exist in the limit, but the limit for the entire expression does exist in many cases of interest. In particular, it exists for so-called stationary disturbances; that is, disturbances whose statistical characteristics do not change with time.

Input-output relations. - The second aspect of the theory to be considered is the relation between a disturbance spectrum and the spectrum of a system response to this disturbance. For linear systems, these spectra are related in a simple manner, and the relation as shown on the upper right side of figure 2 is

$$\Phi_o(\omega) = \Phi_i(\omega)T^2(\omega)$$

In this relation Φ_i and Φ_o are, respectively, the spectra of the disturbance input and the system response. The quantity $T(\omega)$ is the

amplitude of the system frequency-response function and describes the amplitude of the system response to unit sinusoidal disturbances at the various frequencies. The output spectrum is seen from the equation to be given by the simple product of the input spectrum and the square of the amplitude of the frequency-response function.

The application of this relation for the gust load case is schematically illustrated by the sketches shown in figure 2. The upper curve shows a representative spectrum of the vertical component of atmospheric turbulence. Available information on this spectrum will be considered later. The second curve is the amplitude squared of the airplane frequency-response function with the curve shown typical for the normal acceleration response at the center of gravity for sinusoidal gusts at the various frequencies. Airplane modes in this representation show up as peaks, such as the free-body and the fundamental wing-bending mode shown. The output spectrum is obtained by the use of the relation shown and is the product of the first two functions. The result obtained is shown on the bottom curve and is, in this case, the spectrum of normal acceleration.

Relations between spectrum and time-history characteristics. - In addition to the spectrum itself, other statistical characteristics of the response are also generally of interest. Reference 9 provides a comprehensive survey of these relations between the spectrum and some of the other statistical characteristics of the response of interest. This is the third aspect of the theory to be considered and is covered on the left half of figure 3. Item (a) indicates the general relation previously mentioned; namely, that the area under the spectrum is equal to the mean square value. If the disturbance has a zero mean value, which is usually the case, the mean square value provides a useful overall measure of the response intensity. It is also possible to derive other useful statistical characteristics of the time history directly from the spectrum. In the particular case of a Gaussian disturbance, the statistical characteristics are completely defined by the spectrum. Some of the quantities that can be determined readily for this case are listed. Item (b) shows the probability distribution of the amplitude of y and describes the proportion of total time that y has given values. As can be seen, the probability distribution is the normal or Gaussian distribution and depends only on σ, the root mean square value, which is obtained from the area under the spectrum. Item (c) designates that the expected maximum value of y for a given time is proportional to the root mean square value. Relations have also been derived in reference 9 for the Gaussian case between the spectrum and such quantities as the number of times per second a given value of y, for example y_1, is crossed with positive slope (item (d)), marked by the crosses, and the number of peaks per second (item (e)), marked by the circles, that exceed this value y_1. These relations have been particularly useful for fatigue studies.

Estimation of spectra from experimental data. - The final aspect of the theory is concerned with the practical problem of estimating spectra from experimental time-history data. A solution to this problem of spectrum estimation has only recently been achieved (ref. 10) and has contributed significantly to the practicality of this approach. The problems involved are as follows: It will be recalled that the mathematical definitions of the power spectrum involve infinite integrals. Experimental determinations, however, must of necessity be based on finite lengths of record, and because of this, a degree of approximation is immediately introduced. In addition, numerical evaluations are generally restricted to values at discrete intervals of time. The problems introduced by these finite approximations are not trivial and some of them have apparently not been appreciated until recent years.

Two fundamental problems are introduced by the finite approximations and, as indicated on the right half of figure 3, concern the frequency resolution and statistical reliability of the estimates. Frequency resolution problems arise since it takes a finite record length to discriminate between two sinusoidal components of a disturbance whose frequencies are close to each other; the closer the frequencies, the longer the record length required for discrimination. As a consequence, estimates from finite samples are at best averages of the power over a finite frequency range, as shown by the sketch in the figure.

The problem of the statistical reliability of power estimates also arises from the finite length of record since any two sections of record, like two series of coin tosses, will generally not yield identical results. The statistical reliability of the estimates must therefore be established in order to permit the discrimination between actual and statistical fluctuations.

Results obtained in reference 10 permit the estimation of the average power over band widths, as shown by the sketch on the lower right of figure 3. They also permit the determination of the reliability of such measurements in terms of confidence bands, as indicated by the vertical line on the sketch. The width of these frequency bands can be varied in the calculation procedure. The width of the confidence bands can be shown to depend upon this frequency band width and the record length; the wider the frequency band, the greater the reliability; also, the longer the record length, the greater the reliability. Thus, it is possible to tailor the calculations to achieve the best combination of frequency resolution and statistical reliability for a given problem.

The foregoing discussion has briefly outlined the general aspects involved in the applications of the techniques of generalized harmonic analysis. The remainder of this article will be concerned with some results obtained in applications of the foregoing theory.

APPLICATIONS

Spectra of atmospheric turbulence. - The first application concerns some studies of the spectrum of atmospheric turbulence, and the results obtained from various sources are summarized in figure 4. The first of these measurements was made by Clementson (ref. 2) and subsequent measurements were made by the Douglas Aircraft Company (ref. 11), and the NACA (ref. 6). The curves shown on figure 4 represent the various spectra obtained in flight tests under different weather conditions. The ordinate is the power density, the abscissa is the frequency Ω in radians per foot and is equal to 2π divided by the gust wavelength. This frequency argument is useful in airplane gust studies because, insofar as the airplane is concerned, the turbulence is essentially a spacial phenomenon. The data shown cover a range of gust wavelengths from about 10 to 3000 feet.

The spectra in all but one case are for the vertical component of the turbulence. In one case marked by the letter H (the square points) the spectrum is for the horizontal or longitudinal component of the turbulence. The spectra vary considerably in height, reflecting the variations in intensity for the various weather conditions. While the intensity varied considerably, the spectral shapes appear relatively consistent; in all cases the power decreases rapidly with increasing frequency. In fact, in most cases, the spectra appear inversely proportional to the square of the frequency. This spectral shape of $1/\Omega^2$ is in reasonable agreement with theoretical results obtained for the spectral shape at the higher frequencies in the theory of isotropic turbulence. At the low frequencies, the spectral shape has as yet not been adequately established because of the measurement difficulties.

Because of the general characteristics of these spectra, it has been convenient in theoretical studies to use the analytical expression for the turbulence spectrum shown on figure 5. This expression has been useful in wind-tunnel studies of turbulence and can be seen to have the general characteristics of the measured spectra of atmospheric turbulence. The equation has two parameters, the mean square gust velocity $\overline{U^2}$, which describes the turbulence intensity, and the so-called scale of turbulence L. The scale of turbulence L can, in a rough sense, be considered to be proportional to the average eddy size. The curves in figure 5 are for a mean square gust velocity equal to 1 and for values of L = 200, 600, and 1000 feet. The curves at higher frequencies all approach a shape of $1/\Omega^2$, but differ in the frequency at which the flattening out occurs. For large values of L, most of the power is at the very low frequencies. Comparison of these curves with these and other measurements of the spectrum of atmospheric turbulence have suggested that representative values of L for atmospheric turbulence are perhaps several hundred feet to over a thousand feet. For studies of wind-tunnel turbulence, L may be expected to be much smaller, perhaps on the order of an inch.

Effects of short-period damping. - The next application to be described concerns the effects of airplane dynamic stability, particularly the effects of low damping in short period on airplane accelerations in rough air. Theoretical studies based on spectrum analysis (ref. 12) have indicated that the gust loads in continuous rough air are considerably amplified when the short period has low damping. Recently, some test data bearing on this problem have been obtained by the NACA (ref. 5). A swept-wing tailless missile was flown through rough air at low altitudes and high speeds and the results indicated that a very substantial amplification in gust loads was associated with low damping of the short period. Some of the results obtained in this study are shown in figure 6. Results are shown for three Mach numbers: 0.88, 0.91, and 0.95. Over this range of Mach numbers, the short-period damping deteriorated sharply.

Calculations of the expected spectra of normal acceleration were made for these three Mach numbers and are shown in the upper left of the figure. These were obtained from calculated estimates of the missile normal acceleration frequency response function and estimates of the gust spectrum which were based on airplane survey flights over the missile firing range just prior to the tests. The calculated spectra show a progressive movement to higher frequency as the airspeed increases, directly reflecting the variations in the short-period frequency. The spectra are also progressively more peaked, reflecting the deterioration in the damping of the short-period frequency. The relative load levels for the three airspeed conditions as measured by the root mean square values are also given and show a relatively large increase, from 0.48g to 0.65g, almost 40 percent, for the 10 percent increase in airspeed.

For comparison, the measured power spectra of normal accelerations for the same three test airspeeds are shown on the lower right of figure 6. In each case, only very limited samples were available (roughly 2 sec) with the result that only limited statistical reliability could be obtained. In obtaining the power spectrum estimates, statistical reliability considerations dictated a choice of a rather wide frequency-band width; each point represents a weighted average over roughly 3.2 cycles per second ($\pm$1.6 cps about the values shown). The estimates may therefore be expected to provide a "smeared" picture of the real spectrum, and this is borne out by the fact that measured results are flatter in character than are the calculated results.

In order to make a more fair comparison between the calculated and measured results, the calculated results presented were modified by the averaging equivalent to that present in the measured estimates. The results obtained with this modification are shown on figure 6 and are seen to be in good over-all agreement with the measured spectra. In fact, considering the limited statistical reliability present, the agreement seems much better than might have been expected and confirms the expected magnitude and character of amplification in loads associated with low damping.

Effect of wing bending. - As the next application, figure 7 shows some results obtained in a study of the effects of wing-bending flexibility on the root bending moment of a B-29 airplane. The figure shows a comparison of the measured and calculated power spectra of root-bending moment. In each case, the solid curve is for the flexible airplane and the dashed curve is for the airplane considered as a rigid body. For the rigid case, the measured spectrum was obtained from nodal point acceleration measurements and the conversion to bending moment was based on the calibration data obtained in steady pullups. In each case, the first peak is associated with the free body mode, while the second peak at about 3 cycles per second is associated with the fundamental wing bending mode. The effect of wing bending is in both cases given by the bump in the spectrum at the fundamental wing bending frequency. The ratios of the root mean square values are also shown in both cases. Comparison of the measured and calculated results shows rather good agreement in root mean square values and in the size and shape of the bump associated with the wing bending effects.

Span effects. - In these calculations, it has for simplicity been assumed that the turbulence is uniform across the span. Recent studies have indicated that the effects of variations in the turbulence across the span may give rise to significant effects in many problems. Some of the results in regard to the span effects are covered on the next two figures. Figure 8 shows the effect of the span length b on the spectrum of the average gust velocity across the span. These results are for isotropic turbulence and the analytical expression for the turbulence spectrum given earlier. The abscissa is the nondimensional frequency $\omega L/V$ where L is the scale of turbulence and V is the airplane forward speed. Curves are shown for various values of b/L; the curve for $b/L = 0$ giving the spectrum of turbulence at a point, while the other curves give the spectra of average gust velocity across the span. For increasing values of b/L, it can be seen that the effective spectrum is progressively reduced, particularly at the higher frequencies. These results apply directly to wing lift and to over-all airplane accelerations and indicate the amount of attenuation due to spanwise gust averaging. The results, while of significance in gust response studies, are of even greater significance in regard to wind tunnel and buffeting studies where the ratio of b/L is likely to be much greater than for the case of atmospheric turbulence.

Although the effects of nonuniform turbulence appear to attenuate the over-all airplane load and gust response, they may give rise to a different effect when the internal structural response is considered. Figure 9 illustrates this point by showing the effects of spanwise variations in turbulence on the excitation of the structural modes. The results are for a uniform cantilever wing of aspect ratio 5 and show the relative amount by which the first several modes are excited. The various curves show the ratio of the response spectra Φ_s/Φ_u for the first, second, and third symmetric modes, where Φ_s designates the response

spectrum for the condition of turbulence varying across the span and Φ_u designates the spectrum for the uniform turbulence condition. The abscissa is a reduced frequency $\omega L/V$ where L is the scale of turbulence. Results are shown for several values of span-to-scale ratio b/L. For the first mode, the response for the nonuniform gust condition Φ_s is always less than the response for the uniform gust condition Φ_u, the amount of reduction becoming greater as b/L increases. For the second and third modes, however, Φ_s is greater than Φ_u in the range of frequency covered, and for the third mode reaches a peak value of about 2.3 in one case. If the plots were carried out to higher frequency, all the curves would eventually drop off and approach zero. This, of course, is to be expected from physical considerations, since at the very high frequencies, the gust wavelengths are so short that there is effectively a complete cancellation.

It should be mentioned that these peaks in the amplification curves occur at gust wavelengths that are about twice the distance between nodal points for the higher modes. Thus, a spacial resonance condition is suggested in which the loading distribution takes a shape similar to the mode shape.

Results of the type shown on figure 9, of course, do not indicate the superposed effect of all the modes, that is, the net response. The net effect of spanwise gust variations on the airplane response could presumably be greater or less than that for the uniform gust condition, depending on the actual configuration, the response quantity being determined, and which mode, if any, is predominant in the response.

Runway roughness. - As a final example, some results obtained in the problem of loads developed in taxiing over rough runways are described. For this problem, it was desirable to obtain some measurements of the roughness of existing runways. As a first effort in this direction, height surveys were made of two runways at Langley Field, Virginia. One of the runways was considered a relatively smooth runway, while the second runway was known to be rough. The power spectra of runway roughness are shown in figure 10. As can be seen, the spectrum for the rough runway, over the range considered of interest, is considerably higher than for the smooth runway, roughly, ten times as high at the lower frequencies and about twice as high at the higher frequencies. The root mean square values are also given and are seen to be roughly in the ratio of 3:1. These results in describing the characteristics of runways roughness are serving as a useful basis for trend studies of airplane response in ground operations.

CONCLUSION

The foregoing discussion has described some of the aspects of the techniques of generalized harmonic analyses and some of the results obtained in applications. These techniques appear to provide a useful approach for problems involving random disturbances, and their use will probably be expanded in the future.

REFERENCES

1. Wiener, Norbert: Generalized Harmonic Analysis. Acta Math., vol. 55, 1930, pp. 117-258.

2. Clementson, G. C.: An Investigation of the Power Spectral Density of Atmospheric Turbulence. Ph. D. Thesis, M.I.T., 1950.

3. Liepmann, H. W.: On the Application of Statistical Concepts to the Buffeting Problem. Jour. Aero. Sci., vol. 19, no. 12, Dec. 1952, pp. 793-801.

4. Press, Harry, and Houbolt, John C.: Some Applications of Generalized Harmonic Analysis to Gust Loads on Airplanes. Preprint No. 449, Inst. Aero. Sci., Jan. 1954.

5. Vitale, A. James, Press, H., and Shufflebarger, C. C.: An Investigation of the Use of Rocket-Powered Models for Gust-Load Studies with an Application to a Tailless Sweptwing Model at Transonic Speeds. NACA TN 3161, 1954.

6. Chilton, Robert G.: Measurements of Atmospheric Turbulence Obtained from Flow-Direction Vanes Mounted on an Airplane. NACA TN 3313, 1954.

7. Diederich, F. W.: The Response of an Airplane to Random Atmospheric Disturbances. Ph. D. Thesis, C.I.T., 1954.

8. Walls, James H., Houbolt, John C., and Press, Harry: Some Measurements and Power Spectra of Runway Roughness. NACA TN 3305, 1954.

9. Rice, S. O.: Mathematical Analysis of Noise, Pts. I and II. Bell System Jour., vol. XXIII, no. 3, July 1944, pp. 282-332; Pts. III and IV, vol. XXIV, no. 1, Jan. 1945, pp. 46-156.

10. Tukey, J.: The Sampling Theory of Power Spectral Estimates. Symposium on Applications of Autocorrelation Analyses to Physical Problems. Office of Naval Res., Navy Dept., Wash. (D. C.), 1949, pp. 47-67.

11. Connor, R. T., Hawk, J., and Levy, C.: Dynamic Analysis of C-47 Airplane Gust Load Alleviation System. Rep. No. SM-14456, Douglas Aircraft Co., July 1952, p. 114.

12. Press, Harry, and Mazelsky, Bernard: A Study of the Application of Power-Spectral Methods of Generalized Harmonic Analysis to Gust Loads on Airplanes. NACA TN 2853, 1953.

EXAMPLES OF RANDOM DISTURBANCES

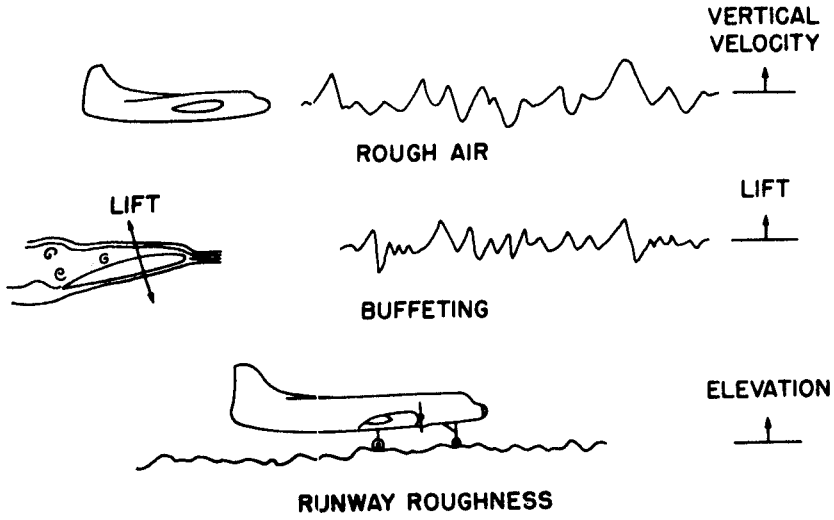

Figure 1

GENERALIZED HARMONIC ANALYSIS

I. POWER SPECTRUM

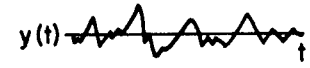

$\overline{y^2(t)}$ = "POWER"

DISTRIB. OF POWER WITH FREQ.

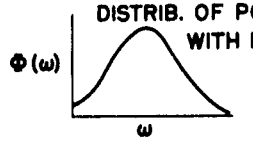

$$\Phi(\omega) = \lim_{T\to\infty} \frac{1}{2\pi T} \left| \int_{-T}^{T} y(t)\, e^{-i\omega t}\, dt \right|^2$$

II. INPUT-OUTPUT RELATION

$\Phi_o(\omega) = \Phi_i(\omega)\, T^2(\omega)$

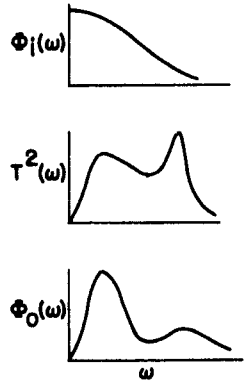

Figure 2

GENERALIZED HARMONIC ANALYSIS

III. RELATIONS BETWEEN SPECTRA AND TIME HISTORIES

(a) $\int \Phi(\omega)\, d\omega = \overline{y^2(t)} = \sigma^2$

(b) $p(y) = \frac{1}{\sigma\sqrt{2\pi}}\, e^{-y^2/2\sigma^2}$

(c) $y_{MAX} \propto \sigma$

(d) NUMBER OF CROSSINGS, ×

(e) NUMBER OF PEAKS, o

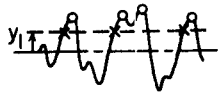

IV. DETERMINATION OF SPECTRA FROM EXPERIMENTAL DATA

(a) FREQUENCY RESOLUTION

(b) SAMPLING RELIABILITY

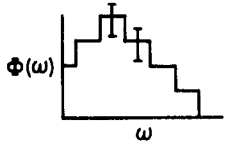

Figure 3

MEASURED POWER SPECTRA OF ATMOSPHERIC TURBULENCE

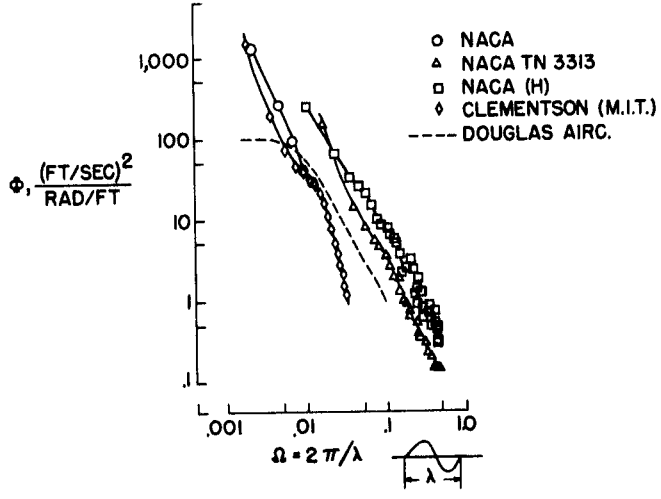

Figure 4

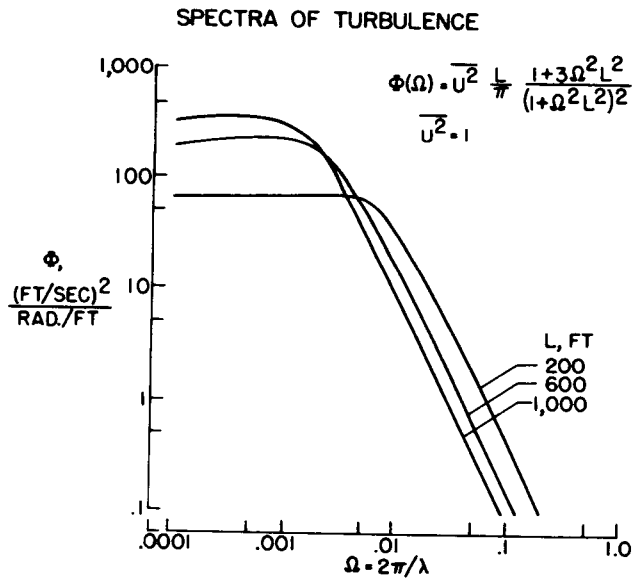

Figure 5

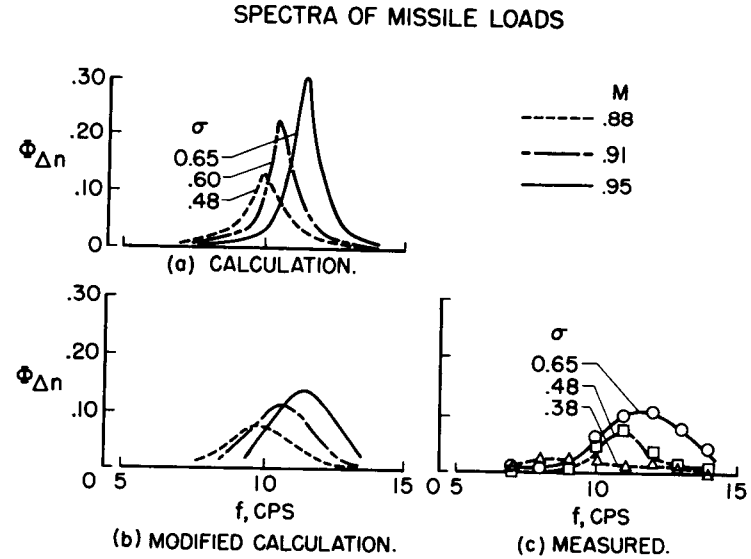

Figure 6

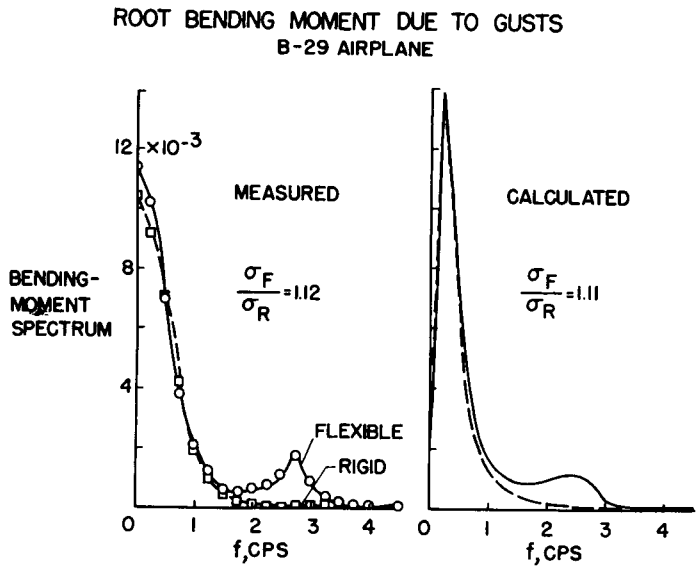

Figure 7

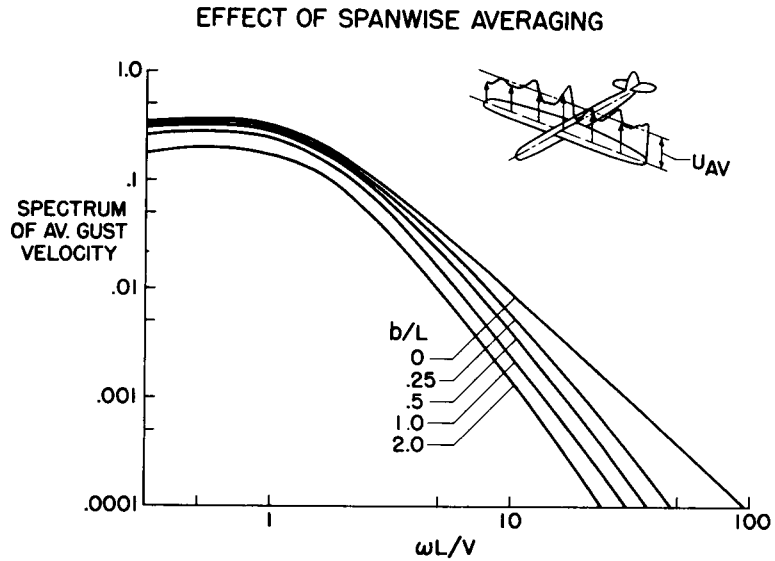

Figure 8

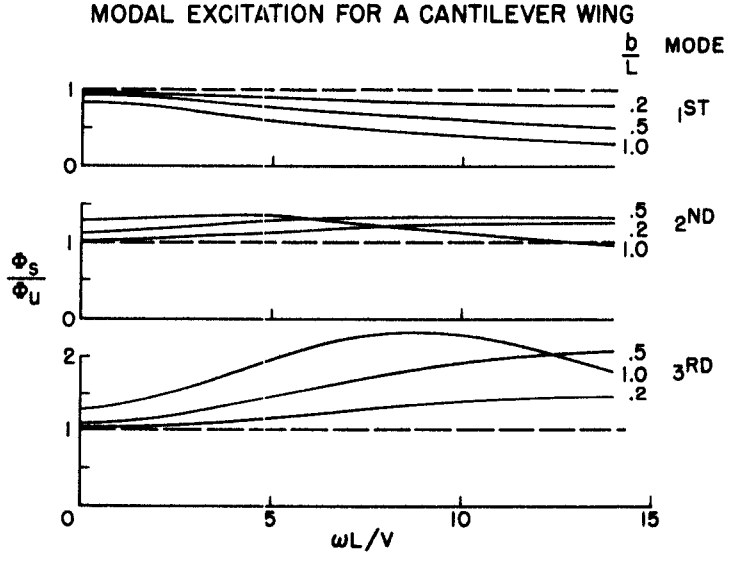

Figure 9

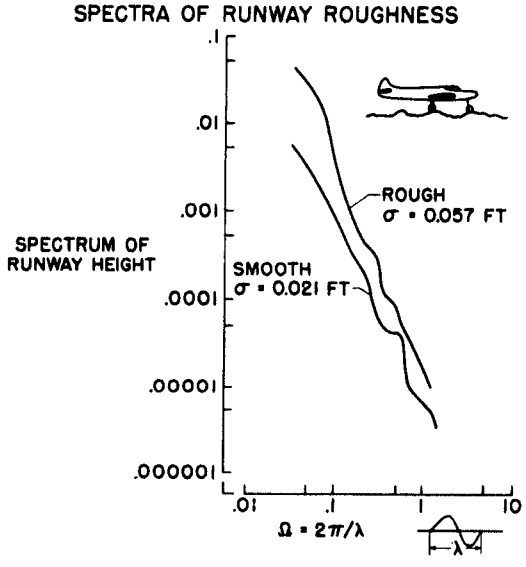

Figure 10

2. SOME RECENT DEVELOPMENTS IN THE AERODYNAMIC THEORY OF OSCILLATING WINGS

By I. E. Garrick and C. E. Watkins
Langley Aeronautical Laboratory

INTRODUCTION

Aircraft companies are making a great effort to treat and to design for aeroelastic problems. These problems, which involve the interaction of the structural deformations and the aerodynamic forces, may be of a static or dynamic nature. An example of a static aeroelastic problem is the determination of the steady load distribution on a deformable wing; an example of a dynamic aeroelastic problem is flutter. Flutter involves the vibration modes of the aircraft with the interaction of the accompanying oscillating air loads as an essential ingredient. It is with this ingredient, the oscillating air loads, that this paper is primarily concerned.

The flutter field is of ever-increasing importance because of higher speeds, diversity of configurations, thinner wing components, and heavier loads and appendages. Problems within the flutter field require a large and continuing effort both on the experimental and theoretical aspects of structures and aerodynamics and on their union.

On the theoretical side, the aerodynamics of flutter has been based mainly on the two-dimensional theory of oscillating wings and has been used in various strip analysis methods with selected structural modes of deformation. Despite its limitations, the two-dimensional theory has been very useful; however, some of the current and future configurations involving plan forms of low aspect ratios and thin wings require improved three-dimensional treatments. This statement, of course, applies to the structural as well as to the aerodynamic analysis.

The present paper is concerned mainly, however, with some recent developments relating to the three-dimensional treatment of the aerodynamics of the finite oscillating wing. A finished report cannot be given, as the subject is in a state of rapid change. The structural side is also in rapid transmutation. For example, the use of simple beam theories, or "beamology," is being questioned as to its relevancy for many modern configurations. Elaborate schemes for accounting for the plan-form elements of low-aspect-ratio wings both aerodynamically and structurally are being developed. These schemes have become not only necessary but also feasible with the notable developments in modern automatic digital computers.

The following subjects are considered in this paper:

(1) The general boundary value problem for oscillating wings and its formulation as an integral equation

(2) Review or recounting of some special solutions, old and recent

(3) The kernel function of the integral equation and its application in determining oscillating air forces on finite wings

(4) The wind-tunnel wall interference problem for oscillating wings and some related experimental measurements

(5) Some supersonic-flow oscillating-wing problems

(6) Reverse-flow reciprocity relations and a few illustrations of their uses

(7) Possible combination of aerodynamic and structural problems

SYMBOLS

The following symbols are used in this report:

A	aspect ratio
a	velocity of sound
b	wing semichord
C_L	lift coefficient
$\left\|dC_L/d\alpha\right\|$	magnitude of oscillating lift coefficient
C_m	moment coefficient
$\left\|dC_m/d\alpha\right\|$	magnitude of oscillating moment coefficient
G	structural-influence function
H	tunnel height
$H_0^{(2)}, H_1^{(2)}$	Hankel functions of second kind of zero and first order, respectively
K	kernel function

k	reduced frequency parameter, $\omega l/U$
L	aerodynamic load distribution
$\lvert L_\alpha/L'_\alpha \rvert$	ratio of magnitude of lift on wing in tunnel to magnitude of lift on wing not in tunnel
l	reference length (often chosen as semichord b)
M	Mach number, U/a
M_3, M_4	components of moment coefficient
p	perturbation pressure
S	projected wing area
s	wing semispan
t	time
U	forward velocity of wing; or, alternatively, velocity of undisturbed stream flowing in x-direction
$V/b\omega_\alpha$	flutter speed coefficient (V denotes speed and ω_α torsional frequency of wing)
w	vertical velocity of fluid or downwash at wing surface, $w(x,y,t) = w^*(x,y)\, e^{i\omega t}$
x,y,z	Cartesian coordinates
Z	normal displacement of mean surface of wing
β	$\sqrt{1 - M^2}$
ξ, η	Cartesian coordinates
ρ	fluid density
Φ	perturbation velocity potential
φ	phase angle
ω	circular frequency of oscillation

$\bar{\omega}$ $\omega/V\beta^2$

ω_r $(\pi\beta/H)(2n - 1)a$, $n = 1, 2, 3 \ldots$

Subscripts:

D direct flow

L lift

m moment

R reverse flow

DISCUSSION AND RESULTS

General Boundary Value Problem for Oscillating Wings

Differential equations and boundary conditions. - The equations that provide the basis for most of the existing theoretical background for unsteady aerodynamics of wings result from a linearization of the boundary value problem for the velocity potential. In equations (1) and (2) are given, respectively, the governing partial differential equation and the main boundary conditions for the problem of the unsteady or the oscillating finite wing:

$$\frac{1}{a^2}\left(\frac{\partial}{\partial t} + U\frac{\partial}{\partial x}\right)^2 \Phi = \nabla^2\Phi \tag{1}$$

On the wing plan form:

$$\left(\frac{\partial\Phi}{\partial z}\right)_{z=0} = w(x,y,t) = \left(\frac{\partial}{\partial t} + U\frac{\partial}{\partial x}\right) Z(x,y,t) \tag{2a}$$

Off the plan form and in its plane:

$$p = -\rho\left(\frac{\partial\Phi}{\partial t} + U\frac{\partial\Phi}{\partial x}\right) = 0 \tag{2b}$$

In addition, there are various conditions to be satisfied at edges of the plan form.

Equation (1) presents the linearized differential equation for the velocity potential Φ based on small perturbations of the flow about the wing in a mainstream of velocity U in the x-direction and of density ρ (see sketch a):

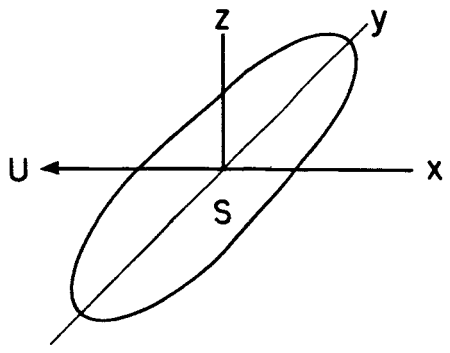

Sketch a

Equation (1) may be recognized as the classical wave equation of acoustics referred to a uniformly moving coordinate system (moving with velocity U in the negative x-direction). In equation (2a) is given the condition that the flow is tangential to the wing surface relating the normal velocity w of the fluid adjacent to the wing surface to the motion of the wing, the displacement of whose mean surface is defined by $Z(x,y,t)$. Equation (2b) is the condition that off the wing surface and particularly in its wake, the pressure difference vanishes. The statement following equation (2b) refers to various edge or tip conditions to be prescribed according to flow regime. In subsonic flow, for example, the pressure difference should go to zero continuously in the immediate neighborhood of all trailing edges. In supersonic flow the trailing edges play no determining part as far as the potential flow is concerned, but leading edges must be assumed to be such that Mach waves remain attached to them.

In this linearized form, the differential equation (1) is satisfied not only by the velocity potential but also by any component of the flow or by the perturbation pressure p, where

$$p = - \rho \left(\frac{\partial \Phi}{\partial t} + U \frac{\partial \Phi}{\partial x} \right) \tag{3}$$

In equation (1), then, Φ may be considered as replaced by the pressure p or by the acceleration potential, which in the linearized form is equivalent to $-p/\rho$.

As a solution of the boundary value problem, the pressure difference or the loading on the wing for arbitrarily given motion or deformation of the wing $w(x,y,t)$ is desired. From a knowledge of the pressure distribution, all forces and moments are directly obtainable by integration. This paper is primarily concerned with the harmonically oscillating type of motion

$$w(x,y,t) = w^*(x,y)\, e^{i\omega t} \tag{4}$$

The integral equation and its kernel. - There are two basic approaches for solution of the boundary value problem. One involves the classical method of separation of variables leading to appropriate solutions of the differential equation and their utilization in infinite series to satisfy the boundary condition of the plan form and the flow. The other involves direct consideration of the integral equation for the pressure into which the boundary value problem of the associated linear differential equations can always be expressed. This latter approach is discussed and used in the present paper. The integral equation can be formulated with the use of velocity potential or with use of the acceleration potential. In the velocity-potential approach the induced effects of the wake, which extends from the trailing edge to infinity, must be taken into consideration; but the acceleration-potential approach is concerned only with integrations over the wing surface alone, the effects of the floating vorticity in the wake being implicitly included.

From this standpoint, the integral equation is readily derived with the aid of the relation between the velocity potential and the pressure difference, which is twice the perturbation pressure p at the surface. The integral equation is given by (see refs. 1 and 2, e.g.)

$$w^*(x,y) = \frac{1}{4\pi\rho} \iint_S L(\xi,\eta)\, K(x-\xi,\ y-\eta)\, d\xi\, d\eta \tag{5}$$

In this equation the normal velocity w^* corresponding to the wing motion (eq. (4)) is assumed to be known. Under the integral which is to be taken over the wing plan form, $L(\xi,\eta)$ denotes the pressure difference or loading to be determined, and K represents the kernel of the integral equation. The kernel function K plays the role of an aerodynamic influence function, in that it gives the induced normal velocity at a point x,y because of unit loading at ξ,η. It is mathematically defined as it arises in the analysis by the rather intricate improper integral given in the following equation:

$$K(x,y;\ M,\omega) = \lim_{z\to 0} \frac{\partial^2}{\partial z^2}\, e^{-\frac{i\omega x}{U}} \int_{-\infty}^{x} \frac{e^{i\bar{\omega}\left(\lambda - M\sqrt{\lambda^2+\beta^2y^2+\beta^2z^2}\right)}}{\sqrt{\lambda^2+\beta^2y^2+\beta^2z^2}}\, d\lambda \tag{6}$$

As indicated, equation (6) expresses the induced velocity field of a uniformly moving unit harmonically loaded element of the plan form and hence corresponds in a sense to a moving acoustic doublet.

A recent reduction of this integral to a proper form given in reference 2 leads to a rather lengthy expression which is given for the general subsonic flow case as a matter of interest:

$$K(x,y) = \frac{k^2}{l^2}\exp(-ikx)\left\{-\frac{1}{k|y|}K_1(k|y|) - \frac{\pi i}{2k|y|}\left[I_1(k|y|) - L_1(k|y|)\right] + \right.$$

$$\frac{iMk|y| + \beta}{M\beta(ky)^2}\exp\left(-\frac{iMk|y|}{\beta}\right) - \int_0^{M/\beta}\sqrt{1+\tau^2}\exp(-ik|y|\tau)\,d\tau -$$

$$\frac{Mkx + \sqrt{(kx)^2+\beta^2(ky)^2}}{M(ky)^2\sqrt{(kx)^2+\beta^2(ky)^2}}\exp\left(\frac{i}{\beta^2}\left[kx - M\sqrt{(kx)^2+\beta^2(ky)^2}\right]\right) +$$

$$\left.\frac{i}{M(ky)^2}\int_0^{kx}\exp\left(\frac{i}{\beta^2}\left[\lambda - M\sqrt{\lambda^2+\beta^2(ky)^2}\right]\right)d\lambda\right\} \qquad (7)$$

where K_1 and I_1 denote modified Bessel functions, L_1 denotes the modified Struve function, and $k = \omega l/U$, where l is an arbitrary reference length often conveniently chosen as a reference semichord b. Other proper forms may be expressed for the kernel function for incompressible flow and for the cases of sonic and supersonic flows.

The kernel function (eq. (7)) can be conveniently separated into two parts. One of these contains all the singularities of $K(x,y)$ but in its application can be treated analytically. The other part contains no singularities and can be numerically tabulated and in application can be dealt with by numerical procedures. The kernel function is therefore capable of being numerically determined and used and, thus, represents the key to some of the developments that are to be discussed. Before coming to these, it may be of value to recall some of the cases for which solutions to the integral equation are already known.

Special Analytical Solutions for Oscillating Wings

By a solution to the equation is meant, of course, an explicit determination of the loading for specified boundary conditions. This has been accomplished analytically exactly, within the framework of the small perturbation theory, for only a few cases. These are listed with regard to flow regime and plan form in the following table:

Flow	Wing plan form
Incompressible	Infinite aspect ratio Very small aspect ratio Circular plan form
Compressible subsonic	Infinite aspect ratio Very small aspect ratio
Supersonic	Infinite aspect ratio Finite, with all-supersonic edges Rectangular plan form Very small aspect ratio

A brief recounting of the procedures, investigators, and approximate dates with which these cases can be associated is believed to be of interest. It should be mentioned first, however, that most of the indicated solutions were not originally obtained by the integral-equation approach.

The closed-form results for the infinite-aspect-ratio wing in incompressible flow (two-dimensional case) were first obtained by consideration of the velocity potential and the infinite vortex sheet to represent the wake. The original methods stem from Birnbaum (1924) and Wagner (1925) who, respectively, considered the infinite oscillating vortex wake and the arbitrary finite wake. General results for the oscillating airfoil are associated with such names as Theodorsen (1934), Cicala (1935), Küssner (1936, 1940), Schwarz (1940), and others. The explicit solution for this case represents a notable landmark in the development of unsteady aerodynamic theory.

Results for the wing of vanishingly small aspect ratio, as indicated under incompressible flow, are due to Miles, Reissner, Garrick, and Ashley and were developed from 1948 to 1951. These results represent an extension of the slender-wing theory for steady flow of R. T. Jones (1946) to unsteady flow.

The oscillating circular plate was first treated by Schade and Kreines (1940-43) who extended Kinner's treatment of the circular plate in steady incompressible flow. It was in connection with this latter problem that Prandtl (1936) first introduced his concept of the acceleration potential for treating linearized problems of aerodynamics. In both the steady- and unsteady-flow cases for the circular plate, the procedure employed was the classical method of separation of variables and the use of appropriate orthogonal functions to obtain the pressure.

The use of orthogonal functions appropriate to the wave equation as a general means of treating the unsteady-flow problem has recently

been discussed by Küssner (ref. 3). Unfortunately, however, appropriate orthogonal systems are possible for only a few special plan forms; and, hence, the general applications are limited. Among the cases that have been treated by the procedure, however, are the wing of infinite aspect ratio and the wing of very small aspect ratio for compressible subsonic flow. Results for the infinite-aspect-ratio wing may be associated with names of Reissner (1944, 1951), Timman (1946), Haskind (1947), and Timman, Van de Vooren, and Greidanus (1951, ref. 4). (Reference 4 supplies various tables that have been corrected as indicated in the reference list.) The results for the oscillating wing of very small aspect ratio extending the incompressible-flow results to include effects of finite sound speed have been given with some numerical tables by Merbt and Landahl (1953, refs. 5 and 6). A more complete numerical set of tables for this case has been prepared by Mazelsky (to be published in Jour. Aero. Sci.).

Before leaving the subject of the use of orthogonal functions, it seems appropriate to mention that among the problems that may possibly be solved by the aforementioned procedure is the important and challenging problem of the oscillating wing of elliptic plan form.

With regard to the cases listed in the table under supersonic flow, it may be mentioned that the two-dimensional oscillating airfoil was first treated by Possio (1937). Garrick and Rubinow in 1947 extended the treatment to apply to any finite wing or portions of a finite wing for which the flow normal to all edges is supersonic. Closed results for the rectangular wing are due to Miles (1949) and Stewartson (1950). Supersonic-flow results for the small-aspect-ratio wing are included in the work of Merbt and Landahl.

The aforementioned list of solutions, it should be remembered, represents only cases for which exact solutions are known and does not include a large portion of knowledge of aerodynamic coefficients that is based on various approximate procedures. Although, for example, the corrected tables based on the exact solution for two-dimensional subsonic flow have become available only within the past few months, the original treatments of the problem and, indeed, accurate tables of coefficients were obtained by approximate procedures through the integral equation for the two-dimensional case long before the exact solution was available. Since a main objective of this paper is to discuss the more general application of these procedures to finite wings, it will be helpful to reexamine some of the pertinent features for the two-dimensional case.

Possio's method for two-dimensional subsonic flow. - The integral equation for two-dimensional flow involves only a single integral taken over the chord, as shown in the following equation:

$$w^*(x) = \frac{1}{4\pi\rho} \int_{-b}^{b} L(\xi)\, K(x-\xi)\, d\xi \tag{8}$$

This equation has become known as Possio's integral equation, since he was the first to treat it and to evaluate its kernel (ref. 7). The kernel which results from an integration of the three-dimensional kernel shown in equation (6) is defined by an improper integral that involves Hankel functions, namely,

$$K(x) = \int_{-\infty}^{\infty} K(x,\, y-\eta)\, d\eta$$

$$= \lim_{z \to 0} \frac{\partial^2}{\partial z^2}\, e^{-\frac{i\omega x}{U}} \int_{-\infty}^{x} e^{i\bar{\omega}\lambda}\, H_0^{(2)}\left(\bar{\omega}\sqrt{\lambda^2 + \beta^2 z^2}\right) d\lambda \tag{9}$$

An explicit expression for K, of which equation (7) is the three-dimensional counterpart is

$$K(x) = -\frac{\pi k}{i\beta}\, e^{-ikx} \left\{ e^{\frac{ikx}{\beta^2}} \left[\frac{iM|x|}{x}\, H_1^{(2)}\left(\frac{kMx}{\beta^2}\right) - H_0^{(2)}\left(\frac{kMx}{\beta^2}\right) \right] + \right.$$

$$\left. \frac{2i\beta}{\pi} \log \frac{1+\beta}{M} + ik \int_0^x e^{\frac{ik\lambda}{\beta^2}}\, H_0^{(2)}\left(\frac{kM|\lambda|}{\beta^2}\right) d\lambda \right\} \tag{10}$$

The method of solution originally employed by Possio was to assume that the chordwise pressure distribution or loading was given by a sum of appropriate modes of load distribution, as in the following equation:

$$L = a_0 \cot\frac{\theta}{2} + a_1 \sin\theta + a_2 \sin 2\theta + \ldots \tag{11}$$

where the angle θ has been introduced as a matter of convenience to replace the chordwise variable ξ by the relation

$$\xi = -b \cos\theta \tag{12}$$

Each modal function in equation (11) is modified by a factor a_i to be determined and which for the oscillating wing (see eq. (4)) must be taken as a complex number in order to yield both magnitude and phase. In steady aerodynamics where the same modes of pressure distribution are commonly used, as in Glauert's thin-airfoil theory, the coefficients a_i are real quantities.

The determination of the a's is brought about by substitution of the assumed loading in the integral equation, thus yielding the normal velocity w^* as a sum of terms involving a. Each term contains as a factor a definite integral that involves the kernel function and one of the assumed modes of pressure distribution. These definite integrals may be evaluated numerically as accurately as desired. Expressing w^* at a desired or sufficient number of control places of the chord leads to a system of linear algebraic equations for determination of the a's.

Analogous method for three-dimensional flow. - Now consider an analogous procedure for treating the integral equation for a finite wing of any plan form, as reproduced from equation (5):

$$w^*(x,y) = \frac{1}{4\pi\rho} \iint_S L(\xi,\eta)\, K(x-\xi,\, y-\eta)\, d\xi\, d\eta \qquad (5)$$

It is recalled that the important kernel K of this equation has been recently put into a form capable of numerical evaluation for any given Mach number, although this evaluation is no simple task. The loading L may again comprise a number of pressure modes, but now must involve besides the chordwise pressure terms, spanwise modifications of these terms involving η:

$$L = \sqrt{s^2 - \eta^2}\left[\cot\frac{\theta}{2}\,(a_{0,0} + a_{0,1}\,\eta + a_{0,2}\,\eta^2 + \ldots) + \sin\theta\,(a_{1,0} + a_{1,1}\,\eta + a_{1,2}\,\eta^2 + \ldots) + \sin 2\theta\,(a_{2,0} + a_{2,1}\,\eta + a_{2,2}\,\eta^2 + \ldots) + \ldots\right] \qquad (13)$$

For example, the first term corresponds to the elliptic type of spanwise loading. The quantity s represents the local semispan and is a function of the local semichord b (see sketch b):

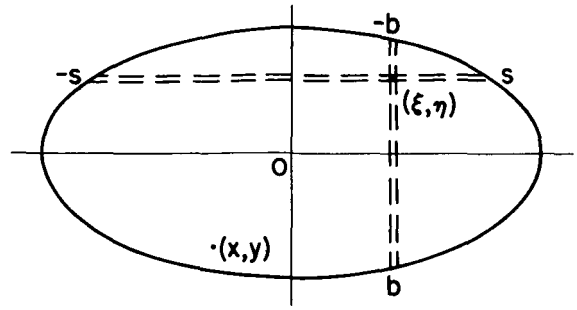

Sketch b

Again the problem is to determine the coefficients $a_{i,j}$ which appear in the expression for the loading corresponding to a specified normal velocity function $w^*(x,y)$. As in the procedures described for the two-dimensional case, the integral equation expressing w^* can be reduced to a sum of terms involving the coefficients $a_{i,j}$. Again, definite integrals occur which involve the kernel K and the assumed modes of pressure distribution and which can be evaluated numerically as accurately as desired. Specification of an appropriate number of control or pivotal points (x,y) will lead to a desired system of simultaneous equations for determining the a's.

The procedure is thus strictly analogous to the two-dimensional one and also bears a resemblance to Falkner's vortex lattice method (ref. 8) of treating finite wings in steady incompressible flow. Other related work of interest is that of W. P. Jones and his associates (e.g., refs. 9 and 10) for treating oscillating wings in incompressible flow based on the velocity potential or vortex lattice approach. The method discussed in the present paper may be more properly termed as a "loaded lattice" approach; however, it will be more simply referred to as lattice approach.

The numerical labor in the three-dimensional lifting-surface method is so great that without the use of modern computing machines it is hardly feasible. There are, of course, many worthwhile short-cuts that can be introduced, but without further details on the methods, some results are presented that have been obtained by these procedures by H. L. Runyan and D. S. Woolston of the NACA Langley laboratory in as yet unpublished work.

Results of application. - The first results presented are for the lift and moment for a rectangular wing of aspect ratio 2 oscillating in pitch about a midchord axis (fig. 1). As no closed-form solution exists for this case, it is necessary to compare results with those of other approximate methods, such as various loaded line or single integral treatments. Among the more recent and outstanding contributions to these approaches is that of Lawrence and Gerber (ref. 11). Their work, which

applies only to incompressible flow, involves approximations in both the loading and the kernel function. In limits with regard to aspect ratio, their results reduce the closed-form results for incompressible flow for wings of infinite aspect ratio and for wings of very small aspect ratio. Their coefficients also agree well with available experimentally determined coefficients for low Mach numbers.

In figure 1 the ordinate on the left is the magnitude of the lift and moment coefficient, and that on the right, the phase angle (angle by which lift or moment vector differs from wing position vector). The abscissa is the reduced frequency parameter commonly used in flutter studies. As indicated by these comparisons, the two methods give essentially the same results for incompressible flow.

For the results covering a range of Mach numbers given in figures 2(a) and (b), the method of reference 10 does not apply and no comparisons with other methods may be made. The magnitudes of lift and moment are given in figure 2(a), and the corresponding phase angles in figure 2(b). These results are also for a wing of aspect ratio 2 oscillating about a midchord axis, but here the reduced frequency is kept constant ($k = 0.22$) and the Mach number is varied. Results for Mach numbers up to and including $M = 1$ were calculated by the lattice approach, while those for $M > 1$ were obtained from supersonic theory for rectangular wings. The subsonic results indicated are, as far as is known, the first such calculations made for the finite oscillating wing. To serve as a basis for comparison of trends with regard to Mach number, results based on closed-form solutions for the corresponding two-dimensional pitching wing are included in figures 2(a) and (b). Examination of the magnitudes and, in particular, the phase angles for finite wings along with those for the two-dimensional wing gives no indication of a simple rule whereby results for one of the wings could be converted into results for the other. It is expected that such an indication would appear less likely as the reduced frequency is increased. For the lower values of the frequency, however, some steady-state rules of conversion should apply. The results shown here were calculated mainly by manual means and required considerable time. A full development of this technique requires a very considerable amount of work and numerical effort. It is readily adaptable to a modern high-speed calculating machine, however, so that the numerical effort required should not stand as an obstacle.

Moreover, and perhaps of greater importance, the procedures are not restricted to the rigid oscillating wing but apply also to the deformable wing; and, as will be briefly indicated in a subsequent section, may be directly combined with structural analysis.

Oscillating Wing in Wind Tunnel

Another result of interest, stemming from the integral equation, relates to the problem of the oscillating wing as affected by the walls of the wind tunnel. Experimental measurement is often required of forces on oscillating wings for studies of flutter, buffeting, and dynamic stability. When such measurements are made in a wind tunnel, it is necessary to know what influence the tunnel walls have on the forces. For simplification, consider the problem of the oscillating wing in a two-dimensional tunnel, as shown schematically in figure 3.

An additional boundary condition that must be observed for solid walls is that the vertical induced velocity at the tunnel wall must be zero. This condition can be met by consideration of a method of images as has been done for the stationary case. To form two walls, an infinite row of images spaced at intervals equal to the tunnel height (as indicated in fig. 3) is required. In addition to the wind-tunnel problem, this reflecting scheme satisfies a main boundary condition for an infinite cascade of oscillating airfoils. The treatment under discussion, therefore, provides a means of calculating forces and moments on such cascades; and these have applications, for example, in problems of flutter of compressor blades. The integral equation for this problem is

$$w^*(x) = \frac{1}{4\pi\rho} \int_{-b}^{b} L(\xi) \left[K(x-\xi) + \sum_{-\infty}^{\infty} K_n(x-\xi,\ nH) \right] d\xi \qquad (14)$$

The kernel for this case consists of two parts, one being the two-dimensional kernel K of Possio's integral equation which is associated with the wing alone, and the other an infinite summation of similar terms that are associated with the images (ref. 12).

In applying the procedures that have been described to this problem, indications of the existence of large effects associated with resonance conditions were soon found. The resonance frequency conditions are given by the relation

$$\omega_r = \frac{\pi\sqrt{1 - M^2}}{H} (2n - 1)a \qquad (15)$$

which has a simple physical basis exactly as organ-pipe resonance. Thus, if the oscillations of the wing occur at frequencies that are equal to or certain multiples of the time required for transverse pressure waves to travel to the tunnel wall and back to the model, this resonant frequency exists, and large and significant resonant-like reactions may be associated with it.

The integral equation has been solved for several specific wind-tunnel problems and, incidentally, for some cascade problems (refs. 13 and 14).

In reference 14 some comparisons are made between calculated and experimental results for the wind-tunnel problem. Some of these results are indicated in figure 4, which applies for a wing oscillating in pitch in a wind-tunnel stream having a Mach number of 0.7. The experimental data were obtained from oscillating pressure distribution measurements by means of pressure cells at 24 stations on the wing. The ordinate on the left is the ratio of lift calculated or measured in the tunnel to the calculated lift without the tunnel. The ordinate on the right is phase angle between lift and position. The abscissa is the ratio of frequency of oscillation of the wing to the calculated resonant frequency. It is not the purpose to labor the differences between theory for the cases of tunnel walls and no tunnel walls, but rather to point to the agreement between theory and experiment. This agreement is noteworthy, particularly since the calculations are intricate and as accurate measurement of oscillating air forces is, indeed, a difficult and delicate undertaking.

Oscillating Wings in Supersonic Flow

Various problems. - The discussion thus far has dealt mainly with problems in subsonic flow. A brief look at the supersonic side is also of interest. The problems of supersonic flow, it will be recalled, can often be treated and synthesized in piecemeal fashion. Thus, the effect at a field point is found by considering only the influences on it in its upstream-facing Mach cone. Moreover, the influence of the point of disturbance reaches only to field points within the aft-cone zone of action.

To indicate the boundary conditions and some regions that are of concern, consider the oval plan form shown in figure 5. The oblique characteristic lines drawn at the Mach angle to the mainstream form a natural coordinate system often more convenient than any other. The tangent characteristic lines that circumscribe the plan form determine several regions and arc segments of the boundary that are of significance. Segment AB is characterized by the fact that the component of the mainstream velocity normal to the edge remains supersonic and is, thus, a supersonic leading edge; similarly DE is a supersonic trailing edge; segments BC and AF are subsonic leading edges; and segments CD and FE are subsonic trailing edges.

The flow problem for the neighborhood of any field point on the plan form influenced only by the supersonic edge, as points of region S_1, has been designated as purely supersonic. A general treatment of

such regions is given in reference 15. Regions like S_2 are influenced by upwash regions ahead of the wing and are, for example, involved in the side edges of the rectangular plan form. Some recent work on rectangular wings is contained in references 16 to 18. The triangular or delta plan form with subsonic edges involves two regions like S_2 and their interaction. Recent reports dealing with this configuration are references 19 and 20. Regions like S_3 are influenced by subsonic trailing edges as well as by the upwash regions ahead of the subsonic leading edges, and their analysis has not as yet been pursued very far.

The references listed are by no means complete, as a large number of investigators have tackled various phases of the unsteady-flow problem for supersonic speeds by the use of many different mathematical techniques. It is appropriate to mention one numerical approach still in a state of development that has recently attracted some attention. This has been termed a "box" method and was proposed by Pines and others in reference 21. In application, it is similar to the lattice approach discussed for subsonic flow, and hence the details will not be given here.

Illustration of two- and three-dimensional effects. - Use may be made of some available numerical results for a wing of rectangular plan form to indicate some pertinent differences between two- and three-dimensional aerodynamic coefficients, and also to indicate some significant effects of these coefficients with regard to calculated flutter speeds.

As a first illustration, figure 6 presents the spanwise distribution of the components of moment coefficients M_3 and M_4 for a rectangular wing of aspect ratio 4 oscillating in pitch about midchord. That for M_3 represents the component in phase with the position of the wing and thus contributes to the aerodynamic stiffness. That for M_4 is the component 90° out of phase with the wing position and thus contributes to the wing aerodynamic damping. The distribution in the tip regions beyond the Mach lines (shown dashed) is significantly different from the two-dimensional type of distribution in the region between the Mach lines. For example, M_4 is negative in the two-dimensional region corresponding to negative aerodynamic damping; whereas, in the tip regions it changes to positive values corresponding to damped conditions. Such variations in coefficients may be of special significance with regard to flutter and dynamic stability of an aircraft. The importance of some of these effects can be seen by referring to figure 7, where some flutter calculations for a cantilever wing of rectangular plan form and of aspect ratio 4 have been made on the basis of two-dimensional and three-dimensional coefficients. Substantial differences of the order of 5 to 30 percent occur in the Mach number range shown. Experimental results for this wing at $M = 1.3$ tend to confirm the three-dimensional or rectangular-wing approach.

It should be pointed out that these examples are based on the motion of the rigid rectangular wing. To obtain aerodynamic coefficients covering various modes of deformation of concern for deformable wings for either supersonic speeds or, as discussed, for subsonic speeds would require a prodigious numerical effort. A recent development of general interest in theoretical aerodynamics that lends hope to greatly alleviate this situation is the subject of reciprocity as it applies to aerodynamics in the form of reverse-flow relations. An indication of the meaning and some possible uses of these relations follow.

Reverse-Flow Relations

Reciprocal relations in aerodynamics may, in fact, be considered as a generalization of classical concepts of reciprocity occurring in dynamics, in structures, and more particularly in acoustics. These, it may be recalled, are related to the broad principle of conservation of energy and to the principle of virtual work.

Thus, in the field of structures, the reciprocity rule is that the displacement at point A due to unit load at point B is equal to the displacement at point B due to unit load at point A. In acoustics, a result of Helmholtz may be recalled: that if, in a space filled with still air (no wind), sound waves are excited at any point A, the resulting velocity potential at a second point B is the same both in magnitude and phase as it would be at A if B were the source of sound.

The generalization of these reciprocal relations to aerodynamics or, for that matter, to acoustics in the presence of a wind involves the consideration of the reverse wind or the reverse flow. The most general results are attributable to Flax (ref. 22), who treated harmonically oscillating wings, and to Heaslet and Spreiter (ref. 23), who considered, in addition, transient flows. To be more concrete, consider a general plan form in direct flow U_D, associated with a normal velocity distribution w_D and the same plan form in reverse flow U_R associated with any other normal velocity distribution w_R:

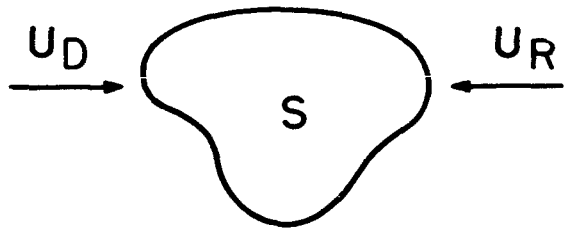

Sketch c

Let L_D represent the pressure loading on the plan form in the direct flow and L_R, the pressure loading on the plan form in the reverse flow. Then, the reverse-flow theorem may be expressed in the form

$$\iint L_D \, w_R \, dS = \iint L_R \, w_D \, dS \tag{16}$$

where each integration is taken over the plan form.

The theorem may be of particular interest for problems of the harmonically oscillating wing, in that it may provide a means for obtaining aerodynamic results for elastic modes from rigid body modes. For example, let w_R refer to uniform harmonic translation of the rigid wing in the reverse flow and let L_R be its associated pressure distribution. Then, the left side of equation (16) is, except for a constant, the integration of the pressure over the surface and defines the total lift; while the right side expresses this lift as an integration over the plan form of the known arbitrary normal velocity w_D and the relatively simple pressure distribution L_R associated with the uniform translation. For example, with $w_R = (\text{constant})\, e^{i\omega t}$,

$$\text{Total lift} = w_R \iint L_D \, dS = \iint L_R \, w_D \, dS \tag{16a}$$

Thus, total lift results for a mode of deformation may be expressed in terms of pressure results for a mode of rigid translation. Indeed, with L_R serving as the appropriate influence or Green's function, it is possible to obtain innumerable solutions from only one known solution. Results of interest are obtained, for example, not only for the lift but also for the pitching, rolling, and aerodynamic-bending moments, as well as control-surface aerodynamic-influence coefficients or generalized forces. Other uses are: it may serve to provide a numerical and analytic check on approximate methods; it may also be of assistance in experimental determination of oscillating air forces. Perhaps one of the most important applications may be in the combining of the aerodynamic and structural analyses by leading to aerodynamic-influence functions associated with structural deformations. The next section touches briefly on this combined aeroelastic problem.

Combined Aerodynamic and Structural Problem

Let $Z(x,y,t)$ represent a normal harmonic deflection of the wing associated with frequency ω; let $G(x,y;\xi,\eta)$ represent the structural-influence function, giving deflections at x,y due to concentrated unit

load at ξ,η; and let $m(\xi,\eta)$ represent the wing element of mass. Then, the general integral equation which combines the aerodynamic and structural problem for any wing capable of harmonic vibrations may be expressed as

$$Z(x,y,t) = \omega^2 \iint G(x,y;\xi,\eta)\, m(\xi,\eta)\, Z(\xi,\eta,t)\, d\xi\, d\eta + \iint G(x,y;\xi,\eta)\, L(\xi,\eta,t)\, d\xi\, d\eta \qquad (17)$$

If L is imagined to be zero - that is, there are no air forces acting - the equation reduces to the vibration problem or eigenvalue problem of determining natural frequencies and modes of the wing. Thus, the first integral term represents the contribution of the inertia forces to the deflection, while the second integral term represents the contribution of the aerodynamic loading to the deflection. Other applied loadings may, of course, be added separately as additional terms. (Since harmonic vibrations are assumed, it is convenient in general to consider ω^2 as a complex frequency of the form $\omega_0^2(1 + ig)$ where g is a measure of the positive or negative damping required in order to permit harmonic vibrations to occur.)

The problem of determining the aerodynamic loading, as has already been discussed, is itself a formidable one and involves the numerical inversion of equation (5) for any plan form. With equation (5) written in the form

$$w(x,y,t) = \frac{\partial Z}{\partial t} + U\frac{\partial Z}{\partial x} = \frac{1}{4\pi\rho}\iint L(\xi,\eta,t)\, K(x,y;\xi,\eta)\, dS$$

it is noted that the derivatives of the deflection function would appear implicitly in L in equation (17) and that this combined problem is of a more general form than that discussed in connection with only the aerodynamics. However, by the methods that have been indicated, L may be determined numerically for a whole matrix of deflection functions, and hence the combined problem may feasibly be treated in a direct numerical manner.

Another approach has recently been suggested by Ashley, Voss, and Zartarian (refs. 24 and 25) in which the reciprocity relations discussed in the preceding topic may play an important role in alleviating the labor. Thus, the second integral term in equation (17)

$$\iint G\, L\, dS$$

may be replaced by its reciprocal relation

$$\int\int \left(\frac{\partial Z}{\partial t} + U \frac{\partial Z}{\partial x}\right) L_G \, dS$$

where L_G is the aerodynamic loading on the plan form in reverse flow with the normal velocity distribution chosen as the influence function G itself. This form has the advantage of making the dependence of the aerodynamic loading on the deflection explicit rather than implicit. It is another example of converting an integral involving the aerodynamic loading on the deformable wing into one that can be expressed in terms of a known type of motion for the plan form in the reverse flow. It is not to be implied that the determination of the structural-influence function G is a simple task. Its determination, experimentally or analytically, is in itself a problem meriting and requiring much additional research.

CONCLUDING REMARKS

This paper indicates that the theoretical aerodynamic problem of the linearized oscillating wing can be resolved in a truly three-dimensional treatment and numerically accomplished. It is not to be implied that the subject is a closed one; it goes without saying that analytical procedures, as, for example, a complete treatment of the elliptic plan form, can supplement and illuminate the work. The aeroelastic problem combining the aerodynamic and the structural problems also gives hope of being resolved in a similar numerical fashion in the not too distant future.

REFERENCES

1. Küssner, H. G.: General Airfoil Theory. NACA TM 979, 1941. (From Luftfahrtforschung, Bd. 17, Nr. 11/12, Dec. 10, 1940, pp. 370-378.)

2. Watkins, Charles E., Runyan, Harry L., and Woolston, Donald S.: On the Kernel Function of the Integral Equation Relating the Lift and Downwash Distributions of Oscillating Finite Wings in Subsonic Flow. NACA TN 3131, 1954.

3. Küssner, H. G.: A General Method for Solving Problems of the Unsteady Lifting Surface Theory in the Subsonic Range. Jour. Aero. Sci., vol. 21, no. 1, Jan. 1954, pp. 17-26.

4. Timman, R., Van de Vooren, A. I., and Greidanus, J. H.: Aerodynamic Coefficients of an Oscillating Airfoil in Two-Dimensional Subsonic Flow. Jour. Aero. Sci., vol. 18, no. 12, Dec. 1951, pp. 797-802. (Corrected tables issued in vol. 21, no. 7, July 1954, p. 499.)

5. Merbt, H., and Landahl, M.: Aerodynamic Forces on Oscillating Low Aspect Ratio Wings in Compressible Flow. KTH Aero. TN 30, Stockholm, 1953.

6. Merbt, H., and Landahl, M.: The Oscillating Wing of Low Aspect Ratio - Results and Tables of Auxiliary Functions. KTH Aero. TN 31, Stockholm, 1954.

7. Possio, Camillo: L'Azione Aerodinamica sul Profilo Oscillante in un Fluido Compressibile a Velocità Iposonora. L'Aerotecnica, vol. XVIII, fasc. 4, Apr. 1938, pp. 441-458. (Available as British Air Ministry Trans. No. 830.)

8. Falkner, V. M.: The Calculation of Aerodynamic Loading on Surfaces of Any Shape. R. & M. No. 1910, British A.R.C., Aug. 23, 1943.

9. Jones, W. P.: The Calculation of Aerodynamic Derivative Coefficients for Wings of Any Plan Form in Non-Uniform Motion. R. & M. No. 2470, British A.R.C., 1952.

10. Lehrian, Doris E.: Calculation of the Damping for Rolling Oscillations of a Swept Wing. Rep. C.P. No. 51, British N.P.L.

11. Lawrence, H. R., and Gerber, E. H.: The Aerodynamic Forces on Low Aspect Ratio Wings Oscillating in an Incompressible Flow. Jour. Aero. Sci., vol. 19, no. 11, Nov. 1952, pp. 769-781. (Errata issued vol. 20, no. 4, Apr. 1953, p. 296.)

12. Runyan, Harry L., and Watkins, Charles E.: Considerations on the Effect of Wind-Tunnel Walls on Oscillating Air Forces for Two-Dimensional Subsonic Compressible Flow. NACA Rep. 1150, 1953. (Supersedes NACA TN 2552.)

13. Woolston, Donald S., and Runyan, Harry L.: Some Considerations on the Air Forces on a Wing Oscillating Between Two Walls for Subsonic Compressible Flow. Preprint No. 446, Jour. Aero. Sci. (To be published in the Jour. Aero. Sci.)

14. Runyan, Harry L., Woolston, Donald S., and Rainey, A. Gerald: Theoretical and Experimental Investigation of the Effect of Tunnel Walls on the Forces on an Oscillating Airfoil in Two-Dimensional Subsonic Flow. (Proposed NACA TN.)

15. Garrick, I. E., and Rubinow, S. I.: Theoretical Study of Air Forces on an Oscillating or Steady Thin Wing in a Supersonic Main Stream. NACA Rep. 872, 1947. (Supersedes NACA TN 1383.)

16. Miles, John W.: The Oscillating Rectangular Airfoil at Supersonic Speeds. Quart. Appl. Math., vol. 9, Jan. 1951, pp. 47-65.

17. Stewartson, K.: On the Linearized Potential Theory of Unsteady Supersonic Motion. Quart. Jour. Mech. and Appl. Math., vol. 3, June 1950, pp. 182-199.

18. Nelson, Herbert C., Rainley, Ruby A., and Watkins, Charles E.: Lift and Moment Coefficients Expanded to the Seventh Power of Frequency for Oscillating Rectangular Wings in Supersonic Flow and Applied to a Specific Flutter Problem. NACA TN 3076, 1954.

19. Watkins, Charles E., and Berman, Julian H.: Air Forces and Moments on Triangular and Related Wings with Subsonic Leading Edges Oscillating in Supersonic Potential Flow. NACA Rep. 1099, 1952. (Supersedes NACA TN 2457.)

20. Watkins, Charles E., and Berman, Julian H.: Velocity Potential and Air Forces Associated with a Triangular Wing in Supersonic Flow, with Subsonic Leading Edges, and Deforming Harmonically According to a General Quadratic Equation. NACA TN 3009, 1953.

21. Pines, S., and Dugundji, J.: Aerodynamic Flutter Derivatives of Flexible Wing with Supersonic Edges. ATC Rep. No. ARTC-7, Feb. 1954.

22. Flax, A. H.: The Reverse-Flow Theorem for Nonstationary Flows. Jour. Aero. Sci., vol. 19, no. 5, May 1952, p. 352.

23. Heaslet, Max A., and Spreiter, John R.: Reciprocity Relations in Aerodynamics. NACA Rep. 1119, 1953. (Supersedes NACA TN 2700.)

24. Ashley, Holt, Voss, Herbert M., and Zartarian, Garabed: The Dynamic Analysis of Low-Aspect-Ratio Wings. Proc. Nat. Acad. Sci., vol. 40, June 1954.

25. Voss, H. M.: On the Use of the Reverse Flow Theorem in the Problem of Aeroeleastic Deflections. Jour. Aero. Sci., vol. 21, no. 8, Aug. 1954, p. 569.

LIFT AND MOMENT FOR PITCHING WING

A = 2; M = 0

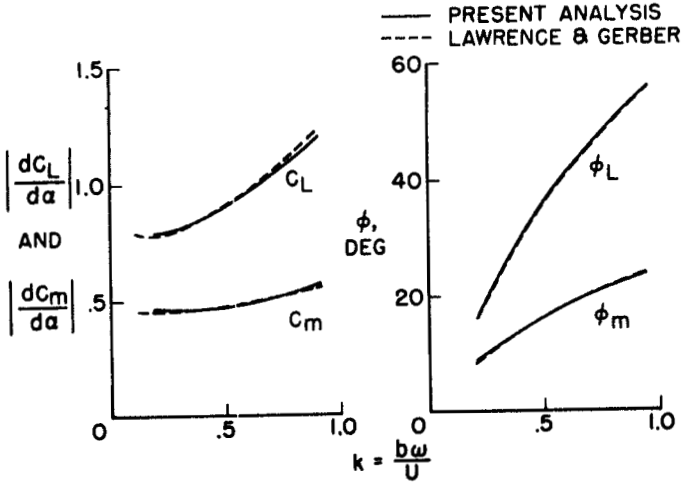

Figure 1

PHASE-ANGLE VARIATION WITH MACH NUMBER

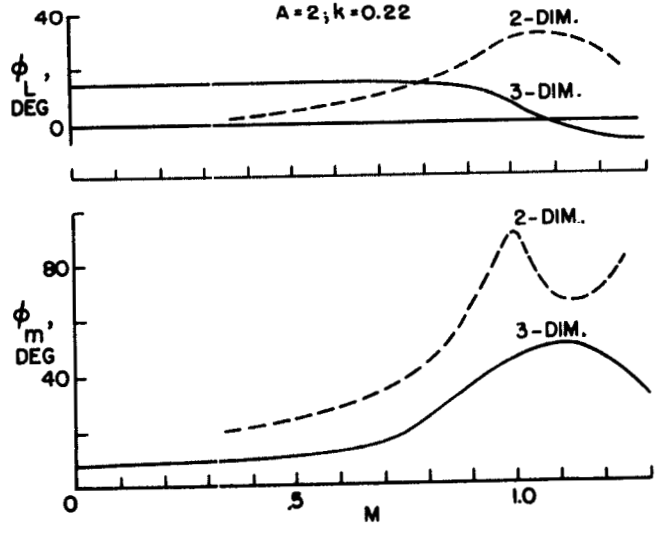

Figure 2b

LIFT AND MOMENT VARIATION WITH MACH NUMBER

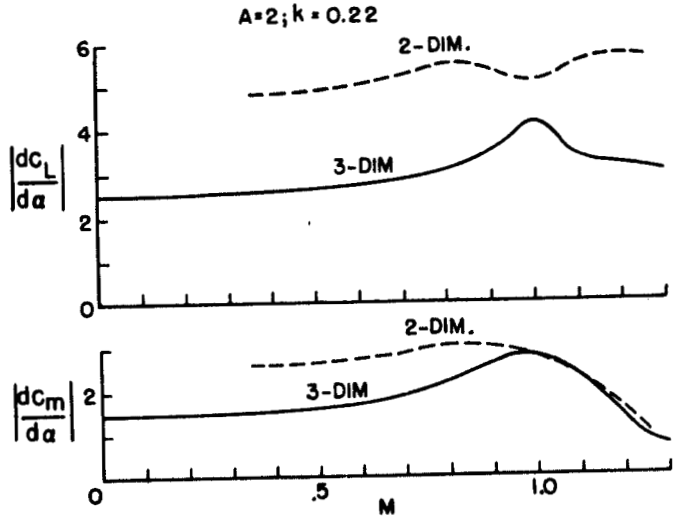

Figure 2a

OSCILLATING WING IN WIND TUNNEL

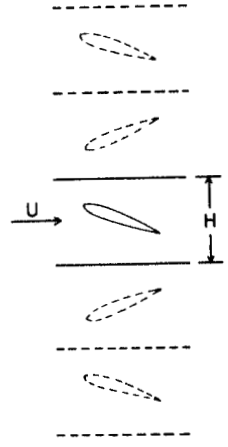

Figure 3

MEASURED AND CALCULATED OSCILLATING LIFT IN WIND TUNNEL
M = 0.7

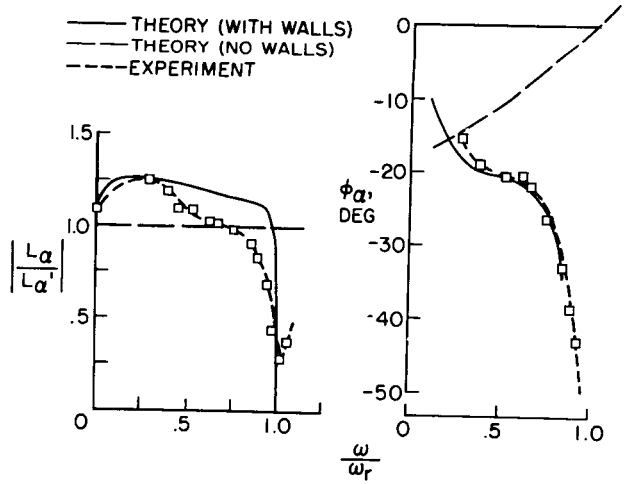

Figure 4

PLAN FORM IN SUPERSONIC FLOW

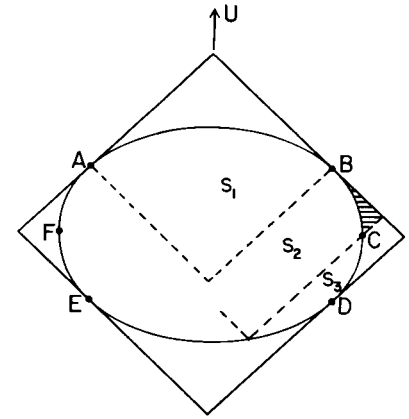

Figure 5

MOMENT DISTRIBUTIONS FOR A WING OF ASPECT RATIO 4
M = 1.3; k = 0.1

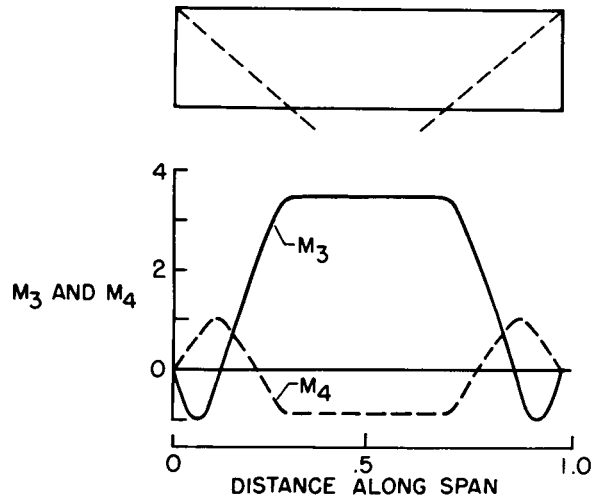

Figure 6

VARIATION OF FLUTTER-SPEED COEFFICIENT WITH M FOR RECTANGULAR CANTILEVER WING
A = 4

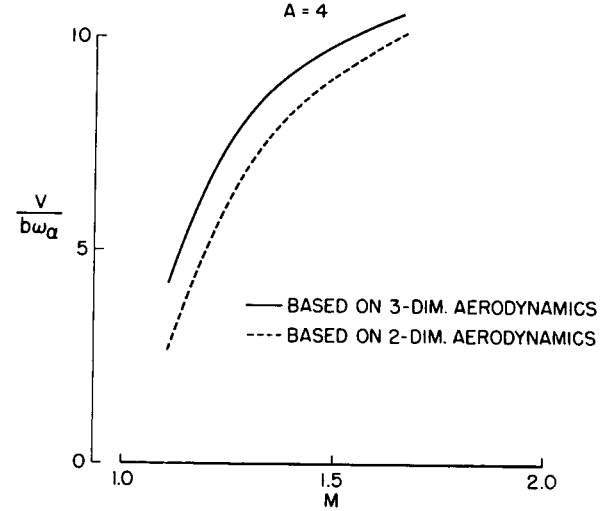

Figure 7

3. STRENGTH ANALYSIS OF MULTIWEB THIN WINGS

By Norris F. Dow and Roger A. Anderson
Langley Aeronautical Laboratory

SUMMARY

Recent investigations of the strength of thin wings of multiweb construction are reviewed. The relation between web support stiffness and ultimate strength is analyzed, and methods are given for evaluating the support stiffness. The results of this analysis are compared with experimental data. Methods are also given for the correlation of the strength of multiweb construction with material stress-strain properties at room and elevated temperatures.

INTRODUCTION

The structural problems associated with current and projected aircraft have given rise to the use of new structural forms and materials. These new forms and materials in turn have required new methods of strength analysis. The present paper is a review of recent NACA investigations pointed toward the extension of knowledge of wing structural strength. In particular, thick-skin construction of the multiweb type (one of the configurations of current interest for thin wings) is considered. This review is divided into two phases. The first phase concerns room-temperature static strength, particularly in regard to the way the skin allowable stresses are influenced by web supporting stiffness. The second covers correlation of strength with changes in material properties.

SYMBOLS

The symbols used for beam dimensions are indicated in figure 1. These and other symbols used are as follows:

b_A distance from rivet line to web center line, in.

b_S web spacing, in.

b_W web height, in.

E_{SEC} secant modulus, ksi

f effective rivet offset distance, in.

t_s skin thickness, in.

t_w web thickness, in.

σ stress, ksi

σ_{cy} 0.2-percent offset compressive yield stress, ksi

$\bar{\sigma}_f$ average stress at failure, ksi

STATIC STRENGTH ANALYSIS

In anticipation of the trend of thick-skin construction, studies were initiated several years ago of multiweb wing construction of the type illustrated in figure 1. This construction is characterized by thick skins which carry 90 percent or more of the bending moment and which are supported by a number of spanwise shear webs as indicated in the sketch at the bottom of the figure. An idealization of this construction for analysis is indicated in the enlarged view at the top of the figure. The symbols for the various dimensions used in this paper are identified in the figure.

The allowable compressive stress for the skin in this type of construction depends on the restraint offered the skins by the internal webs. In a strength analysis of multiweb construction given in reference 1, buckling coefficients were computed for the skin assuming an idealized integral type structure (as indicated in the enlarged view in fig. 1), which provides a rigid deflectional support for the cover skins along the web lines. Subsequent experimental results (ref. 2) on a systematic series of built-up beams, however, showed poor correlation in many cases with the buckling behavior calculated from this analysis. Two basic types of characteristic behavior at buckling were noted in these tests. This behavior is illustrated in figures 2 and 3. In beams of certain proportions the mode of buckling that occurred corresponded to local buckling as assumed in the integral web analysis. As shown in figure 2, it is characterized by a sinusoidal wave pattern that is suppressed along the web support lines so that the buckles do not extend across the support lines, and from bay to bay the buckles appear out of phase. In beams of other proportions, however, the buckles were not suppressed along the web lines; instead they formed crests and troughs extending across the entire width of the beam as shown in figure 3. Here the buckles might be considered "in phase" across the beam. This in-phase buckling, which occurred at lower stresses than would be predicted for local buckling, has been called "wrinkling instability."

The reductions in buckling stress associated with wrinkling instability are illustrated in figure 4. Here experimentally measured buckling coefficients are plotted as in reference 3 against a parameter representative of the cell geometry of the beam, namely the ratio of web height to thickness over the ratio of web spacing to skin thickness. The curve gives the prediction for the buckling stress coefficients based on the integral web analysis. A significant point here is that the assumption of integral type joints between webs and cover skins gives the upper limit to the buckling coefficients actually achieved, and for most of the thick-skin proportions the measured coefficients were substantially lower than the predictions.

The reason for the failure of fabricated beams to achieve the buckling modes and stresses for the idealized integral web construction is associated with the inherent flexibility of the attachment flanges and riveted joints between the webs and the skins. The source of this flexibility is illustrated in figure 5. In actual practice the beam webs have an attachment flange riveted to the skins at an offset from the web plane. Because of the bending flexibility of this cantilever type connection, buckling of the compression cover can occur by displacements relative to the tension cover; that is, the compression cover can move up or down relative to the tension cover as if the compression cover were a wide column on an elastic foundation. This mode of distortion in which the buckle deflections grow across the support lines is in contrast to the localized rotational distortions that are assumed to take place on local buckling of the idealized integral web beam.

An analysis of the supporting stiffness provided to the cover skins by this cantilever type connection must take into account not only the geometrical offset of the rivet line from the web plane, but also must attempt to evaluate the location of a line along which the rivet pattern effectively clamps the attachment flange to the skin. An important factor influencing this clamping is the pitch and diameter of the rivets used. In general, a given combination of geometrical offset, rivet pitch, and diameter, will produce an effective offset that does not coincide with the line of rivets. The effective offset distance is denoted by the symbol f.

An analysis of the strength of multiweb beams in which the allowable compressive stress in the skin is related to the effective rivet offset distance f has recently been made. Essentially, this bending-strength theory is based upon the behavior of a wide plate supported on flexible line supports (see ref. 4). The f distance associated with various attachment flanges and rivet patterns was determined empirically from a large number of tests on skin-stringer compression panels (ref. 5), giving the results shown in figure 6. From this diagram the ratio of f to t_w for a given attachment flange design can be determined for

specified values of the pitch-to-diameter ratio for the rivets and the ratio of the geometrical offset of the rivet line b_A to the web thickness t_w. The absolute diameter of the rivet was not found to be important independently but only as it affected the ratio of pitch to diameter. When the f value is read from this diagram and used in the strength analysis for multiweb beams, the results are as shown in figure 7. The test points here are for the same beams as those shown in figure 4, and the curves now represent failing stress coefficients calculated for these beam proportions at the various indicated values of effective rivet offset distance divided by the web height. In this series of beams the details of the web skin joints were held constant and only the web height was varied to give these values of f/b_w. Satisfactory agreement is indicated between the calculated curves and the test points for the corresponding beam proportions.

The importance of the offset distance in the determination of the failing strength is indicated by the results of tests of four beams (ref. 6) in which all proportions were held constant except for the value of f/t_w. The results of these tests are shown in figure 8. For a change in value of f/t_w from 9 to 5, which represents a change in f of only 1/4 inch for these beams, the ultimate stress was changed from approximately 30 ksi for the wide offset to nearly 50 ksi for the small offset. The implication is clear that, with high-strength materials such as the 75S-T6 aluminum alloy used for these beams, substantial increases in strength can be obtained by improved connection design.

A further possibility is that, if true integral construction were utilized, thereby eliminating the attachment flange and the attendant support flexibility, a further increase in ultimate strength can be realized. For example, a recent large deflection analysis of plates supported in such a manner that the plate edges are constrained to remain straight long after buckling indicated ultimate plate compressive strengths appreciably higher than had been obtained experimentally. According to this analysis (ref. 7), which was made for 24S-T3 aluminum alloy, the results of which are plotted in figure 9 as calculated curves of average stress against unit shortening, the average stress in the plate continues to increase as the plate shortens after buckling, with no maximum stress occurring within the usually encountered range of shortening. These calculations were made for four plate proportions buckling at the four stress levels indicated, and the calculated (dashed) curves are compared in figure 9 with load-shortening curves (solid) measured for plates tested in V-groove edge fixtures. The behavior of a plate tested in V-groove fixtures probably corresponds quite closely to that of plates supported by stiff webs as in a multiweb beam. That is, the V-grooves are capable of forcing the plates to buckle in a local mode but assuredly fail to prevent displacement of the plate edges in the post-buckling range of loading, with the result that a maximum load is reached at fairly small end shortenings.

The implication of this analysis is that the provision of very stiff supports may increase the ultimate strength of plates, but then the high strength will not be achieved within the usual range of deformation. What this means in terms of a very thin wing structure is illustrated by the frames taken from a short movie (fig. 10) of a test of a 4-percent-thick airfoil section having a single solid shear web down its center.

The wing section was mounted horizontally in the Langley combined load testing machine and loaded in pure bending by the loading unit rising and rotating at the right-hand end of the specimen. The bending moment continued to increase until the test was halted, because the angular travel of the loading unit was used up without failing the specimen. The total tip rotation was 35° in a specimen length of only $1\frac{1}{2}$ times the wing chord (see bottom frame of fig. 10). Obviously, for very thin wings such as this, if maximum load is not achieved within the usual range of deformation it becomes important to consider the deflections and rotations associated with maximum load as well as the ultimate strength.

EFFECT OF MATERIAL CHANGES ON ULTIMATE STRENGTH

Because of the effects of aerodynamic heating, the effects of changes in wing material are becoming of increasing interest. Material properties change with temperature, and the use of new materials to withstand elevated temperatures with respect to both stiffness and strength must be considered.

In order to predict the effect of a change in material on the known strength of a beam constructed of another material, work has been done to determine how a correlation of structural strength with material properties may be made. This work (ref. 8) shows that this correlation can be effected by means of easily defined parameters determined by the overall shape of material compressive stress-strain curves. For example, a material parameter $\sqrt{E_{SEC}\sigma_{cy}}$ can be defined (see fig. 11) which combines the usual 0.2-percent offset compressive yield stress and the secant modulus to the compressive stress-strain curve at the failure stress for the structure. If the failure stresses of geometrically similar structures are divided by this material parameter, the results are as shown in figure 12. This figure shows the results of V-groove fixture tests to determine the ultimate strength of plates of a number of width-thickness ratios, tested in materials having wide variations in yield stress and slope of the stress-strain curve. The materials used were a magnesium alloy, three aluminum alloys, and two steels. When the ultimate strengths of the plates divided by the material parameter are plotted against the plate width-thickness ratio, the test results for all materials lie essentially along a single curve. These results are

typical of those found for other plate structures as well as for plates in V-groove fixtures, when tested at room temperature. The same technique appears to be applicable to the prediction of the reduction in strength of a given structure when subjected to elevated temperature. A convenient method of making short-time elevated-temperature strength predictions using this parameter is illustrated in figure 13.

From compressive stress-strain curves obtained for the material at various temperatures, a plot of σ against σ divided by the material parameter can be made for each temperature. The rounding off of each curve corresponds to the changes in the secant modulus in the plastic range at the given temperature. The use of a plot such as this avoids the necessity for a trial-and-error procedure. To predict the steady-state elevated-temperature strength of a structure that fails at approximately 62 ksi at 80° F, for example (fig. 13), the corresponding strength at elevated temperatures is found by dropping vertically at a constant value of the abscissa to the desired elevated-temperature curve and then reading the failure stress on the ordinate. This technique has been found to be applicable to structures such as skin-stringer panels and multiweb beams that fail by compressive crippling. When applied to multiweb beams, the results are shown in figure 14.

The failing stresses for two multiweb beam configurations are plotted in figure 14 against the steady-state temperatures at which the tests were run. The curves represent failing stresses predicted by this method based upon room-temperature strength for beams at stabilized elevated temperatures, and the test points indicate the experimental values of failing stress. The accuracy of prediction here appears to be at least as satisfactory as found previously for correlation among entirely different materials at room temperature.

CONCLUDING REMARKS

The investigations reviewed indicate the important relation between the allowable stresses that can be developed in thick-skin, thin-wing structures and the web support stiffness provided to the skins. Strength analyses based upon the stiffness of riveted attachment flanges show that the ultimate bending strength of fabricated structures can be predicted. These analyses also show that the ultimate strength is extremely sensitive to small changes in the effective offset distance of the riveted flanges and increases substantially as the effective offset is decreased. Accordingly, the details of attachment flanges and connections become an important design and production consideration. These conclusions regarding effects of geometry are independent of material properties. Satisfactory correlation with material properties of the strength of thick-plate type structures is obtained through use of a suitably defined

material parameter. This parameter appears to give good correlations of the static strength of plate structures made of different materials or subjected to different steady-state temperature environments.

REFERENCES

1. Schuette, Evan H., and McCulloch, James C.: Charts for the Minimum-Weight Design of Multiweb Wings in Bending. NACA TN 1323, 1947.

2. Pride, Richard A., and Anderson, Melvin S.: Experimental Investigation of the Pure-Bending Strength of 75S-T6 Aluminum-Alloy Multiweb Beams with Formed-Channel Webs. NACA TN 3082, 1954.

3. Semonian, Joseph W., and Anderson, Roger A.: An Analysis of the Stability and Ultimate Bending Strength of Multiweb Beams with Formed-Channel Webs. NACA TN 3232, 1954.

4. Anderson, Roger A., and Semonian, Joseph W.: Charts Relating the Compressive Buckling Stress of Longitudinally Supported Plates to the Effective Deflectional and Rotational Stiffness of the Supports. NACA TN 2987, 1953.

5. Dow, Norris F., and Hickman, William A.: Effect of Variation in Rivet Diameter and Pitch on the Average Stress at Maximum Load for 24S-T3 and 75S-T6 Aluminum-Alloy, Flat, Z-Stiffened Panels that Fail by Local Instability. NACA TN 2139, 1950.

6. Anderson, Roger A., Pride, Richard A., and Johnson, Aldie E., Jr.: Some Information on the Strength of Thick-Skin Wings with Multiweb and Multipost Stabilization. NACA RM L53F16, 1953.

7. Mayers, Jean, and Budiansky, Bernard: Analysis of the Behavior of Simply-Supported Flat Plates Compressed Beyond the Buckling Load into the Plastic Range. (Proposed NACA TN.)

8. Anderson, Roger A., and Anderson, Melvin S.: Correlation of Crippling Strength with Changes in Material Properties. (Proposed NACA TN.)

IDEALIZED MULTIWEB WING

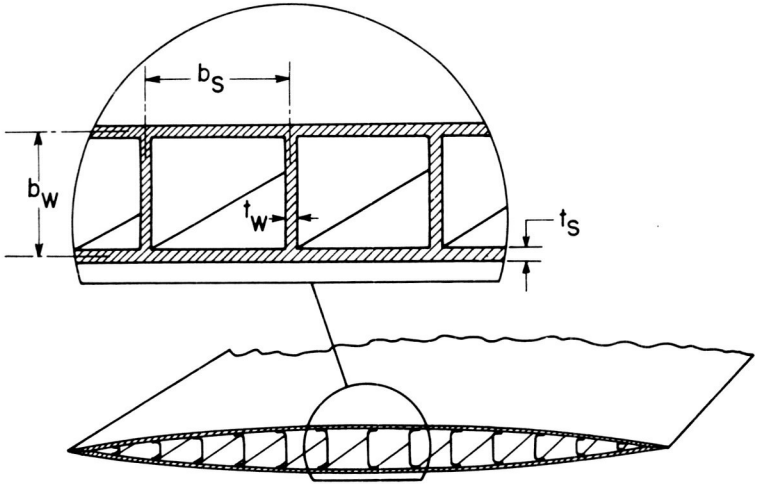

Figure 1

PLATE BUCKLING

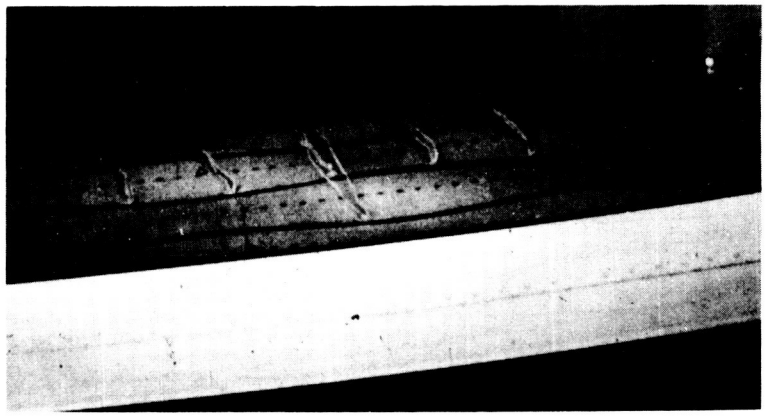

Figure 2

WRINKLING INSTABILITY

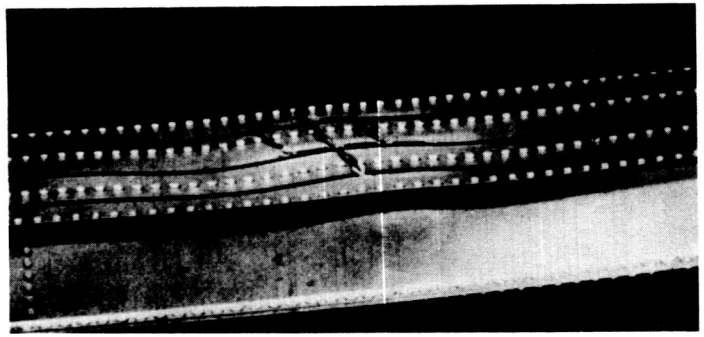

Figure 3

BUCKLING OF MULTIWEB BEAMS

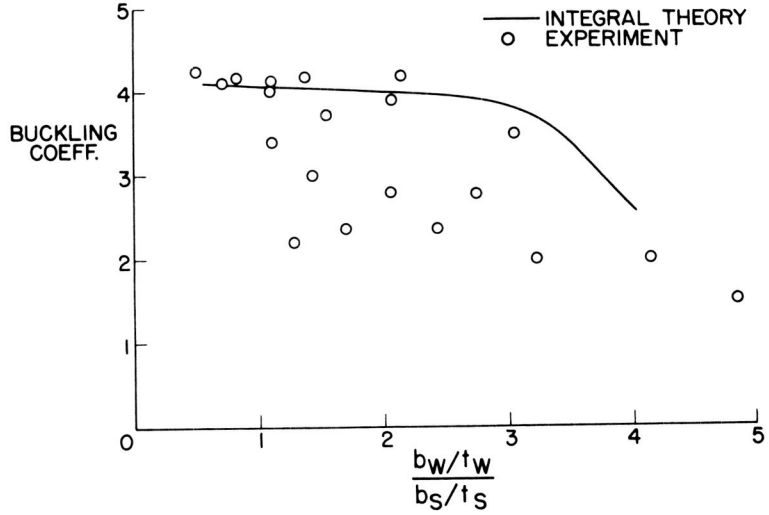

Figure 4

EFFECTIVE RIVET-OFFSET DISTANCE

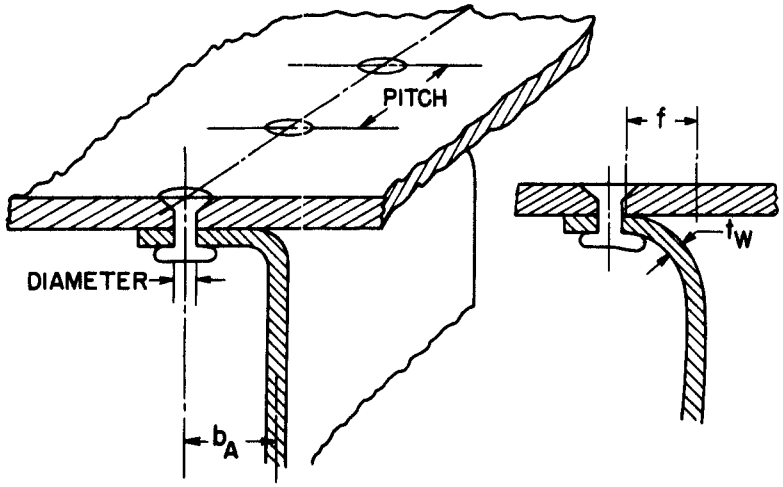

Figure 5

EVALUATION OF EFFECTIVE RIVET-OFFSET DISTANCE

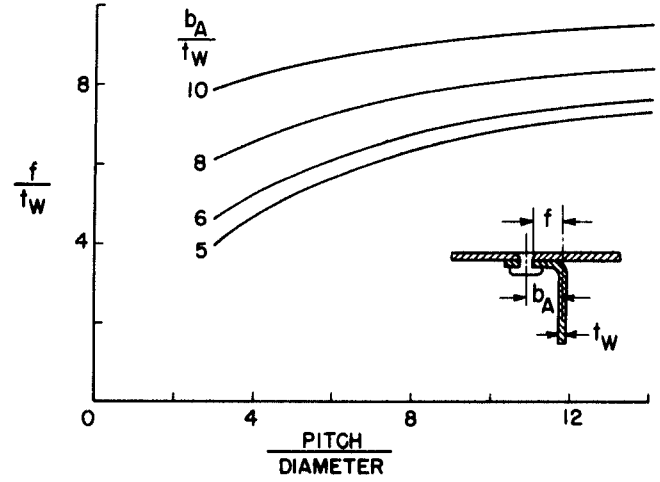

Figure 6

WRINKLING INSTABILITY OF MULTIWEB BEAMS

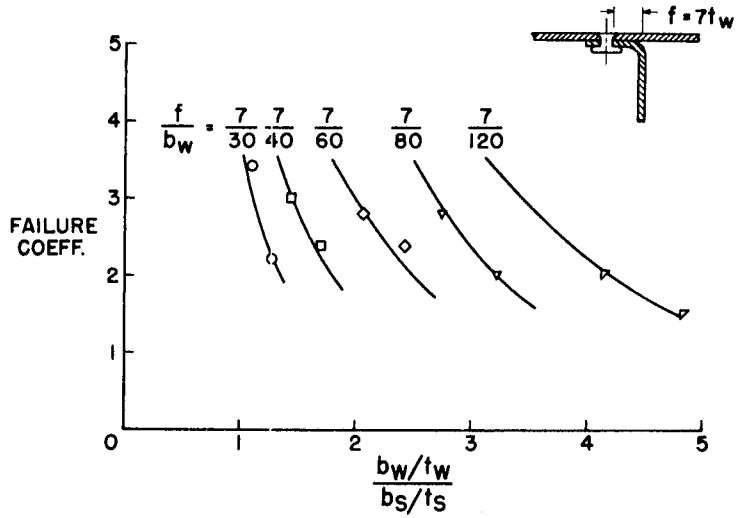

Figure 7

EFFECT OF OFFSET DISTANCE ON BEAM STRENGTH

75S-T6 ALUMINUM-ALLOY BEAM

$\frac{b_S}{t_S} = 30;\ \frac{t_W}{t_S} = 0.26;\ \frac{b_W}{t_S} = 21$

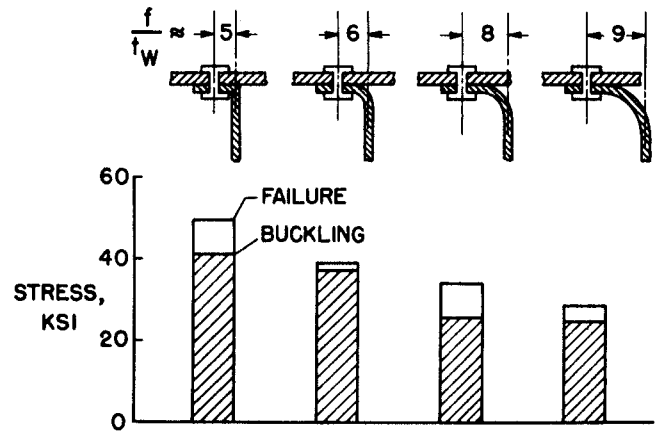

Figure 8

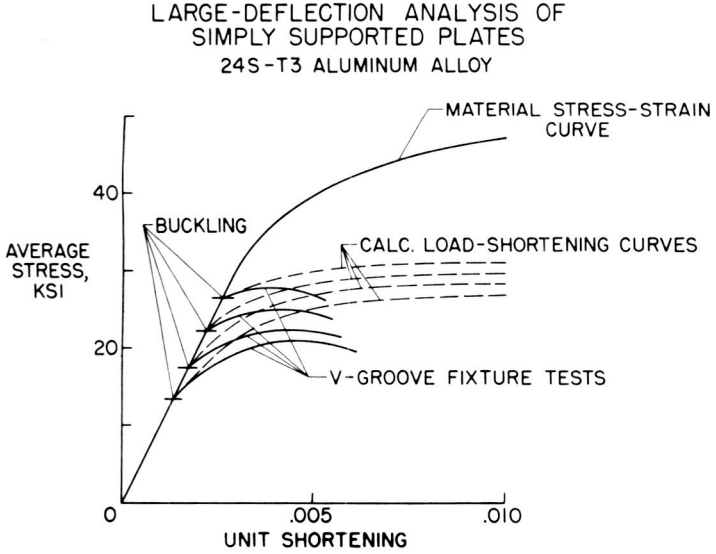

Figure 9

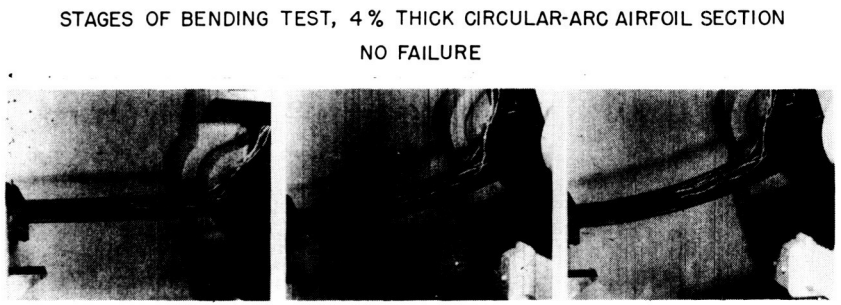

Figure 10

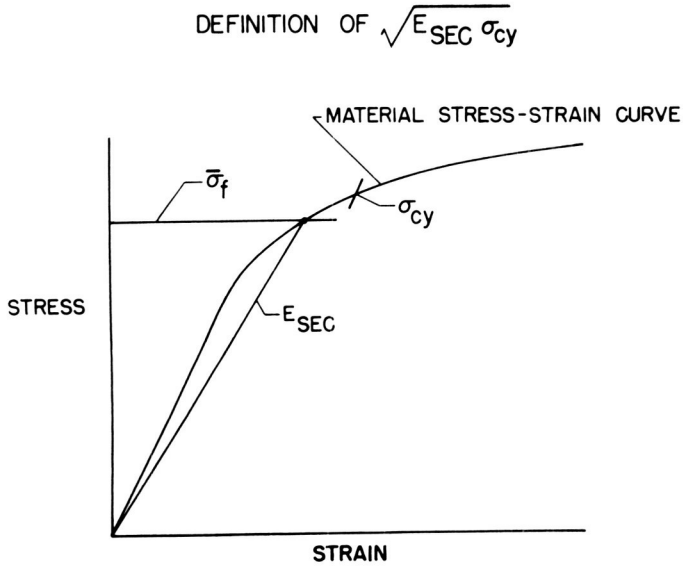

Figure 11

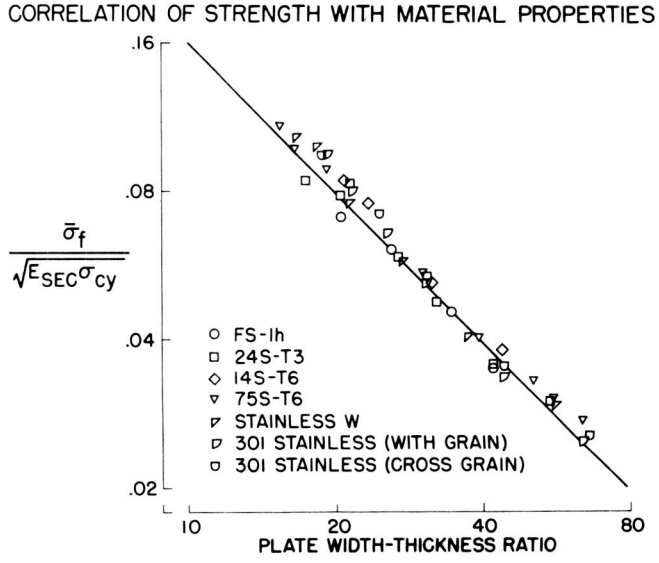

Figure 12

STRENGTHS AT ELEVATED TEMPERATURE
75S-T6 ALUMINUM ALLOY

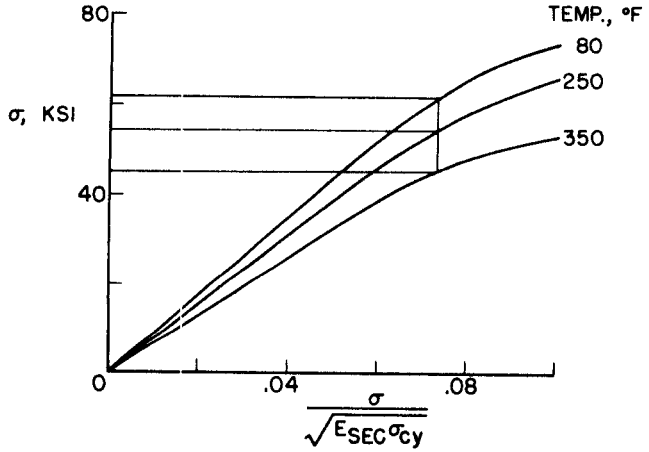

Figure 13

BEAM STRENGTHS AT ELEVATED TEMPERATURE
75S-T6 ALUMINUM ALLOY

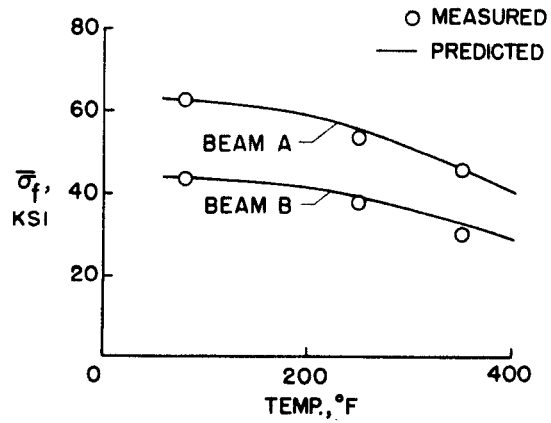

Figure 14

4. SOME STRUCTURAL EFFECTS OF AERODYNAMIC HEATING

By R. R. Heldenfels, E. E. Mathauser, and W. A. Brooks
Langley Aeronautical Laboratory

INTRODUCTION

The structural effects of aerodynamic heating have become the subject of much research in recent years because they limit flight speeds attainable in the atmosphere. Many papers have been written about these effects (refs. 1 to 3, e.g.), but some aspects of the resulting structural problems are still only vaguely understood or as yet uninvestigated. This paper will review some of these effects that may be significant in the design of man-carrying aircraft that fly at moderate supersonic speeds. The effects discussed will be illustrated by examples taken from NACA research, both published and unpublished.

TEMPERATURES ENCOUNTERED IN FLIGHT

Before discussing the structural problems, the temperatures experienced by supersonic aircraft will be considered. The magnitude of the maximum temperatures encountered is shown in figure 1, which is the familiar plot of adiabatic wall temperature against Mach number for an altitude of 40,000 feet. The adiabatic wall temperature is the equilibrium temperature attained at the surface of an aircraft structure during sustained flight. It can be seen that the temperatures are beyond human endurance at $M = 2$ and that the failure of common aircraft materials becomes a problem. At higher speeds, structural materials lose strength, and sustained flight for even pilotless aircraft is impossible without substantial cooling.

The structure does not attain these temperatures instantaneously because of the heat capacity of the structure and the time required for heat to be transferred from the boundary layer to the structure. This temperature lag is very beneficial, since short flights are possible at high Mach numbers without excessively high temperatures. The times involved depend on the flight path and the configuration of the structure. An example of the temperature history of a representative aircraft structure is given in figure 2. The Mach number and two structural temperatures are plotted against time in minutes for a short flight at 40,000 feet altitude. The airplane, initially cruising at Mach number 0.75, accelerates at 1 g to Mach number 3.0 and then flies steadily at this speed. The structure considered is one of the skin and web combinations that forms a multiweb beam. The temperature is shown for a point on the skin and for a point on the center line of the web. The variation of adiabatic wall temperature with time is also included. The curves show that considerable time is required for the skin to stabilize at T_{AW} and that the interior temperature lags the skin temperature.

The maximum temperature difference occurs at about 1.2 minutes. The temperature distribution at this time is shown in figure 3, which presents details of the structural component, the temperature distribution along the surface, and the temperature variation down to the center line of the web. The rapid heating experienced by this structure has resulted in temperature differences that will induce thermal stresses. The nature of these thermal stresses is considered in more detail later.

STRUCTURAL EFFECTS

The times and temperatures associated with aerodynamic heating of structures can be used to classify some of the more important structural effects. In the following table, these effects are divided into two groups, those resulting from uniform elevated temperatures and those resulting from nonuniform temperature distributions produced by changing flight conditions:

	Structural effects
Uniform elevated temperature	Loss of strength and stiffness Creep
Nonuniform temperature distribution	Thermal stresses Reduced stiffness Buckling

Uniform elevated temperature implies flight under stabilized conditions with a general deterioration of material properties that leads to loss of strength and stiffness and to creep. When a structure creeps, continual deformation occurs under load, and failure results at a load level less than the load that can be supported in a short-time test. When a nonuniform temperature distribution exists in the structure, thermal expansion will have a similar variation that will induce thermal stresses. These thermal stresses may have an adverse effect on the strength and deformation of the structure. One of the more complex phenomena associated with them is a reduction in effective stiffness produced by small thermal stresses - this is different from changes in stiffness that result from a reduction in the elastic modulus. Thermal stresses may also become large enough to produce buckling. Buckling and reduced stiffness of an aircraft structure may be very important, because they could lead to serious aeroelastic problems, such as flutter, that otherwise might not occur.

The general nature of the effects listed is the same regardless of temperature level or Mach number, but the magnitude and relative importance of these effects will vary with the flight conditions. Insulating

or cooling the structure can greatly alleviate these problems by reducing both the temperature level and temperature differences. Likewise, better materials could greatly reduce or eliminate these problems which arise because materials expand and lose strength as temperature increases. The structural designer can also partially solve these problems by devising structures that are not susceptible to aerodynamic heating effects, particularly those arising from rapid heating. In the remainder of this paper the effects shown in the table will be discussed in greater detail. The structural effects of uniform elevated temperatures are considered first.

Uniform Elevated Temperature

Elevated temperatures produce changes in material properties, such as loss of ultimate tensile strength as shown in figure 4. Ultimate tensile stress of 24S-T3 aluminum alloy is plotted against temperature for preheating times, that is, time exposed to temperature before loading, ranging from 1/2 to 1000 hours (ref. 4). A large decrease in the ultimate tensile stress can be noted for temperatures above 300° F and for increased preheating times. A small increase in strength occurs for long preheating times at about 300° F because of artificial aging. The stiffness of the material, as given by the elastic modulus, also shows a reduction with temperature, but preheating time has no significant effect. The elevated-temperature properties of structural materials and the most efficient materials for various structural applications are discussed in paper number 5.

Information of the type shown here can be used directly in the design of tensile members such as the tension cover plate of a box beam; however, determination of the elevated-temperature strength of compression members is more complex, because both material and structural properties must be considered. Previous investigations have shown that, if the behavior of compressive members is known at room temperature, the behavior of these members at elevated temperature can be predicted satisfactorily by substituting the elevated-temperature stress-strain curve for the root-temperature curve (ref. 5). Methods for predicting the compressive strength of wing structures are discussed in the preceding paper.

The techniques obtained from such studies were applied in an investigation of the static strength and creep behavior of box beams at elevated temperatures (ref. 6). Details of the aluminum-alloy multiweb box beams used in this investigation are shown in figure 5. The beams were 96 inches long supported at the center and loaded at the tips. Each beam had five webs and was tapered in depth as shown.

Static strength. - Results obtained from the static strength investigation are shown in figure 6. The strength of the tension and compression cover plates of the box beam is plotted against temperature for preheating times of 1/2 and 2 hours. The tensile strength of the cover plate was obtained from the material data shown in figure 4. The compressive strength was determined from material stress-strain curves and the given cross-sectional geometry; this strength corresponds approximately to the compressive yield stress of the material. These curves indicate that the tension cover is stronger at all temperatures for 1/2-hour preheating time, and consequently compressive failure of the beams is expected. For 2-hour preheating, the tension cover is stronger up to approximately 375° F. Above this temperature, the strength of the cover plates is approximately equal. Thus, for this preheating time, either type of beam failure may occur, depending on the temperature. A comparison between these predictions and limited test data is shown; the circles represent compressive failure of the beams and the square indicates tensile failure. These test results are in agreement with the predictions.

Creep. - The results of three creep tests on the multiweb beams are shown in figure 7. Tip deflections determined experimentally are plotted against time. The test temperatures, the maximum bending stresses, and the applied load expressed as a percentage of the load that would produce immediate failure of the box beam at the test temperature are indicated. The percentages with the 425° F tests are based on the same short-time load; that with the 375° test is based on a slightly higher value. At 425° F, the beams failed in relatively few hours when the applied loads were only 56 and 61 percent of the load required to produce immediate failure at this temperature. In addition, at the 425° F test temperature, a decrease of about 10 percent in the applied load increased the lifetime approximately 70 percent.

Tensile rupture failure occurred in two of the creep tests, but the beam tested at 425° F with 56 percent of the short-time load applied experienced a buckling failure. In this particular test, the beam was not held at 425° F continually but was cooled to room temperature and reheated to 425° F at the times indicated by the tick marks. The time at room temperature is not included on the plot.

Attempts were made to predict the type of failure in the creep tests; however, the results were not successful. The prediction of creep buckling of the compression cover plate requires a knowledge of the creep behavior of plates that is not available at present. When failure of the tension cover is assumed to occur, however, the time to failure can be predicted satisfactorily from material tensile creep data.

Figure 8 shows tensile rupture stress plotted against a time-temperature parameter (ref. 7). Data in this form are convenient for predicting failure time for the tension cover. In the time-temperature parameter, T_R is temperature in ^{o}R, t is rupture time in hours, and 17 is a material constant. The results of tensile creep tests ranging from 300° to 600° F define the master rupture curve. The box-beam creep test results are indicated by the larger symbols. The two large open symbols represent tensile failure of the beams, and compressive failure is denoted by the large solid symbol. In this particular case, compressive failure of the beam occurred in a shorter time than was predicted for tensile failure.

If it is assumed that the limited results shown for the box beams can be extended to a more general investigation of the effects of creep on the weight of an aircraft wing structure, results such as shown in figure 9 can be obtained. The increase in weight of a 24S-T3 aluminum-alloy multiweb beam, similar to those used in the test program, is plotted as a function of temperature. The solid lines indicate the weight of a beam designed to support a given load for 1/2, 10, and 1000 hours. The dashed lines indicate the weight of a beam that fails immediately at the given design load after preheating times of 1/2, 10, and 1000 hours.

In this example, which concerns a particular family of multiweb beams, preheating and creep increase the weight of the beam considerably, especially at the higher temperatures. The largest part of the weight increase results from loss of material strength caused by preheating before load is applied. For example, if the beam is preheated for 1000 hours at 400° F and is designed to have the same ultimate load after this preheating as at room temperature, the beam weight increases to 2.30 times the room-temperature weight. If the beam is designed for a creep lifetime of 1000 hours - that is, the beam is required to support the given load for 1000 hours while at 400° F - an additional weight increase of approximately 15 percent is required. Thus the severest case for the beam, that is, supporting the given load continually while at temperature, requires only a 15-percent weight increase over that required for the preheating case. Since airplanes are expected to encounter design loads only a small percentage of actual flying time, it appears that for aluminum-alloy structures at elevated temperatures, the major portion of the increased weight will result from loss of material strength with exposure; an additional but less significant weight increase will result from material creep.

Nonuniform Temperature Distribution

Primary thermal stresses. - Turning now to problems associated with rapid heating, consider first the nature of thermal stresses. As previously mentioned, thermal stresses are developed, in general, when the

thermal expansion of a body is not uniform. These thermal stresses can be determined from the equations of elasticity, provided the stress-strain relations are modified to include thermal expansion. The established techniques of the theory of elasticity provide considerable insight to the nature of thermal stresses in simple bodies, but for actual structures the application of these techniques is often difficult and impractical. However, a simpler approach (ref. 8) can be used to solve thermal stress problems if one accepts the usual limitations of beam theory; that is, secondary stresses are unimportant.

The elementary theory that plane sections remain plane yields the following equations:

Load stress:

$$\sigma_L = E\left(\frac{P}{EA} + \frac{M_x}{EI_x}\,y + \frac{M_y}{EI_y}\,x\right) \tag{1}$$

Thermal stress:

$$\sigma_T = -E\alpha T + E\left[\frac{\int_A (E\alpha T)\,dA}{EA} + \frac{\int_A (E\alpha Ty)\,dA}{EI_x}\,y + \frac{\int_A (E\alpha Tx)\,dA}{EI_y}\,x\right] \tag{2}$$

where

$$\left.\begin{aligned} EA &= \int_A d(EA) \\ EI_x &= \int_A y^2\,d(EA) \\ EI_y &= \int_A x^2\,d(EA) \end{aligned}\right\} \tag{3}$$

Equation (1) is the familiar stress equation resulting from applied moments and axial load. Equation (2) is an analogous form for thermal stresses in a shell-type structure. The first term in equation (2) is the stress that results from complete restraint of thermal expansion. The terms within the brackets provide the stress relief that occurs when the expansion is only partially restrained, as is the case when thermal stresses arise from unequal expansion of parts of a free body. The first term inside the brackets is analogous to P/EA and is the relaxation required to satisfy thrust equilibrium. The last two terms are analogous to Mc/EI and ensure moment equilibrium for unsymmetrical temperature distributions. If the distribution of $E\alpha T$ over the area is uniform or linear, the terms within the brackets add up to αT, with the result that the thermal stress is zero.

If the temperature distribution is nonuniform and the temperatures are sufficiently high, the modulus of elasticity will vary across the area and will differ from the room-temperature value. By defining EA and the EI's as shown in equation (3), the effects of the variable modulus of elasticity, whether resulting from temperature variation or the use of different materials, are included in the stress analysis.

If these equations are applied to a simple beam with the cross section and temperature distribution shown in figure 3, the results shown in figure 10 are obtained. Two stress distributions are shown for a representative portion of the section, the stress being plotted against distance measured along the upper skin to the web, down through the web to the lower skin, and then along the lower skin. The load stresses produced by a bending moment are indicated by the dashed curve. As usual in a wing structure, there are compression stresses in the upper skin and tension in the lower skin. The solid curve represents the thermal stresses produced by the temperature distribution of figure 3. The thermal stresses produce some compression in both skins and tension in the web. It is evident that when the load and thermal stress are superimposed, the stress condition in the compression skin is aggravated, whereas that in the tension skin is alleviated.

The fact that thermal stresses aggravate the stress condition on some portions of the beam is a serious design problem. Design ingenuity can be used, however, to reduce the thermal stresses and alleviate the problem. For example, the area ratio of the skin and web can be changed, the coefficients of thermal expansion may be favorably altered by using different materials for skin and web, or the mutual restraint existing between the skin and the web may be reduced. Of these approaches, changing the degree of restraint between the skin and the web seems to offer the best remedy for general use. If the web were designed to provide very little restraint to the thermal expansion of the skin, while continuing to perform its function of preventing premature skin buckling, the thermal stresses would be negligible.

Figure 10 also shows that the thermal stresses and the load stresses are dissimilar in distribution, a fact that must be considered in a stress analysis based on a simplified idealized representation of the structure. For the load-stress problem, the maximum stress occurs in the skin and is uniform over the skin. In the thermal-stress problem the stress varies over the skin, and substantial stresses occur in the web; in fact, in this example the maximum thermal stresses are in the web.

Secondary thermal stresses. - The preceding discussion has been concerned with the primary thermal stresses. Secondary thermal stresses arise from stress diffusion in the vicinity of discontinuities in the structure or spanwise temperature distribution. Stress diffusion results from shear deformation of the structure combined with boundary

conditions that are not consistent with elementary theory. Although basically similar, the stress diffusion problems of load and thermal stresses differ in detail because of differences in the elementary stress distribution. In addition, the free end of a beam subjected to thermal stresses presents a thermal-stress diffusion problem not usually present in the load case, although it is basically similar to the cut-out problem.

The diffusion of thermal stresses near a free end can be demonstrated by a stress analysis of the simple structural element shown in figure 11. The rectangular flat plate subjected to a tent-like temperature distribution is a simplified structure susceptible to analysis and has practical significance because it resembles the skin panel between adjacent webs of a multiweb beam. The temperature difference ΔT induces the thermal stresses; the edge temperature exists uniformly over the plate and thus produces no thermal stress. The total temperatures involved in this example are at a low level, and thus any changes in material properties from those at room temperature may be neglected. Because of the symmetry of the temperature distribution, only the shaded quadrant need be considered in the stress analysis.

Figure 12 shows the three types of thermal stress produced in the midplane of the plate by the temperature distribution of figure 11. The distributions of the longitudinal direct stress σ_x, the transverse direct stress σ_y, and the shear stress τ_{xy} are shown, each stress distribution consisting of a transverse and longitudinal plot of the particular stress along the line where the maximum values occur. Along the transverse center line, the longitudinal direct stress σ_x has its maximum values and is approximated by elementary theory. However, the transverse edges of the plate are stress-free, and σ_x decays to zero at the transverse edges. Both the transverse direct stress σ_y and the shear stress τ_{xy} result from the condition that σ_x must be zero at the transverse ends of the plate. These stresses were calculated by the energy method and were published along with some experimental measurements that agree well with calculated values (ref. 9). Substantial compression stresses, both transverse and longitudinal, exist at the center of the plate, and it could be expected to buckle as a result of these stresses. In fact, the stresses shown are the theoretical thermal buckling stresses for this plate when it is simply supported at the edges.

Buckling. - The buckling of the plate was investigated both theoretically and experimentally (ref. 10) with the results shown in figure 13. The temperature difference ΔT is plotted against w_a, the center deflection that exists in addition to the initial center deflection w_i. The critical temperature difference, determined by small deflection

theory, and the growth of center deflection, given by large deflection theory, are shown by the upper curve for a perfectly flat plate. The lower curve is given by large deflection theory for a plate with initial curvature similar to the buckling mode and with an initial center deflection equal to 18 percent of the plate thickness. Some experimental measurements for such a plate are also shown. It is evident that, as far as buckling is concerned, the behavior of the plate under thermal stress is very similar to its behavior under an applied compressive load, with one exception not shown; that is, thermal buckling is independent of the modulus of elasticity.

At the critical temperature difference, calculated by small deflection theory for the flat plate, the deflection of the initially curved plate is relatively small and approximately equal to the plate thickness. Thus, the small-deflection-theory critical temperature difference, although somewhat unconservative, is a good approximation to the thermal buckling of the initially curved plate.

Reduced stiffness. - Some objectionable results of buckling are the deformation of aerodynamic surfaces and reduction of stiffness. However, the reduction of stiffness is not confined to the buckling or post-buckling region. Loads well below the buckling load will also cause reductions in stiffness that may be indicated by changes in the natural frequencies of vibration and increased deflections under load.

Figure 14 illustrates reduction of stiffness due to thermal stresses. On the left, center deflection produced by a lateral pressure load is plotted as a function of the temperature difference, or thermal stress, in the simply supported plate. As the temperature difference increases, the deflection increases without change in the load. When the temperature difference approaches its critical value, the center deflection of the plate theoretically becomes infinite, which is equivalent to zero stiffness. A similar effect on frequency change is shown on the right, where the frequency of the first two symmetrical modes is plotted as a function of temperature difference. A very substantial decrease in the frequency of the first symmetrical mode, which is similar to the buckling mode, is evident. The second mode does not show as large a percentage decrease in the temperature range considered. The results shown were obtained from small deflection theory and thus are in error near the points of theoretical zero stiffness; elsewhere the results should be valid. Again it should be emphasized that the effects shown in this figure do not result from changes in material properties; they result from the stresses in the midplane of the plate. Any midplane stress, whether load or thermal, would produce similar results; but the net effect on the structure would differ because of basic differences in the distribution of load and thermal stresses.

CONCLUDING REMARKS

Some of the structural effects of aerodynamic heating have been described and illustrated with examples from NACA research. The effects considered may be significant factors in the design of supersonic aircraft, but considerable research is needed to determine their exact nature and magnitude.

REFERENCES

1. Hoff, N. J.: Structural Problems of Future Aircraft. Proc. Third Anglo-American Aero. Conf., Brighton (England), 1951, The Roy. Aero. Soc., pp. 77-114.

2. Loveless, E., and Boswell, A. C.: The Problem of Thermal Stresses in Aircraft Structures. Aircraft Eng., vol. XXVI, no. 302, Apr. 1954, pp. 122-124.

3. Hibbard, Hall L., and McBrearty, J. F.: Structures for High Speed Aircraft. Aviation Age, vol. 20, no. 5, Nov. 1953, pp. 32-51; and vol. 20, no. 6, Dec. 1953, pp. 116-123.

4. Doerr, Dale D.: Compressive, Bearing, and Shear Properties of Several Non-Ferrous Structural Sheet Materials (Aluminum and Magnesium Alloys and Titanium) at Elevated Temperatures. Proc. A.S.T.M., vol. 52, 1952, pp. 1054-1078.

5. Mathauser, Eldon E., and Libove, Charles: Preliminary Investigations of Strength Characteristics of Structural Elements at Elevated Temperatures. NACA RM L53E04a, 1953.

6. Mathauser, Eldon E.: Investigation of Static Strength and Creep Behavior of an Aluminum-Alloy Multiweb Box Beam at Elevated Temperatures. NACA TN 3310, 1954.

7. Larson, F. R., and Miller, James: A Time-Temperature Relationship for Rupture and Creep Stresses. Trans. A.S.M.E., vol. 74, no. 5, July 1952, pp. 765-771.

8. Heldenfels, Richard R.: The Effect of Nonuniform Temperature Distributions on the Stresses and Distortions of Stiffened-Shell Structures. NACA TN 2240, 1950.

9. Heldenfels, Richard R., and Roberts, William M.: Experimental and Theoretical Determination of Thermal Stresses in a Flat Plate. NACA TN 2769, 1952.

10. Gossard, Myron L., Seide, Paul, and Roberts, William M.: Thermal Buckling of Plates. NACA TN 2771, 1952.

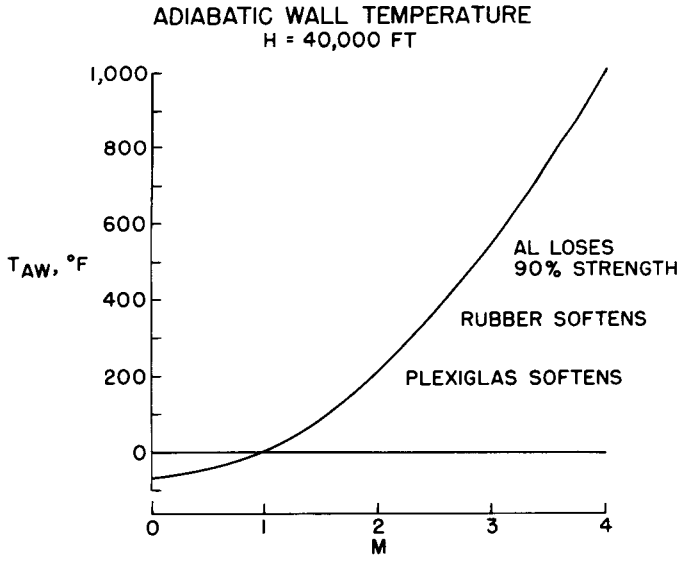

Figure 1

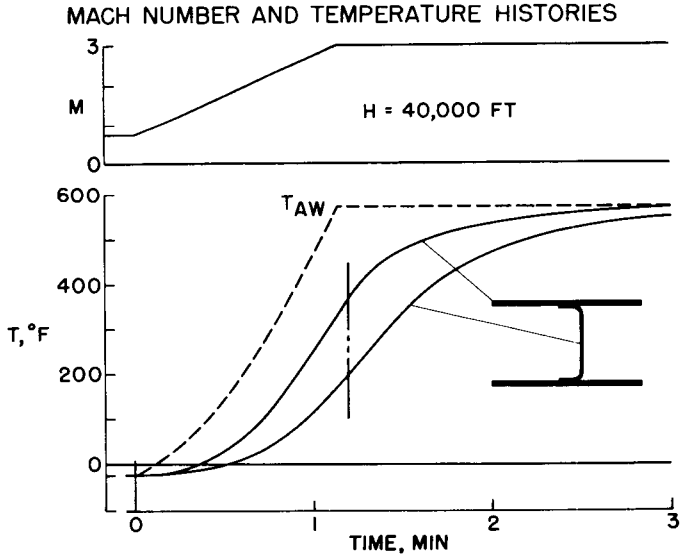

Figure 2

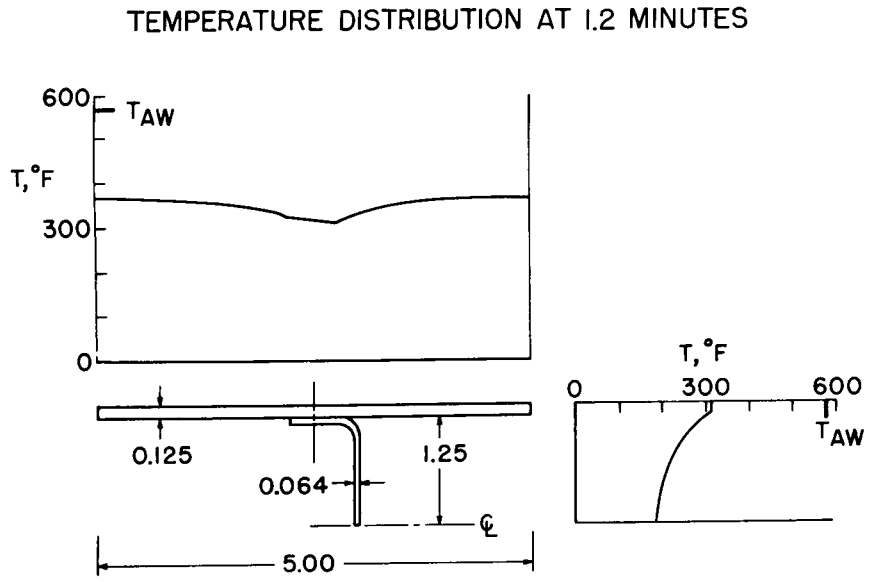

Figure 3

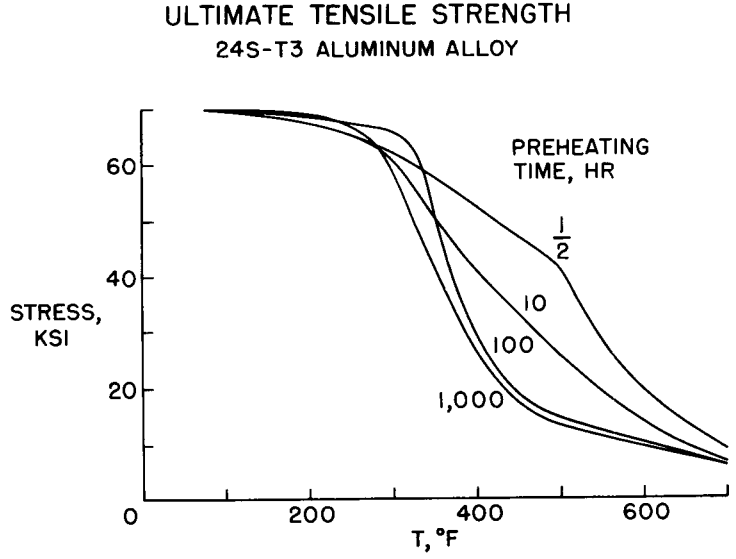

Figure 4

MULTIWEB-BOX-BEAM DIMENSIONS

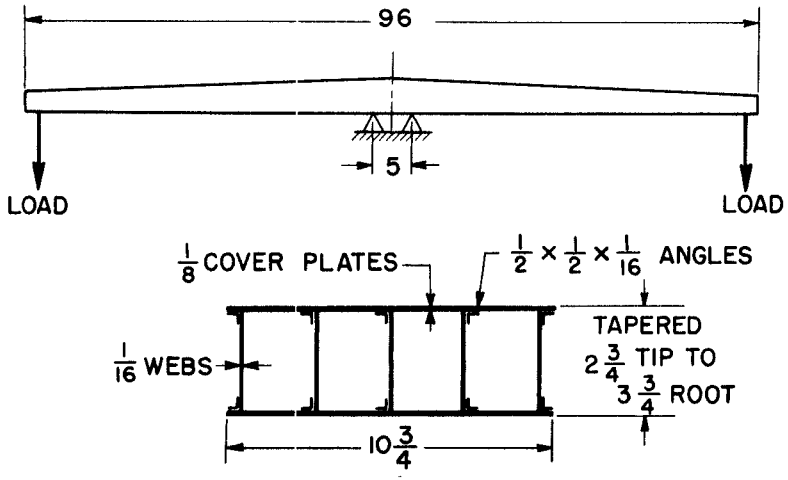

Figure 5

FAILURE STRESSES FOR MULTIWEB BOX BEAM

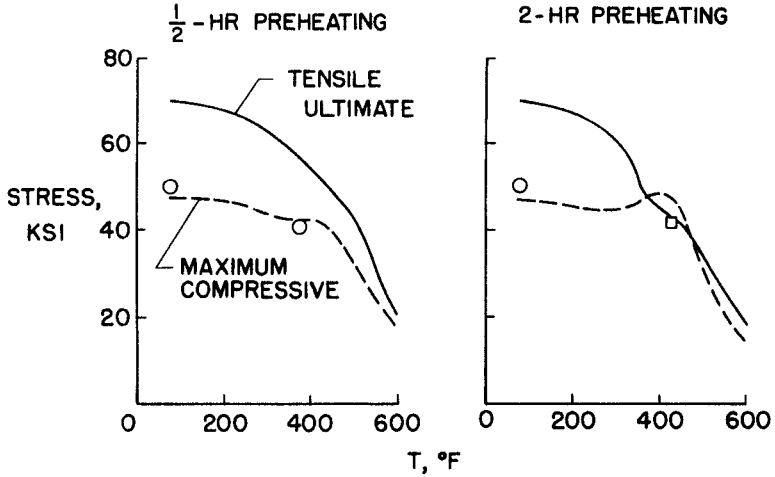

Figure 6

CREEP DEFLECTIONS OF MULTIWEB BOX BEAMS

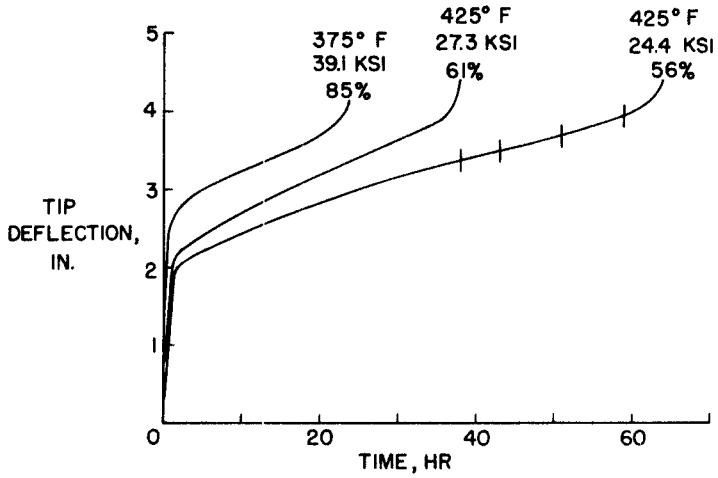

Figure 7

MASTER CREEP RUPTURE CURVE
24S-T3 ALUMINUM ALLOY

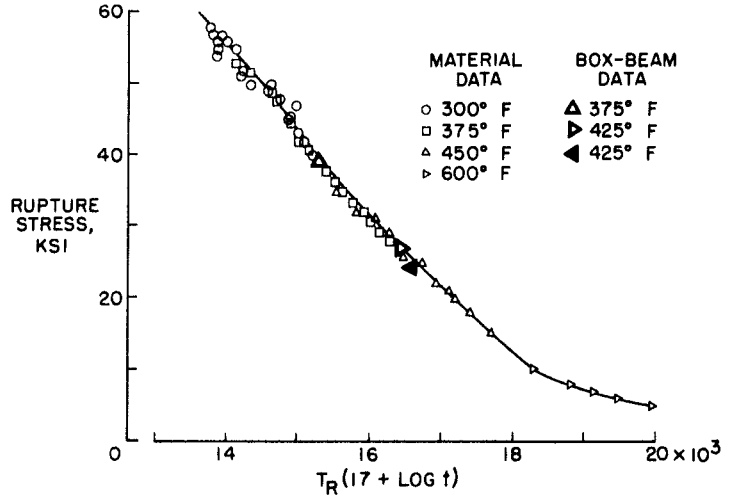

Figure 8

WEIGHT OF MULTIWEB BOX BEAMS FOR EQUAL LOADS

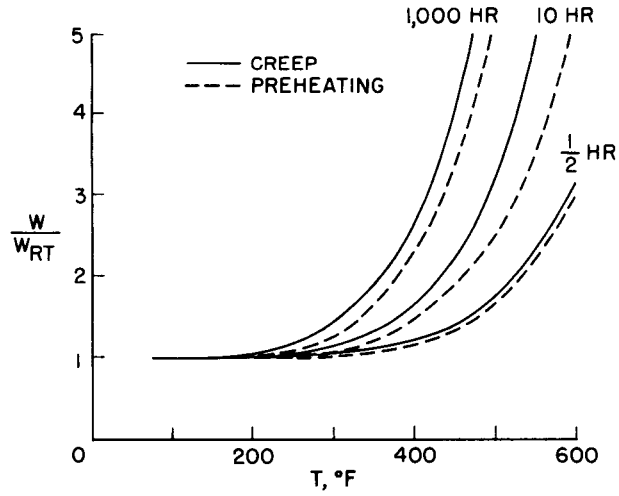

Figure 9

STRESS IN BEAM SECTION

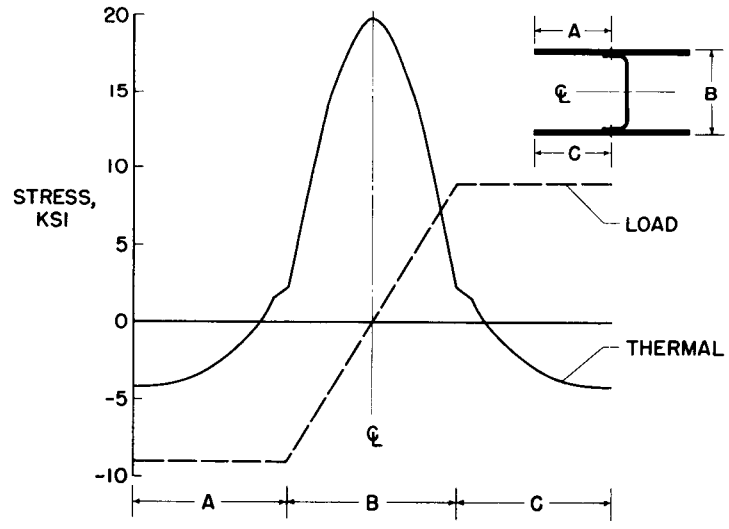

Figure 10

TEMPERATURE DISTRIBUTION ON PLATE
75S-T6 ALUMINUM ALLOY

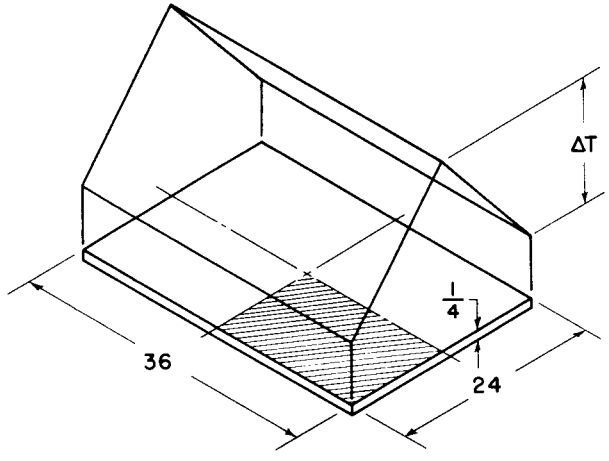

Figure 11

THERMAL-STRESS DISTRIBUTION IN PLATE

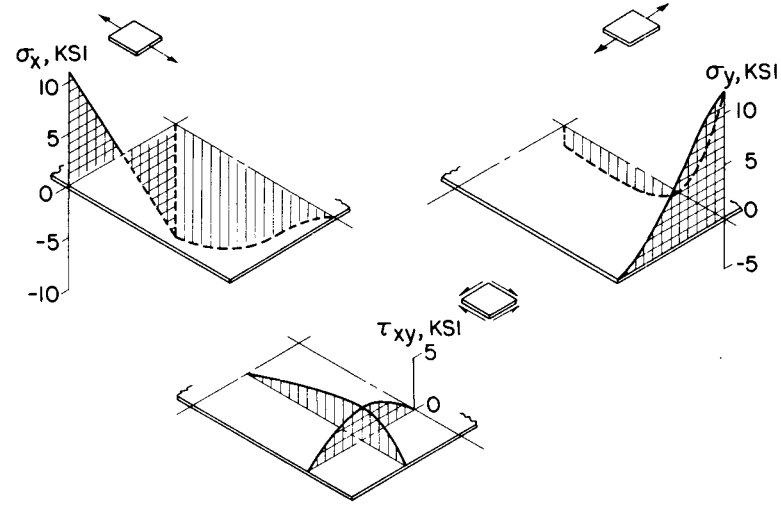

Figure 12

THERMAL BUCKLING OF A SIMPLY SUPPORTED PLATE

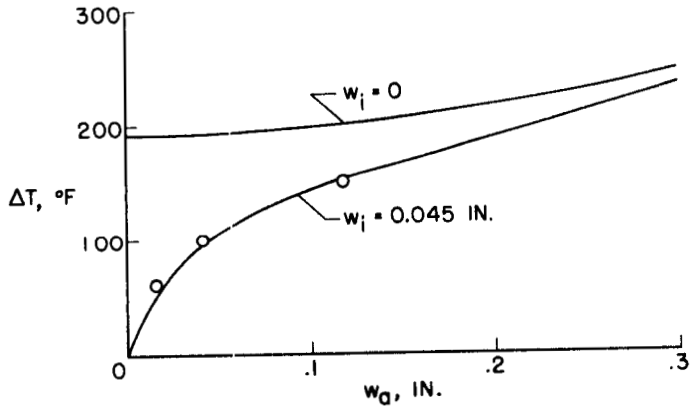

Figure 13

EFFECT OF THERMAL STRESS ON DEFLECTION AND FREQUENCY

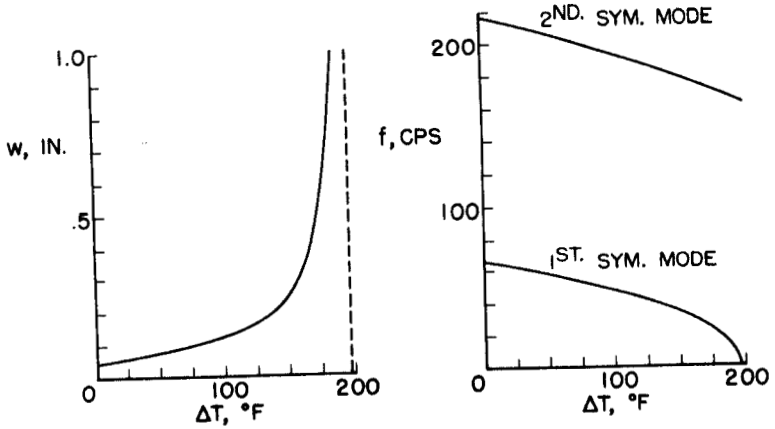

Figure 14

5. SOME CONSIDERATIONS ON AIRCRAFT STRUCTURAL MATERIALS FOR HIGH-SPEED FLIGHT

By George J. Heimerl
Langley Aeronautical Laboratory

Until recently, there has been no immediate need for concern as to the effects of elevated temperatures on the properties of aircraft structural materials except in regions close to power-plant systems. Supersonic speeds of Mach 2 to 2.5 have now been achieved, however, and boundary-layer temperatures have risen as much as 450° F. As speeds increase still further, the effects of elevated temperatures on the properties of structural materials will constitute one of the major obstacles to very high-speed flight.

Some of the material properties requiring consideration under elevated-temperature conditions are as follows:

Properties of materials	
Mechanical	Strength Stiffness Creep
Physical	Thermal Corrosion Weight

This paper is concerned chiefly with the effects of elevated temperatures on the mechanical properties of strength, stiffness, and creep; and, except for the weight, the physical properties will not be taken into account, although they also play an important part in material and structural behavior at elevated temperatures.

The chief effect of elevated temperatures on materials is to alter their properties. Ordinarily, the strength and stiffness are reduced, the extent depending upon the material, the exposure time, and the temperature. The strength problem will be difficult to cope with because of the varied temperature and exposure conditions which will be the rule rather than the exception under actual flight conditions. Stiffness is an important consideration in the design of high-speed aircraft because of the greater possibility of flutter, divergence, or excessive distortion. Although the stiffness is reduced by elevated temperatures, it fortunately is independent of time effects as long as the material remains elastic.

At elevated temperatures, materials tend to creep or strain while under load. This time-dependent strain may require consideration, as permanent set, excessive distortions, and even rupture may occur under tensile loading. Creep buckling of structural elements loaded in compression may also take place. As high-speed flight will be maintained only for relatively short periods of time, short-time creep behavior will have to be taken into account. Cumulative effects over longer periods, however, will also need to be considered. Some of these effects are covered in paper 4 on "Structural Aspects of Aerodynamic Heating."

Many materials that are satisfactory for use at normal temperatures may corrode or oxidize badly at elevated temperatures. Materials may require special surface protection or treatment if they are to be serviceable under such conditions. At elevated temperatures, the weight of the aircraft structure is as primary a consideration as at normal temperatures. Consequently, the weight as well as the strength of the materials must be taken into account for the different structural applications.

Three examples illustrating the effect of temperature and time on the properties of materials will now be given. The first of these shows the effect on the tensile yield stress for a high-strength aluminum alloy 75S-T6 (fig. 1). The solid curves are obtained from stress-strain tests under constant temperature and strain rate conditions for various exposure times. At 400° F, the yield stress for 1/2-hour exposure is about half that at normal temperatures. Longer exposure times reduce the stress still further. The dashed curve is obtained from tests in which the material is kept under constant load while it is heated at 100° F per second until yield and failure occur. In this case, a considerable increase in yield stress is found over that obtained from tests at constant temperatures for 1/2-hour exposure. Consequently, temperature, time, and heating rate may all be important factors.

An example of the possible magnitude of the creep obtained for short times under load is shown in figure 2 (ref. 1) by design curves for the same aluminum alloy at 500° F. These results were obtained from short-time creep tests in which the material was first loaded and then heated at 70° F per second to the test temperature. The curves show the stress required to produce different amounts of total strain in various times. A 1-percent total strain occurs in only 1 minute for a stress of about 22 ksi. Although these curves do not show the permanent creep strain, a 0.2-percent permanent strain occurs in about 20 minutes at 15 ksi at this temperature. Even though this example is an extreme one, as 500° F is considerably above the working range for this material, it affords an illustration of what can occur in the creep of materials.

The last example shows the effect of varying the rate of straining on the strength of a material. This effect is unimportant at normal temperatures for the structural aluminum alloys, but may be pronounced for other materials, particularly at elevated temperatures. Figure 3 shows the increase in average stress with strain rate obtained for an annealed 7 percent manganese titanium-base alloy at normal temperatures and at 800° F (ref. 2). This stress is a measure of the average height of the stress-strain curve and is somewhat greater, in general, than the conventional yield stress. Strain rates usually employed in tests of materials are on the order of 10^{-2} to 10^{-3} per minute. Strain rates of 10^{4} per minute are obtained under impact conditions. An appreciable increase in stress with strain rate is obtained for this material especially at 800° F. This effect appears to be quite general at elevated temperatures for many materials and may alter the strength considerably from that established by conventional or standard tests.

With few exceptions, current practice has been to employ high-strength aluminum alloys for the bulk of the aircraft structure. Although these materials have made possible the construction of light-weight efficient structures, their use in supersonic aircraft will be limited because of the adverse effects of elevated temperatures on their properties. As their use for structural purposes will be generally inadvisable if temperatures should go above 300° to 400° F at the most, other more temperature-resistant materials are required for the next higher range. The need for temperature-resistant substitute materials that can provide light-weight structures is apparent. The remainder of this paper shows what can be expected with some currently available structural materials under constant temperature conditions up to about 1000° F, taking into account strength, stiffness, and weight for a number of structural applications.

The materials selected for this purpose include a high-strength aluminum alloy that serves as an efficiency yardstick, a titanium alloy, an ultra-high-strength steel, and a high-temperature nickel-base alloy. The titanium alloys, like the aluminum alloys, are characteristically light-weight, high-strength materials, which show promise of meeting aircraft structural requirements up to about 800° F. The ultra-high-strength steel, although heavier than the other materials, has been utilized at normal temperatures at very high strength levels and under such circumstances can compete with the lighter materials. The high-temperature alloy is included for comparative purposes.

As no single criterion or basis can be found for making such comparisons for all the various possible structural applications, some of the principal cases will be covered. These include the tensile yield strength, stiffness, and the buckling of columns and plates under compression loading. The comparisons are based upon the use of tensile and compressive stress-strain data obtained under constant-temperature and strain-rate conditions for 1/2-hour exposure time.

Creep is assumed not to be a factor. The properties of the ultra-high-strength steel at elevated temperatures were assumed and taken to be the same at 800° F as the same material heat-treated to high- instead of ultra-high-strength levels. The tensile properties of the aluminum alloy at elevated temperatures were assumed to be the same as the compressive properties for which data were available. Except for the tensile properties for the titanium alloy and the ultra-high-strength steel at normal temperatures, the results are based on data for sheet materials. Data were taken from various sources (refs. 3 to 5).

Values of the tensile yield stress, Young's modulus, and the density for the various materials are given in the following table:

Material	Tensile yield stress, ksi	Young's modulus, psi	Density, lb/cu in.
78S-T6	82	10.5×10^6	0.10
RC-130-A	138	16.0	.17
SAE 4340	242	29.5	.28
Inconel X	110	32.0	.30

The aluminum alloy 78S-T6 is one of the newest and strongest of the aluminum alloys. The titanium alloy RC-130-A is an 8 percent manganese titanium-base alloy. SAE 4340 is a low-alloy, nickel-chromium-molybdenum steel that has been heat-treated to ultra-high-strength levels, 280 ksi tensile ultimate stress in this case. Inconel X is a 70 percent nickel, 15 percent chromium alloy that has high strength up to about 1500° F. These materials cover a wide range of properties. Tensile yield stresses vary from 82 to 242 ksi, moduli run from 10.5 to 32×10^6 psi, and densities vary from 0.10 to 0.30 pound per cubic inch.

The strength efficiency of the various materials at elevated temperatures is shown in figure 4. The tensile yield stress is taken as the criterion for strength, and the efficiency is measured by the yield stress-density ratio. Except for Inconel X, these materials all have about the same efficiency at normal temperatures. The efficiency of the steel is somewhat greater than that for the titanium alloy at elevated temperatures. Inconel X is the most efficient material above about 850° F, but it has a relatively low efficiency at normal temperatures. Temperatures up to 1200° F have very little effect on this material, whereas the efficiency of the aluminum alloy drops off rapidly with temperature.

The elastic stiffness efficiency of the various materials at elevated temperatures is shown in figure 5. The stiffness is given by Young's modulus, and the efficiency is determined from the modulus-density ratio. The moduli used for this purpose are those obtained from compression loading, which run slightly higher than for tensile loading. The efficiencies of the materials are all about the same at normal temperatures. At elevated temperatures, Inconel X is the most efficient on a stiffness basis, and the steel and titanium alloy are next in order. The efficiency of the aluminum alloy drops off the most rapidly with temperature.

Compression loading dictates a considerable portion of the aircraft design. Unfortunately, simple comparisons of materials such as those just given are not possible for compression loading, because failure may occur by buckling, and both the properties of the material and the structural characteristics are involved. Comparisons of the various materials will next be given for columns and plates loaded in compression, using the structural index method (ref. 6). For column buckling, the tangent modulus formula was utilized. For the plate compressive strength, the relation for the average stress at failure for simply supported plates, which was shown earlier in the program to hold for many materials, is used. This relation is

$$\sigma_f = 1.60 \, (E_{sec} \, \sigma_{cy})^{1/2} \, \frac{t}{b}$$

where σ_f is the average stress at failure; E_{sec} is the secant modulus associated with σ_f; σ_{cy} is the 0.2-percent offset compressive yield stress; and t and b are the plate thickness and width, respectively. Both the column and plate formulas are assumed to be valid at elevated temperatures, because such relations have been shown to apply at elevated as well as at normal temperatures under comparable conditions (refs. 7 and 8). The compressive stress-strain curves are required for these calculations. Only the detailed comparisons at normal temperatures will be given.

The efficiency of the various materials for column buckling at normal temperatures is shown in figure 6. The structural index $P_{cr}cf/L^2$ comprises the buckling load P_{cr}, the end fixity c. the shape factor f, and the column length L. The efficiency is given by the stress-density ratio, where the stress is the buckling stress associated with P_{cr}. The relative efficiencies of the materials vary with the value of the index. Small index values correspond to small loads, low stresses, and long columns. In this region, the most efficient materials are, in order: the aluminum alloy, the titanium alloy, and then the steel and high-temperature alloy. For large index values, which correspond to large loads, high stresses, and short columns, the ultra-high-strength steel is now slightly more efficient than either the aluminum or titanium alloy. Inconel X is comparatively inefficient for use in columns under both low and heavy loading conditions.

Similar comparisons of the various materials on the basis of plate compressive strength are given in figure 7. The structural index P/b^2 includes the load P at failure and the plate width b. The efficiency is measured by the stress-density ratio, where the stress is the average stress at failure which corresponds to the load P. Small index values correspond to small loads, low stresses, and wide plates; and large values, to large loads, high stresses, and narrow plates. The relative efficiencies of the materials remain about the same for the plate compressive strength over a wide range of index values. The aluminum alloy is the most efficient, and the titanium alloy, steel, and nickel-base alloy follow in that order. If very high loadings and stresses are involved, however, materials such as the ultra-high-strength steel can give efficiencies about as high as those obtained with the lighter materials, which level off at the very high stresses.

The relative efficiency of the various materials at 80° and 800° F is summarized in figure 8. Comparisons are given at 800° F, because this is probably close to the upper limit of the working range for the titanium alloy and the ultra-high-strength steel. The various applications include tensile yield strength, elastic stiffness, column buckling, and the strength of compressed plates. The first pair of bar graphs represents in each case the aluminum alloy; the second, the titanium alloy; the third, the steel; and the last, the nickel-base alloy. The efficiency of the high-strength aluminum alloy at normal temperatures is taken as unity for each application and as a base for determining the relative efficiencies of the other materials at both 80° and 800° F. Comparisons for column buckling and plate compressive strength are given for high index values of 400 and 8 ksi, respectively. An examination of these results shows that at normal temperatures the titanium alloy is about as efficient or nearly as efficient as the aluminum alloy for the different applications. Further improvement in the titanium alloys may provide an appreciable increase in efficiency over the high-strength aluminum alloys for some of the applications. Ultra-high-strength steel can also provide high efficiencies at normal temperatures, except in the case of compressed plates, where the relative efficiency is about 3/4. For very high plate loadings, however, the steel may be almost as efficient even in this instance. At 800° F, the efficiencies of the titanium alloy and the steel are only about 1/2 to 3/4 of those obtainable at normal temperatures with the aluminum alloy. The efficiency of the titanium alloy at 800° F is about the same or slightly better than that for the steel at 800° F, except as regards stiffness. Inconel X is only 40 to 50 percent as efficient at 80° and 800° F as the aluminum alloy at normal temperatures, except in the case of stiffness.

In this talk, some of the properties of materials that require consideration under elevated temperature conditions were pointed out,

and a few examples were given of the effects of time and temperature. Some structural efficiency comparisons were then made for various applications, which showed that materials such as a titanium alloy and an ultra-high-strength steel could provide efficient structures at normal temperatures if high stresses were employed. The efficiency of these materials for such purposes, however, was substantially reduced for temperatures of 800° F and above. Consequently, the weight of the aircraft structure for very high-speed flight will increase substantially. In order to reduce this handicap in the temperature range up to 1000° F, improved elevated-temperature properties are needed for materials such as the titanium alloys and ultra-high-strength steels, which initially have very high strengths. At still higher temperatures the situation is less promising, as the high-temperature alloys that may be required under such conditions are generally relatively inefficient both at normal and elevated temperatures compared to present aircraft materials. In closing, it should be emphasized that the aircraft structural materials problem is greatly complicated by elevated temperatures, and that many of the mechanical and physical properties will have to be taken into account under varied conditions in the actual application.

REFERENCES

1. Van Echo, J. A., Page, L. C., Simmons, F., and Cross, H. C.: Short-Time Creep Properties of Structural Sheet Materials for Aircraft. Tech. Rep. No. 6731, Battelle Memorial Inst., Dec. 1951. (WADF Contract AF-33(038)-8743.)

2. Luster, D. R., Wentz, W. W., and Catlin, J. P.: Effect of Strain Rate on the Mechanical Properties of Titanium-Base Materials. WADC Tech. Rep. 53-71, Air Res. and Dev. Command, USAF, Wright-Patterson Air Force Base, Sept. 1953. (Materials Lab. Contract AF33(038)-21912, RDO No. 614-13.)

3. Hughes, Philip J., Inge, John E., and Prosser, Stenley B.: Tensile and Compressive Stress-Strain of Some High-Strength Sheet Alloys at Elevated Temperatures. NACA TN 3315.

4. Melcon, M. A.: Ultra High Strength Steel for Aircraft Structures. Product Eng., vol. 24, no. 10, Oct. 1953, pp. 129-141.

5. Heimerl, George J., and Hughes, Philip J.: Structural Efficiencies of Various Aluminum, Titanium, and Steel Alloys at Elevated Temperatures. NACA TN 2975, 1953.

6. Heimerl, George J., and Barrett, Paul F.: A Structural-Efficiency Evaluation of Titanium at Normal and Elevated Temperatures. NACA TN 2269, 1951.

7. Heimerl, George J., and Roberts, William M.: Determination of Plate Compressive Strength at Elevated Temperatures. NACA Rep. 960, 1950. (Supersedes NACA TN 1806.)

8. Mathauser, Eldon E., and Brooks, William A., Jr.: An Investigation of the Creep Lifetime of 75S-T6 Aluminum Alloy Columns. NACA TN 3204, 1954.

STRENGTH OF 75S-T6 ALUMINUM ALLOY AT ELEVATED TEMPERATURES

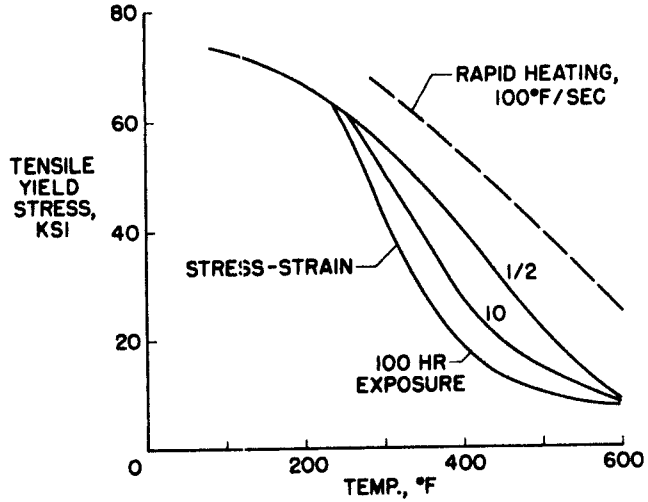

Figure 1

SHORT-TIME CREEP
75S-T6 ALUMINUM ALLOY AT 500°F

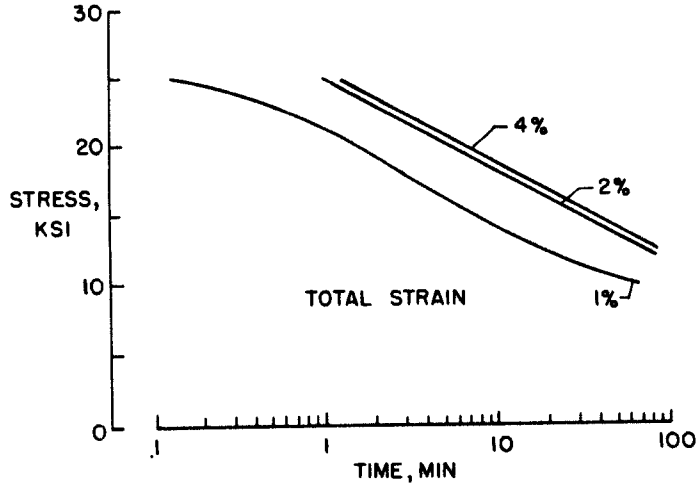

Figure 2

EFFECT OF STRAIN RATE
7% MN-TI ALLOY

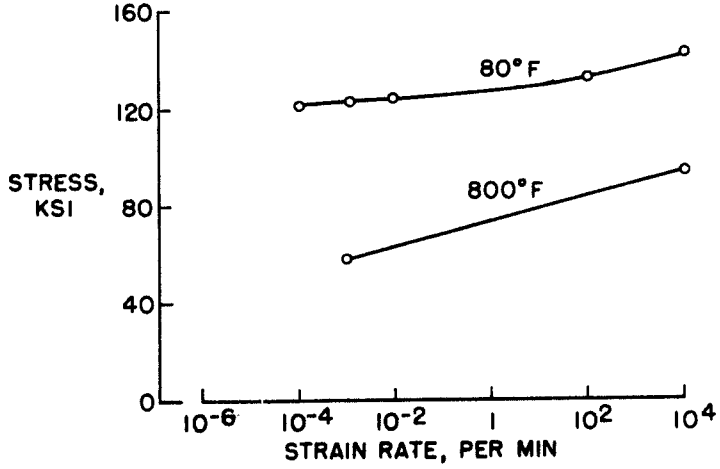

Figure 3

TENSILE-STRENGTH EFFICIENCY AT ELEVATED TEMPERATURES

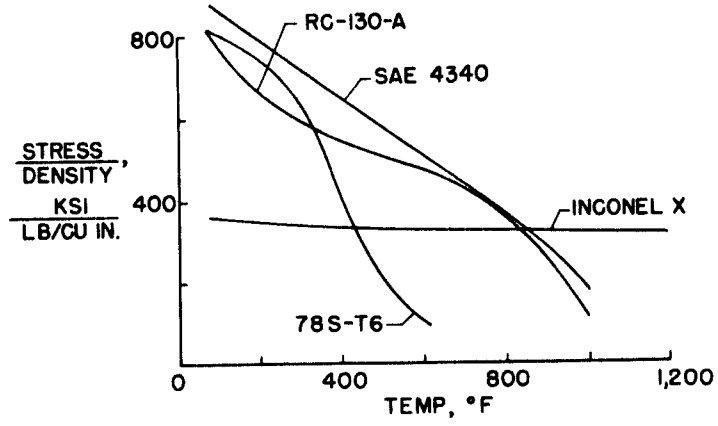

Figure 4

STIFFNESS EFFICIENCY AT ELEVATED TEMPERATURES

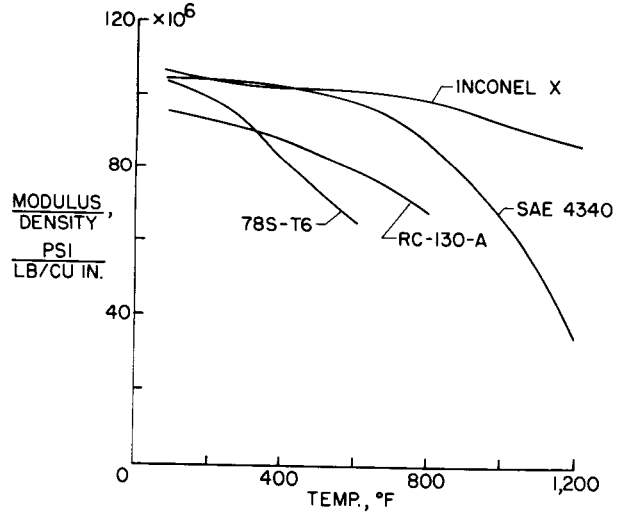

Figure 5

COLUMN-BUCKLING EFFICIENCY AT NORMAL TEMPERATURES

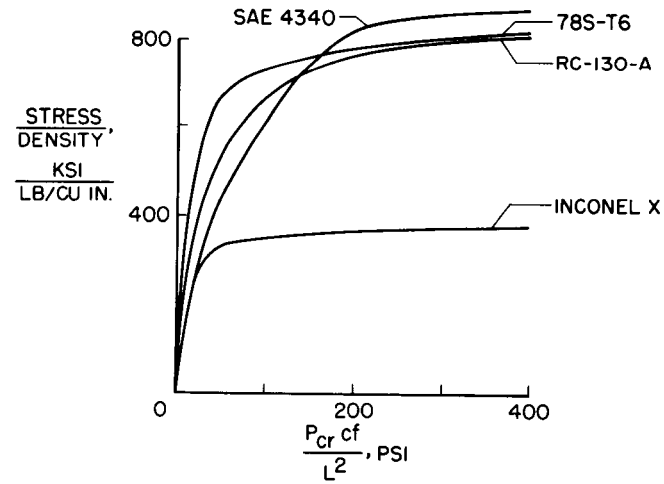

Figure 6

PLATE COMPRESSIVE-STRENGTH EFFICIENCY AT NORMAL TEMPERATURES

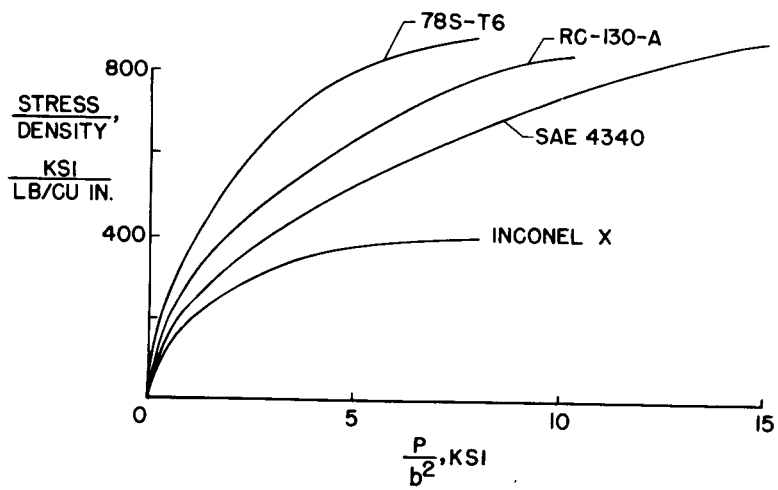

Figure 7

RELATIVE EFFICIENCY FOR VARIOUS APPLICATIONS AT 80° AND 800° F

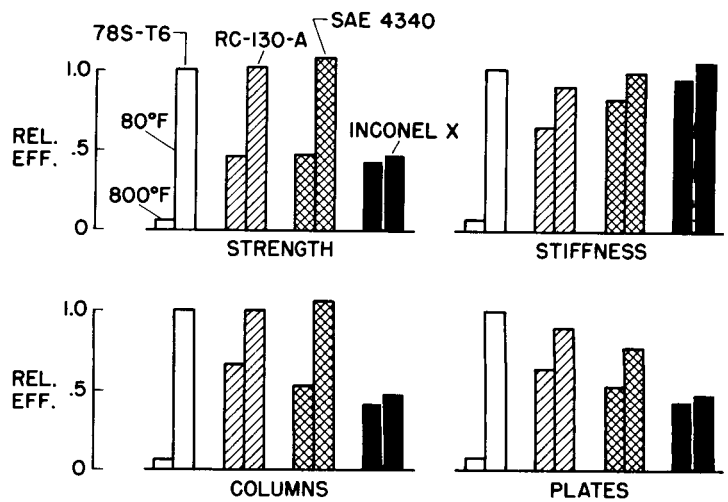

Figure 8

6. REVIEW OF MATERIALS FOR JET ENGINES

By G. Mervin Ault and George C. Deutsch
Lewis Flight Propulsion Laboratory

INTRODUCTION

The jet engine depends for its effectiveness on the availability of materials that can withstand severe operating conditions. During the early development of the jet engine, a class of materials known as super alloys was created without which the engine as it is known today would not have been possible. The competition for higher performance is creating a demand for even better materials, particularly those that would permit higher operating temperatures.

In studies to obtain better materials, the availability of the constituent elements must also be considered. It would, of course, be very desirable for these materials to contain solely those elements that are domestically available in sufficient amounts for use during wartime. The super alloys in widespread use today are generally based on systems employing cobalt, nickel, and chromium. One such material, S-816, consists of 40 percent cobalt, 20 percent chromium, and 20 percent nickel. In addition, minor alloying agents, such as niobium, tungsten, and molybdenum, are used. Because of the very limited supplies of these elements, particularly cobalt, tungsten, and niobium, the number of engines that could be built using S-816 as a blade material would fall far short of the required number in an emergency. The current cobalt-base alloys also have another serious disadvantage in that they are limited in the temperature that they can withstand. If the desired higher operating temperatures are to be attained, new alloys must be developed for use as turbine blades.

While the materials problem in the turbine blades is probably the most critical in the jet engine, materials problems exist in other components, and research is being directed toward investigating a vast variety of materials that might ultimately replace many of those in use today. This discussion will outline the present status of the materials problem in each of the critical components of the jet engines and will mention several of the directions from which these problems are being attacked. It is useful to bear in mind the relative location of the particular component to be discussed and the approximate temperature to which this component is subjected by making reference to figure 1. This is a cross section of a typical turbojet engine. Air is drawn in through the inlet, its pressure is raised in the compressor, fuel is added, and the mixture is ignited in the combustor. The hot gases are directed onto the rotating turbine blades at the correct angle by the nozzle guide vanes. The expanded gases issue through the nozzle and thereby provide the

propulsive thrust of the engine. Typical temperatures in a current engine are shown in the figure. For example, current turbine blades operate at maximum material temperatures of about 1500° F. The temperatures specified in figure 1 are, in many cases, determined by the properties of materials available at the present time. Higher temperatures would be desirable if suitable materials were available. A very important objective of materials research, therefore, is to permit the elevation of some of these temperatures.

ROTATING AND STATIONARY TURBINE BLADES

The component that most limits gas temperatures is the rotating turbine blade because it is subjected to a severe combination of stress and temperature.

The nozzle vanes are another component of the turbine that operates at very high temperatures - as much as 200° F above that of the turbine blade. However, because the blades are stationary, they are subject primarily to the thermally induced stress with, in addition, a small bending stress due to the gas load. Because of the low stress state existing in the nozzle vanes, alloys similar to those used for turbine blades are satisfactory and in many cases acceptable blade lives are obtained with lower alloy materials. For these reasons, the nozzle vane alloys will not be considered separately. As has already been mentioned, the alloy of greatest use for the turbine blade up to the present time has been the super alloy S-816, containing large amounts of the strategic elements cobalt and columbium. Considerable research is being directed toward replacing this alloy by newer cobalt-base alloys or preferably nickel-base alloys. There is evidence that alloys exist having not only less strategic material content but higher temperature limits of operation.

In figure 2 are shown several alloys of this type which are currently under development. (The compositions of these alloys as well as others referred to in this paper are shown in table I.) In the figure the stress that a material can support for 100 hours without fracture is plotted against temperature. This stress would represent the centrifugal stress applied to the blade. In addition to this stress, a turbine blade must withstand vibratory and thermal stresses and a severly oxidizing atmosphere, and must not elongate excessively. The first criterion, however, is time-to-rupture under the centrifugal load and, for the sake of brevity, comparisons will be made on this basis only. The horizontal dotted lines in the figure are the range of typical centrifugal stress levels encountered in current engines. For a majority of current engines, a stress of about 13,000 psi would exist in the blade at midspan, the point where it is most likely to fail. For

some highly stressed engines, the stress is approximately 22,000 psi. Since the trend in future engines appears to be to toward higher stresses, comparisons will be made on the basis of the highly stressed engine, labeled "Engine A." The lowest curve on this figure refers to S-816, and the next higher curve designated "current cobalt-base cast" represents the best properties of other currently well-developed blade alloys.[1] It will be noted that for the highly stressed engine the temperature limit of S-816 is in the neighborhood of 1525° F, and for the best of these current alloys, about 1600° F. The other curves show the properties of new alloys under development. Most recent effort has been devoted to the development of nickel-base wrought alloys because these contain much less critical material than those of cobalt base. Nickel-base wrought alloys have been developed that may permit engine operating temperatures of 1650° F at the high stress level. New cast alloys of both cobalt and nickel base (ref. 1) also are being developed, and these are shown by the upper two curves. Blade temperatures up to 1700° F, or about 175° F higher than S-816, may be possible with these materials.

Another means of increased turbine temperatures is the use of alloys of chromium (ref. 2) and molybdenum (refs. 3 and 4). Figure 3 shows the stress-rupture properties of the strongest of these alloys. Again the stress that can be withstood for 100 hours prior to rupture is plotted as a function of temperature. In this case, a correction has been made for the density to take into account the fact that molybdenum alloys are approximately 20 percent heavier than the cobalt or chromium alloys. It is seen that, with the chromium alloys, temperatures of about 1850° F may be possible, whereas with the molybdenum alloys temperatures of 2000° F are indicated. Molybdenum, however, is severely attacked by oxygen at temperatures above 1100° F and must be protected. Many types of coatings and alloy additions to prevent oxidation have been attempted, but none has proved completely satisfactory. Most of the coatings are either too brittle and have very low impact strength or when used on large numbers of parts, such as turbine blades, cannot be applied perfectly on all pieces. The oxidation of molybdenum is so rapid that a small pin hole resulting from an imperfect coating or from impact of small particles in the gas stream can be expected to result in complete oxidation of the blade in a few minutes under engine operating condition. The current consensus is that a coating on molybdenum for a part subjected to impact (such as a turbine blade) must be ductile, as may be expected with diffused metallic coatings as contrasted with ceramic or vitreous coatings. The protection of molybdenum presents one of the most difficult coating problems ever encountered, and considerable effort is being expended on this problem at the present time.

---

[1]Throughout this discussion, only data which are not readily available are referenced.

The best molybdenum alloys at present are made by melting in a vacuum or neutral gas atmosphere followed by extrusion or working by other methods. The alloys have maximum strength in the as-worked condition and lose considerable strength when recrystallized. Molybdenum alloys are malleable and can be forged into blades.

The best chromium-base alloys contain about 60 percent chromium, 15 percent iron, 25 percent molybdenum, and about 2 percent titanium. They are fabricated by casting, usually in a vacuum. They have satisfactory oxidation resistance but are extremely brittle with no measurable ductility at room temperature and negligible impact strength even at high temperatures. The brittleness of these alloys completely prohibits their use currently. Chromium-base alloys are being studied extensively in several laboratories, primarily for the purpose of improving ductility.

In addition to the new alloys, a different class of materials is being investigated for potential use as turbine blades. These are called "cermets" (ref. 5), and are combinations of ceramics and metals. By suitably combining these components, materials have been developed that possess many of the high-strength characteristics of ceramics at the elevated temperatures while retaining some of the advantages of alloys, such as resistance to thermal shock. Figure 4 shows the stress-rupture properties of a number of cermets under investigation. Again the stress that can be withstood for 100 hours without fracture is plotted against the temperature limit of operation. An adjustment of the stress is necessary to take into account the fact that the density of these cermets is about 25 percent less than that of S-816. Two classes of cermets are shown. The line labeled "TiC + alloy cermet" is typical of a class of materials that are well along in their development, meaning that their properties have been fairly well defined, they have good thermal shock resistance, and techniques for production of intricate shapes have been developed. The data indicate that they are usable at temperatures up to about 1800° F, or 250° F above current alloys and 100° F above the best developmental cobalt- and nickel-base alloys. The second class of cermets consists of materials not so far along in their development, but which serve to indicate furture strength potentialities of this type of material. This is shown by the curve labeled "Al_2O_3+Cr." Temperatures in excess of 2000° F may be possible if these materials can be properly developed for practical application.

Such materials, in addition to allowing higher temperatures, are lighter in weight; consequently, engine weight will be lowered and even higher thrust per unit engine weight can be obtained.

While a number of methods are being explored for increasing the temperature limits and reducing the strategic element content, each

approach has problems that will have to be solved before it can be adopted for practical application. Nearest ready for use are the wrought nickel-base alloys because they are so similar to the currently used materials and yet have higher strength. The cast nickel-, cobalt-, and chromium-base alloys involve problems of brittleness or low ductility. Figure 5 shows, for example, the room-temperature ductility of a number of materials plotted against the allowable metal temperature. It can be noted that the wrought cobalt-base alloy (S-816) has a ductility of over 30 percent. The wrought nickel-base alloy permits higher allowable metal temperature, but does not reduce the ductility below 10 percent. Actual engine experience has indicated that this ductility level is acceptable for turbine application. The cast cobalt- and nickel-base alloys show ductilities in the neighborhood of only 1 or 2 percent. Vacuum melting is now being vigorously pursued, partly in an attempt to increase the ductilities of both the cast and wrought alloys. As mentioned previously, the brittleness of the higher strength alloys prohibits their current use. The best combinations of strength and ductility are indicated for molybdenum alloys — the best of which have the 30 percent ductility when severely cold-worked. Molybdenum alloys require suitable coatings as was mentioned previously.

Although not indicated in figure 5, cermets, too, are very brittle but appear to be somewhat superior to the high-strength chromium-base alloys.

Very low ductilities imply two problems: high sensitivity to stress concentrations and poor impact strength. The stress concentration problem comes in connection with the method of fastening the turbine blade into the disk. Figure 6 shows various turbine blade fastenings. On the left is the conventional fir-tree root used with ductile alloy blades. This has sharp radii which are not serious in ductile blades, but lead to very early failure when the material is brittle. The alloy design also involves a large number of mating teeth. In brittle materials which are not capable of easy deformation, slight manufacturing tolerances may result in a concentration of load on one or only a few of the teeth, thereby resulting in premature fracture. For brittle materials, therefore, it is desirable to use designs involving large radii and a small number of mating surfaces. Several designs that have been evolved for use with cermet blades and with alloy blades of low ductility are shown to the right of the fir tree. In the first, ductile pins of large diameter serve to retain the blade in the wheel. The blade-root temperature is much lower than is that of the airfoil, thus permitting the use of soft stainless-steel pins at this point. In the interlock design, only one mating surface is provided, and again a ductile pin is inserted between the blade and the wheel. The dovetail design makes use of very large radii and of a ductile screen (which is not shown) between the wheel and the blade. Some of these designs have been successfully used in overcoming the stress concentration factor associated with fastening cermet blades into wheels.

The impact problem may be more difficult to solve. Part of the problem arises because of foreign objects ingested into the engine. This part may perhaps be solved by suitable screening devices; however, missiles may be generated within the engine. Fragments of combustor liners and transition pieces have been known to pass through the turbine. A failed turbine blade may be thrown against adjacent blades. If the impact resistance of the material is poor, extensive damage to the blades will occur. Impact resistance of potential turbine-blade materials has been evaluated by a special apparatus devised at this laboratory. Typical results are shown in figure 7. The impact resistance is measured in inch-pounds and should not be confused with conventional values obtained on Charpy or Izod machines, since a special apparatus has been used. The first vertical bar indicates the impact strength of alloys that are currently widely used as turbine-blade materials and thus are known to be satisfactory. The value for these alloys is 40 inch-pounds and above. It is not known at this time how much less than 40 inch-pounds can be tolerated. Cermets have impact strengths in the range of 2 to 20 inch-pounds, as indicated by the cross-hatched area of the second bar. Cermets with impact strengths of 4 to 6 inch-pounds have been run in engines and found to be definitely unsatisfactory. Molybdenum alloys have impact strengths ranging from 15 to 25 inch-pounds, but the strength goes to over 60 inch-pounds if the temperature is raised slightly and these alloys are thus believed to be satisfactory. The experimental nickel- and cobalt-base alloys for higher temperatures have impact strengths ranging from 5 to 25 inch-pounds. Much research must be directed toward overcoming the impact problem in the cermets and some of the experimental nickel- and cobalt-base alloys. It is also necessary to define the minimum impact resistance required for satisfactory operation in an engine.

The method thus far discussed for increasing turbine-blade temperature has been the direct replacement of current alloys by materials of higher strength at higher-than-current temperatures. It should be borne in mind that the sole purpose of increasing the temperature is to obtain higher engine thrust. The parameter that governs engine performance, however, is the ratio of the thrust to unit engine weight. It is therefore also important to decrease engine weight. The use of hollow blades permits the reduction in engine weight, and cooling these hollow blades will permit an increase in gas temperatures and engine thrust.

The effect of lighter turbine blades will be reflected in lighter turbine wheels for carrying these blades, lighter shafts for carrying the wheels, and so forth, so that small gains in turbine blade weight may reflect as large weight savings in the over-all airplane. Figure 8 is a sketch of a typical turbine wheel using hollow blades. The massive solid turbine wheel has been replaced by two disks which are adequate for carrying the lighter blades. The passage between the two disks may, if necessary, serve for the introduction of cooling air to the blades.

The introduction of cooling air to the blades will alter the materials requirements just discussed. Substantial increases in temperature can be achieved with cooling while using materials similar to those currently being used uncooled.

Figure 9 shows typical weight saving that can be achieved by the use of sheet metal blades in conjunction with more efficient wheel structures. Total wheel weight (that is, disks plus blades but without shaft) is plotted on the ordinate as a function of the individual blade weight for various arbitrary design stress levels in the center of the disk. Two blade weights are considered. The one at 0.6 pound represents a conventional solid blade and the one at 0.3 pound represents a hollow blade of comparable aerodynamic design. For an arbitrary stress level in the center of the disk, say 70,000 psi, wheel weight could be reduced about 50 percent by replacing the solid blade with a hollow blade. If through cooling the allowable design stress could be increased, even greater weight saving might be accomplished.

For the turbine blade, studies are underway that, if successful, can ultimately increase blade operating temperature, reduce strategic material content of the blades, and reduce engine weight.

COMPRESSOR BLADES

Another area in the turbojet engine where blades present a materials problem is in the axial-flow compressor. The temperatures in the compressor have been increasing because of higher compression ratios and higher flight speeds, and the trend of increasing temperatures is expected to continue. Figure 10 shows the relation of compressor outlet temperature to compression ratio and flight speed. Early designs had compression ratios of about 4 with temperatures of about 250° F. Current designs have compression ratios as high as 12 with outlet temperatures approaching 550° F. Increased flight speeds can increase these temperatures up to about 1000° F or even higher. These temperatures for the latter stages of compressors exceed those allowable with current compressor materials and enter the range of operating temperatures for current turbine disks. It is apparent that some of the materials now used in the hotter turbine disk must be used for the compressor blades and compressor disks of future engines.

In addition to complications introduced by the trend toward higher operating temperatures, the axial-flow compressors operating at current temperatures have problems in blade vibration which may lead to blade failure. The failure of one compressor blade can initiate a disastrous chain reaction that at its worst can completely destroy the engine. A primary cause of blade failure is fatigue induced by fluctuating air flow in the compressor. Currently the most widely used compressor-blade alloy

is 403 stainless steel containing about 12 percent chromium. To reduce the weight of the blades, as well as the weight of the supporting wheels, consideration is being given to the use of both plastics and titanium and titanium alloys. The plastics which are being considered are laminates composed of glass fibers bonded together with bakelite cement or phenolic resins. These have about 25 percent the weight of steel, and the titanium alloys are about 60 percent the weight of steel. In addition, of course, the strength must be adequate. An important criterion, then, is strength-to-weight ratio. For rotating parts where the load is determined by centrifugal force, the load or stress is directly related to the density; rotating parts made from titanium, for example, would be subjected to 40 percent less centrifugal stress than if made of steel. The strength-weight ratios of several materials are shown in figure 11 (from ref. 6) as a function of temperature. It can be seen that the titanium alloy is superior to aluminum alloy, 1/2 hard stainless steel, glass-cloth laminate, and a high-temperature alloy Inconel X up to 900° F. The plastic or glass-cloth laminate with its very low density is quite competitive with other materials at moderate temperatures.

In addition to being about one-fifth the weight of the steel blade which it is to replace, the plastic blade has another advantage which makes it of particular interest - this is damping capacity. For a particular root mounting, it is the aerodynamic plus the internal or material damping which determine the vibratory stress to which a material will be subjected. The magnitudes of these factors for plastics and titanium as well as for more conventional compressor-blade materials are shown in figure 12.

On the left side of the figure the aerodynamic damping is plotted as a function of density for the various materials. When a blade vibrates freely in an air stream, the air removes energy from the blade, thus decreasing the vibrational energy of the blade. This removal of energy is known as aerodynamic damping. The higher the aerodynamic damping, the less is the tendency for such excitations as rotating stall to induce destructive vibrations. It can be seen that the plastic has an aerodynamic damping of 20.8 percent, which is considerably higher than that of the other applicable materials and is 4.5 times that of 403 stainless steel.

On the right side of the figure is a comparison of the internal or material damping of the same materials, plastic, aluminum, titanium, and 403 stainless steel. For some materials, the internal damping depends on the stress level; this is the case with the plastic considered, a laminated fiberglass impregnated with a phenolic resin. For example, an internal damping of 9 percent occurs at a vibratory stress level of plus or minus 5000 psi, and a damping of 20 percent occurs when the vibratory stress level is at the endurance limit of 25,000 psi. For comparison, the material damping for 403 stainless steel is only about 1

percent at 5000 psi and 3 percent at the endurance limit of 50,000 psi. Although one reason for the choice of 403 stainless steel for compressor blades has been its high material damping, plastics are even better. The high material damping of the plastic is particularly advantageous when the aerodynamic damping cannot be relied upon; this can occur in stall flutter.

In addition to the ability to dampen vibrations, the ability of the material to withstand vibrational stresses is, of course, also of concern. This ability is defined by the endurance limit in fatigue. The endurance limit for plastics is about one-half that of the stainless steel. It remains for actual experience in engines with these materials to determine whether the greatly improved aerodynamic damping and material damping of plastics will overcome their lack of fatigue strength and permit the designer to take advantage of their light weight. Preliminary engine tests have been promising.

For titanium alloys the reported room-temperature fatigue strengths are of the order of 60 percent better than 403. It is thus indicated that on the basis of these factors, titanium alloys will find application for compressor blading. Complexities in melting and fabrication and some as yet undetermined properties such as notch fatigue strength may retard this application, however.

TURBINE AND COMPRESSOR DISKS

As the trend toward higher operating speeds and/or higher operating temperatures for compressor blades is realized, there are, of course, greater demands put on the blade supporting structure, the disk; and it becomes obvious that when the temperature limitations of the compressor disks are exceeded, materials currently being used for the hotter turbine disks may be required. It is convenient, therefore, to discuss all disk materials together, again keeping in mind that the same materials may also be used for compressor blading.

The wheels are designed to withstand the combined effects of centrifugal, thermal, and fastening stresses. In the wheel hub where the temperature is lowest, the design is based on the short-time yield strength of the material. In the high-temperature rim, the design is based on the long-time stress rupture and creep properties.

Because of the difficulty in obtaining comparative data for all these properties as well as for the sake of simplicity, the available materials are compared (fig. 13) on the basis of stress-rupture strength. In this figure is plotted the stress which can be sustained for 1000 hours to rupture for various temperatures. The values of aluminum and

titanium are shown as dashed lines. Because of the large differences in densities between these materials and the remaining alloys, they are also shown (as solid lines) after an adjustment to the average density of the other alloys is made. For stresses in the neighborhood of 40,000 to 60,000 psi, the ferritic steel and the titanium alloy are about equivalent in strength and offer a 400° to 500° F temperature advantage over the aluminum alloys. They are also somewhat superior to the simple 18-8 austenitic steels. The utilization of the titanium alloys poses several problems and the alloy shown (data from ref. 7) is in its very early stages of development. Also shown is an austenitic steel that derives its strength by being work-hardened in an operation known as hot-cold working or warm working. For the same stress levels, this alloy permits operating temperatures in the neighborhood of 1200° F or about 150° F over the ferritic steel and the titanium alloy. This work-hardenable alloy is now the most widely used turbine-rim material. A more recent alloy and one which is very promising, although it has only a slight temperature advantage, is the heat-treatable austenitic. As the name implies, this again is an austenitic steel, but one that derives its strength from heat treatment. The final alloy shown on the figure is Inconel X. This is a nickel-base, heat-treatable alloy. With this alloy, temperatures in the neighborhood of 1400° F could be attained at similar stress levels.

Thus it can be seen that with regard to strength there exists a wide choice of materials which will keep the compressor and turbine disk from limiting jet-engine operating temperatures. For some of the materials, however, there is very little operational experience; as experience is accumulated, difficulties not previously considered may be revealed and may necessitate additional developmental work on the alloys.

One such property receiving increased attention is that of long-time notch sensitivity (ref. 8). An example of this is shown in figure 14. On the figure is plotted the stress-rupture life in hours for the alloy 17-22A(S) in both the notched and unnotched condition. It can be seen that for short lives the notched strength exceeds that of the unnotched strength and the material is said to be notch ductile. At the longer rupture times, because of structural instabilities, this situation reverses and the alloy becomes notch-sensitive. This notch-sensitivity may develop in a much shorter time, should the alloy be subject to over-temperature of the type that could be encountered with a turbine wheel during a hot start. It is in this notch-sensitive area that difficulties with the fastening may develop. As is shown on the figure, at the very longest rupture times the notch ductility is recovered.

This discussion of turbine and compressor wheels has attempted to present the materials that are available rather than indicate what materials are to be used. As was indicated in the discussion of turbine blades, the designer may chose to increase the operating temperature

through the use of more refractory blade materials. In this case he would be forced to use more temperature-resistant wheel materials or to cool the wheel rim, or he might increase operating temperature through the use of cooled blades. In this case he might actually reduce the rim temperature and he could then reduce the weight of the wheel by allowing the rim to run at a higher stress level, or perhaps he could go to a less strategic or more easily fabricated alloy.

SHEET MATERIALS

In considering sheet materials for the jet engine, it is necessary to discuss only those areas of the engine in which the sheet problem can be critical. These involve the hot parts of the engine such as combustion chamber liner and transition piece, the tail pipe, and the afterburner components. Of first importance is that the sheet materials withstand the oxidation and corrosion conditions of the engine atmosphere. This resistance is achieved either by the inherent oxidation resistance of the sheet alloy or by coating with ceramic or metallic coatings - particularly aluminum. Next, it is important that the materials withstand the stresses to which they are subjected. Stresses to be considered are the hoop stresses caused by differential pressures, the stresses of supporting the components' own weight, and the thermal stresses. Most important usually is the ability to withstand without buckling and cracking the stresses resulting from the repeated severe thermal gradients existing in most hot engine components. Since stresses from thermal gradients are very important, sheet materials should also be considered as to minimizing these gradients and resultant stresses. This requires high thermal conductivity, low coefficient of thermal expansion, and low modulus of elasticity. Figure 15 (from ref. 9) indicates the relative thermal conductivities of some typical sheet alloys. Some of the high-temperature alloys are quite poor when compared with low-alloy steels in this respect. Because of high thermal conductivity, molybdenum alloys are very attractive. They also have a coefficient of expansion that is appreciably less than that of conventional alloys, and molybdenum alloys are extremely strong at high temperatures. The modulus of elasticity is about 1.6 times that of conventional alloys. Molybdenum alloys are very promising for sheet, but the coating problem may be very difficult to solve.

The Inconel-clad copper alloy, combining the strengths of the Inconel with the thermal conductivity properties of copper, is very attractive. The thermal conductivity of this material is about 10 times that of Inconel.

The strengths of some current sheet materials are shown on figure 16 (principally from ref. 10). Essentially the sheet materials are comparable in strength to the wrought alloys except that some strength

may be lost as a result of the very high surface-to-area ratio. Also, it is desirable to use alloys that achieve good strength in the solution or annealed condition. Materials requiring elaborate heat treatments have usually been avoided. As temperature is increased, the usual trends are observed, going from low-alloy steels to stainless steels to precipitation-hardened stainless steels and finally to cobalt-base alloys. As indicated previously, where the stresses are primarily thermal, properties such as high conductivity along with good strength are more important than very high strength alone (ref. 9).

SUMMARY

The materials research for jet engines has as its objective the development of materials to permit higher operating temperatures, higher operating speed, lower weight, and greater reliability. For the compressor blades the principal new materials being considered are plastics and titanium. For the compressor and turbine disks there is a wide assortment of materials available, ranging from the lightweight titanium to the highly temperature-resistant Inconel X, a material which is also being considered for turbine blades.

Because the turbine blade operates under the more severe stress, temperature, and atmospheric environment, it presents the most crucial materials problem. As a consequence, many different types of material are being considered for this component. These include new nickel- and cobalt-base alloys, the refractory molybdenum and chromium alloys, and cermets.

Problems also are anticipated in the high-temperature sheet metal parts of the engine. Solutions to these problems are being sought through the use of coatings for oxidation resistance and the consideration of materials of improved thermal properties to minimize thermal stresses.

Studies are also underway to reduce the engine weight through the use of hollow turbine blades and built-up wheel structures, which in addition may be cooled to permit higher operating temperatures.

REFERENCES

1. Guy, A. G.: Nickel-Base Alloys for High Temperature Applications. Trans. A.S.M., vol. 41, 1949, pp. 125-140.

2. Havekotte, W. L., Greenidge, C. T.: Final Report on Chromium-Base Alloys. Battelle Memorial Inst., Mar. 31, 1950. (Contract No. N5ori-111, Task Order I, Proj. NR 031-003, Office Naval Res., Navy Dept.)

3. Semchyshen, M., and Hostetter, H. E.: Arc-Cast Molybdenum Base Alloys. Third Annual Rep. NR 034-401, Climax Molybdenum Co. (Michigan), 1952. (Contract N8onr-78700, Task Order N8onr-78701, Proj. NR 034-401, Office Naval Res., Navy Dept.)

4. Harwood, J. J.: Molybdenum - Our Most Promising Refractory Metal. Product Eng., vol. 23, no. 1, Jan. 1952, pp. 121-132.

5. Ault, G. M., and Deutsch, G. C.: The Applicability of Powder Metallurgy to Problem of High-Temperature Materials. Jour. Metal, Nov. 1954.

6. ASM Committee on Titanium: Titanium and Titanium Alloys. Metal Prog., vol. 66, no. 1-A, July 15, 1954, pp. 80-89.

7. Hutchinson, G. E., Kaufmann, D. W., and Durstein, R. C.: New Weldable Titanium Alloy. Materials and Methods, vol. 39, no. 4, Apr. 1954, pp. 91-93.

8. Newman, D. P., Jones, M. H., and Brown, W. F., Jr.: Time-Temperature Dependence of the Notch Effect and Influence of Notch Depth in Stress Rupture Tests on a Cr-Mo-V Steel. Proc. A.S.T.M., vol 53, 1953, p. 677.

9. Haythorne, P. A: Sheet Metals for High Temperature Service. Iron Age, vol. 162, no. 13, Sept. 23, 1948, pp. 89-95.

10. Preston, D.: Exploratory Investigation of High-Temperature Sheet Materials. Proc. A.S.T.M., vol. 52, 1952.

TABLE I. - COMPOSITION OF ALLOYS OF INTEREST FOR JET ENGINES

Type	Designation	Nominal composition, percent by weight												
		Co	Ni	Cr	Mo	W	Fe	Ti	Al	C	B	Nb	Mn	Other
Turbine-blade alloys														
Current cobalt-base, wrought	S-816	44	20	20	4	4	3	-------	----	0.4	---	-------	-------	4.0 Cb + Ta
Current cobalt-base, cast	X-40	55	10.3	25	----	7.4	1	-------	----	0.48	---	-------	-------	
Nickel base, wrought	Inconel 700	29	Bal	15	3.7	0.5 max	4.0 max	2.25	3.0	0.16 max	---	-------	3.0 max	
New nickel-base, cast	Guy alloy	---	67	13.5	5.5	-------	4.5	-------	6.25	0.1 max	0.5	2.0	0.5	
New cobalt-base, cast	H.E. 1049	44	10	26	----	15	3	-------	----	--------	0.4	0.4	-------	
Chromium cast	----------	---	------	58	35	-------	15	2	----	--------	---	-------	-------	
Molybdenum	----------	---	------	-----	97.5	-------	-------	2.5	----	--------	---	-------	-------	
Compressor-blade alloys														
75S-T Aluminum	75S-T	---	------	0.3	----	-------	-------	-------	Bal	--------	---	-------	0.2	1.6 Cu, 2.5 Mg, 5.6 Zn
Titanium & Manganese	----------	---	------	-----	----	-------	-------	92	----	--------	---	-------	8	
Heat treatable nickel base	Inconel X	---	70 min	15	----	-------	7	2.5	0.7	--------	---	0.85	0.65	0.50 max Si
1/2 Hard stainless steel	----------	---	------	-----	----	-------	-------	-------	----	--------	---	-------	-------	
403 stainless steel	A.I.S.I. 403	---	------	12.25	----	-------	Bal	-------	----	0.15 max	---	-------	-------	
Compressor and turbine disk alloys														
Aluminum alloy	24S-T	---	------	-----	----	-------	-------	-------	Bal	--------	---	-------	0.6	4.5 Cu, 1.5 Mg
Titanium alloy	A-110AT	---	------	-----	----	-------	-------	Bal	5	--------	---	-------	-------	2.5 Sn
Austenitic stainless steel	A.I.S.I. 321	---	10	18	----	-------	Bal	4xC min	----	0.08 max	---	-------	2.0 max	
Ferritic steel	17-22A(S)	---	------	1.24	0.50	-------	-------	-------	----	0.45	---	-------	0.48	0.60 Si, 0.20 V
Heat-treatable austenitic steel	A-286	---	26.1	15.8	1.4	-------	Bal	1.6	0.14	0.7	---	-------	1.6	1.00 Si
Work-hardenable austenitic steel	16-25-6	---	25	16	6.25	-------	Bal	-------	----	0.9	---	-------	2.0 max	1.0 Si, 0.15 N
Ferritic steel	17-22A(S)	---	------	1.25	0.5	-------	Bal	-------	----	0.30	---	-------	0.55	0.65 Si, 0.25 V
Sheet materials														
302 stainless steel	302	---	9	18	----	-------	Bal	-------	----	0.14	---	-------	2.0 max	
347 stainless steel	347	---	10	18	----	-------	Bal	-------	----	0.10 max	---	8xC min	2.0 max	
Cobalt-base	L-605	Bal	11	21	----	15	1.6	-------	----	0.08	---	-------	1.64	0.6 Si, 0.03 N
Cobalt-base	V-36	Bal	13	25	4	2	1.9	-------	----	.27	---	1.7	0.9	0.2 Si
Iron-base	Incoloy T	---	32	20	----	-------	Bal	1	----	.1	---	-------	1	0.4 Si
Nickel-base	Inconel	---	78	14	----	-------	6.5	-------	0.25	.05	---	-------	.15	0.25 N
	N-155	20	20	20	3.5	2.5	Bal	-------	----	0.20 max	---	1.25	1.8	0.5 Si, 0.15 N

TYPICAL OPERATING TEMPERATURES OF A TURBOJET WITH THRUST AUGMENTATION

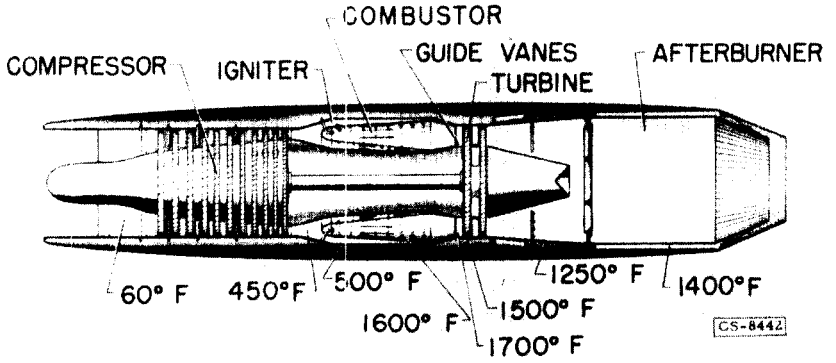

Figure 1

COMPARISON OF 100-HOUR STRESS-RUPTURE STRENGTHS OF BLADE ALLOYS

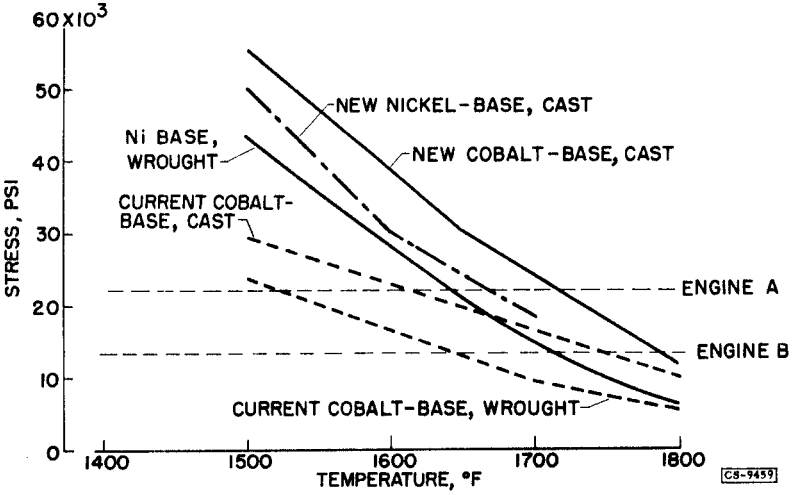

Figure 2

COMPARISON OF 100-HOUR STRESS-RUPTURE STRENGTHS OF ALLOYS ADJUSTED TO DENSITY OF S-816

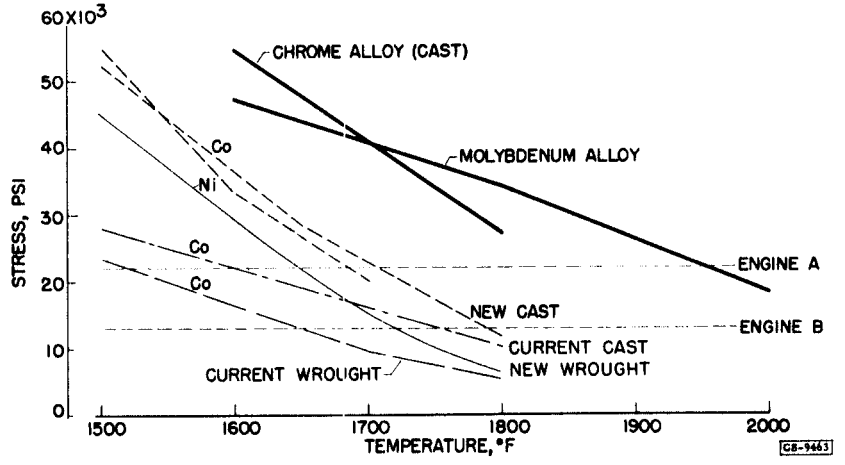

Figure 3

COMPARISON OF 100-HOUR STRESS-RUPTURE STRENGTHS OF CERMETS AND ALLOYS ADJUSTED TO DENSITY OF S-816

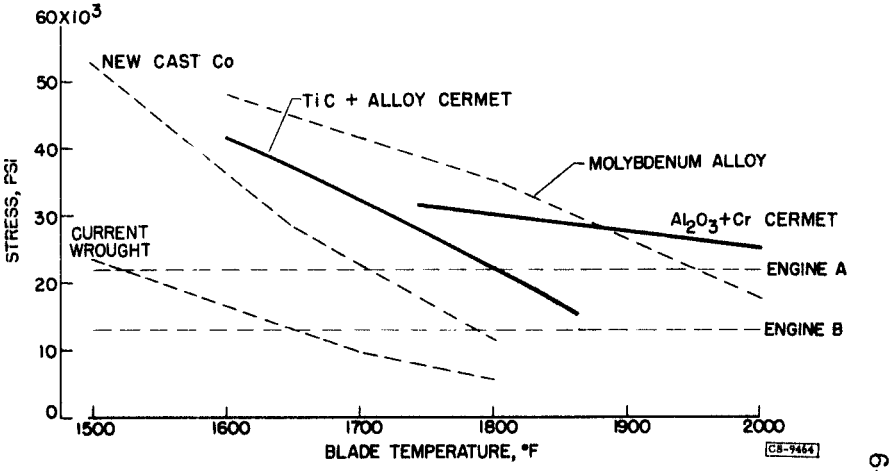

Figure 4

RELATION BETWEEN ROOM TEMPERATURE DUCTILITY AND ALLOWABLE BLADE TEMPERATURE FOR RUPTURE IN 100 HOURS AT 22,000 PSI

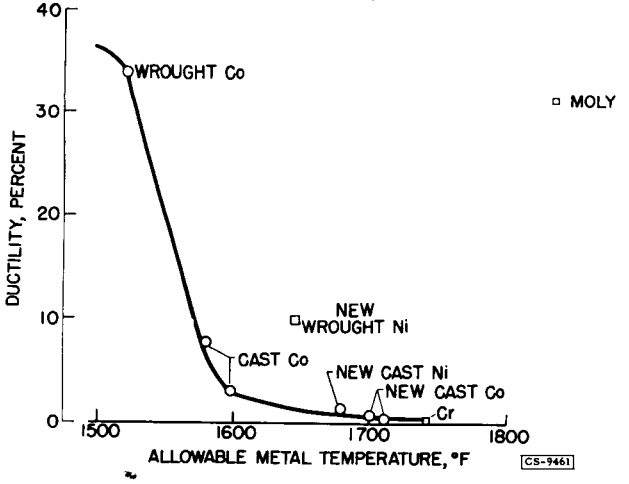

Figure 5

CERMET BLADES HAVING VARIOUS ROOT CONTOURS

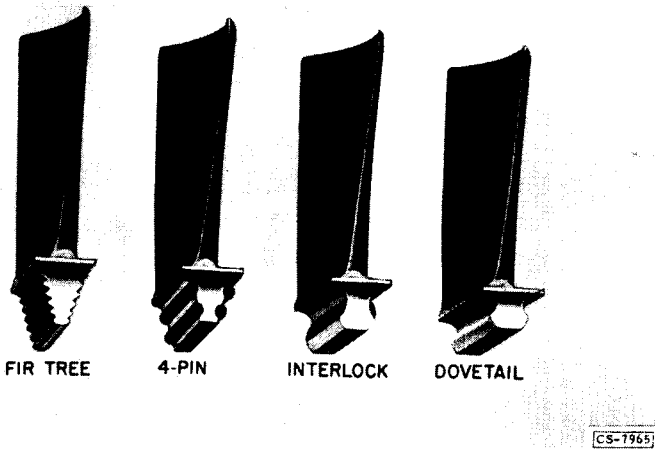

Figure 6

IMPACT STRENGTH OF BLADE MATERIALS AT ROOM TEMPERATURE

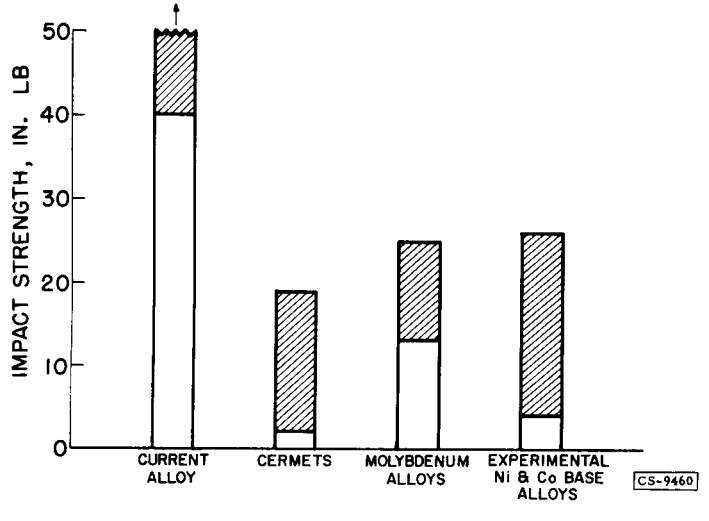

Figure 7

LIGHT WEIGHT TURBINE BLADE AND WHEEL ASSEMBLY

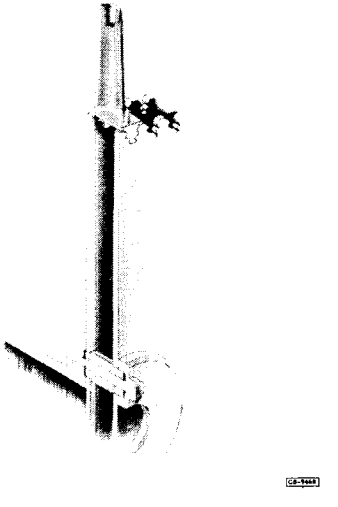

Figure 8

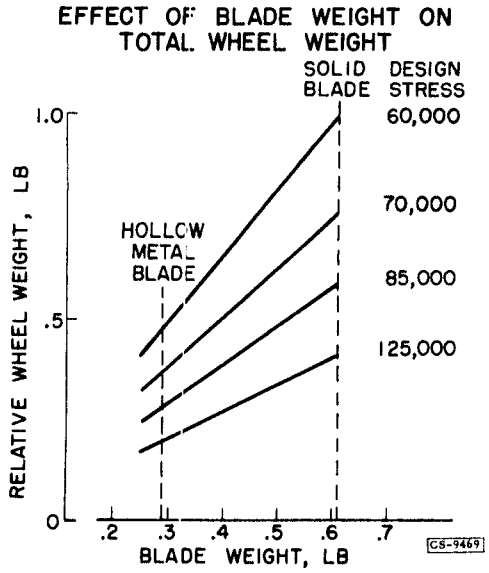

Figure 9

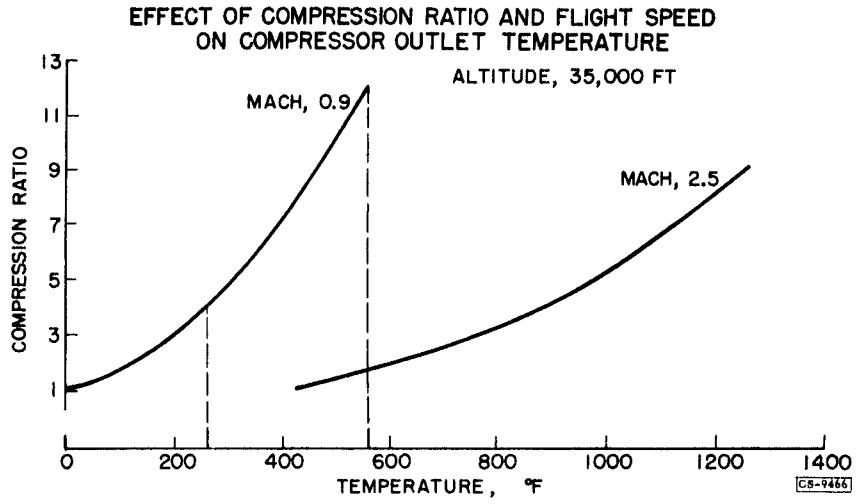

Figure 10

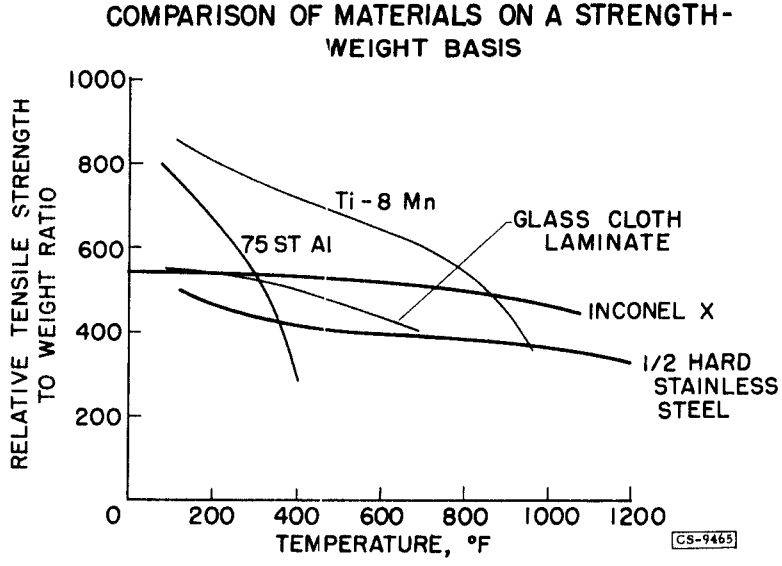

Figure 11

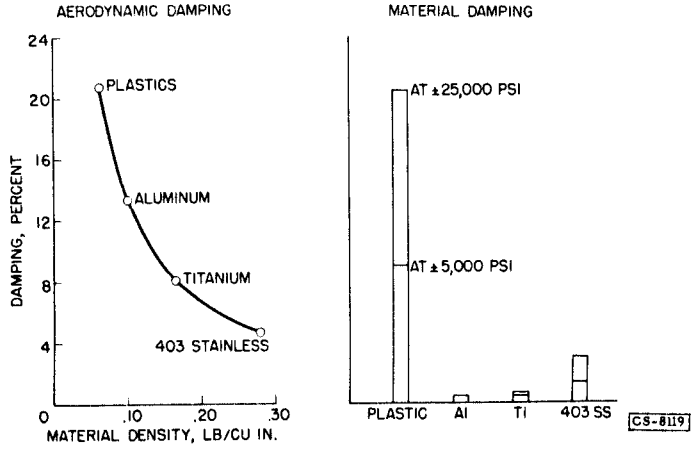

Figure 12

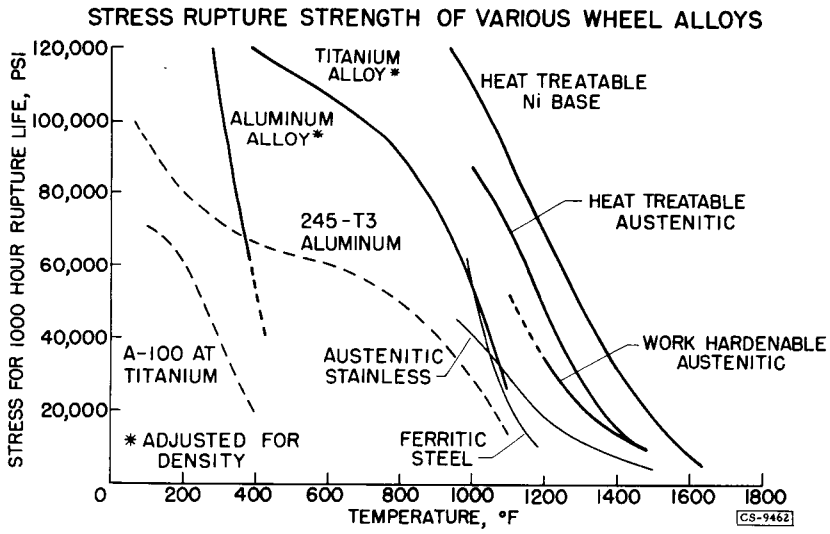

Figure 13

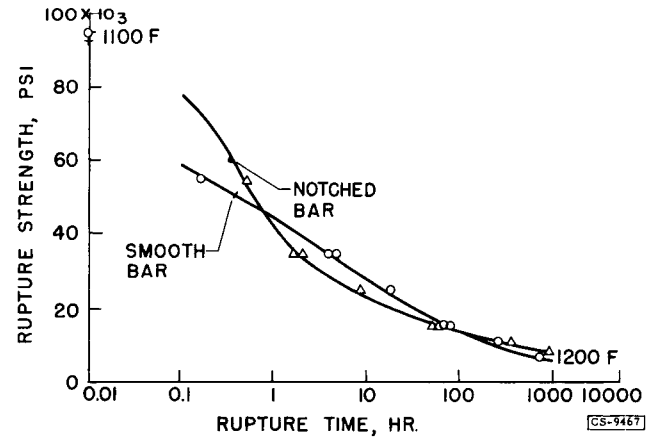

Figure 14

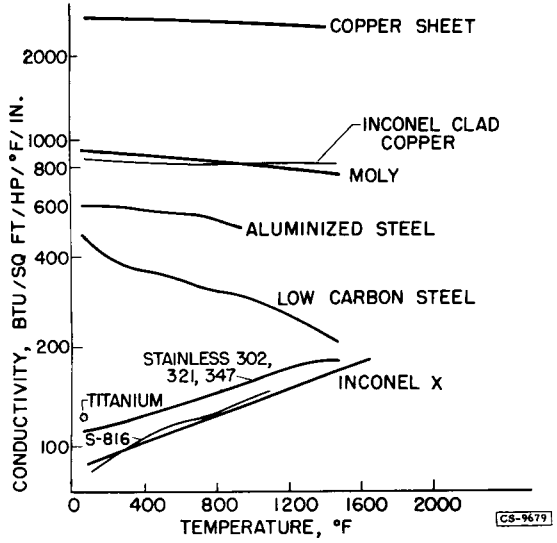

Figure 15

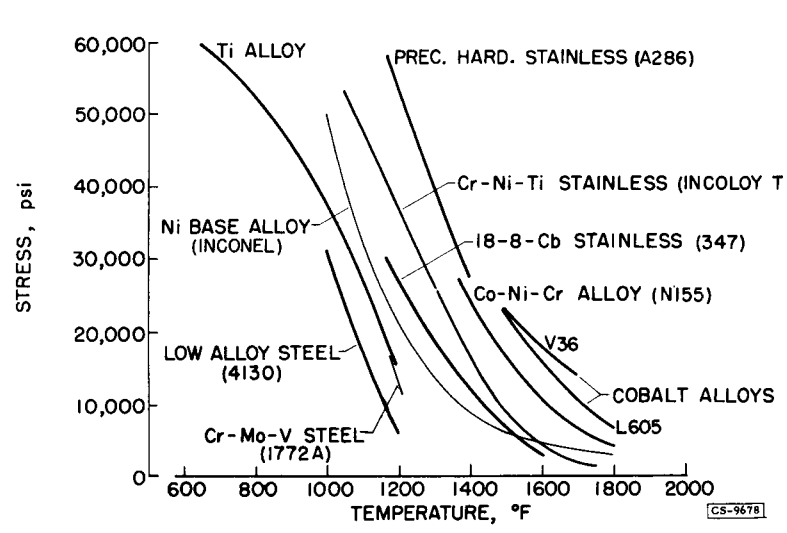

Figure 16

7. PHYSICS OF SOLIDS AND AERONAUTICAL MATERIALS

By S. L. Simon
Lewis Flight Propulsion Laboratory

In the history of the development of aeronautical materials, two features are noteworthy: (1) the repeated success in supplying materials to meet the demands of airplane and engine designers and (2) an almost complete absence of a basic understanding of why these materials worked. Since it is becoming more and more difficult to find new materials as readily as in the past, the basic understanding becomes more and more necessary.

In aeronautical materials development, it would be desirable to know, for example, why materials flow under stress, why they fracture, and why working or heat-treating increases strength. Moreover, the materials of interest are nearly always alloys of complex composition, structure, and shape and are exposed to changing temperatures and stresses.

The field of solid-state physics is the study of the basic behavior of materials and is therefore the eventual source of the general understanding of materials. However, at present most of the questions and materials of practical interest to materials development are far too complicated for direct attack by the physicist.

In order to make any progress, the physicist must ask much simpler questions, use simpler materials, and do simpler experiments. Although, at first sight, some of these simplifications have been carried so far as to make the experimental situation seem unrealistic, considerable advances in the basic knowledge of materials have been obtained in this way and much more may be expected. On the other hand, the mass of test data which has been accumulated in the course of the development of materials for aircraft has not contributed significantly to our basic knowledge, although it has been essential to the practical development.

The physics of solids work at this laboratory uses the approach, the methods, and the simplifications of academic solid-state physics. The problems chosen are those whose solutions are expected to contribute most to an understanding of the behavior and properties of aeronautical materials. Since the field of physics of solids is relatively new, some of its methods and techniques will be discussed more specifically.

The simplest metallic material to work with is a low-melting-point metal as a single crystal. The simplest nonmetallic material is a single crystal of an alkali halide. "Simplest" in this sense means that the atomic structures of these materials are the best understood theoretically. They do, however, contain imperfections whose behavior is

not yet completely understood and this behavior constitutes one of the main objects of present-day research in solid-state physics. Because single crystals do not have grain structure, it often does not have to be taken into account.

In addition to the simple materials mentioned, there are occasional special materials which lend themselves to basic studies. An excellent example is the order-disorder alloy of copper and gold (fig. 1). In this alloy a continous series of states is possible ranging from one in which the copper atoms occupy extremely regular positions in the lattice, as on the left side of the figure, to one in which their distribution is entirely random, as on the right. Since the electrical resistivity depends on the state of "order," it is possible, for example, to deform or heat a piece of this alloy, thereby changing its state of order, and by measurement of the change in electrical resistivity, to gain an idea of what has happened to the metal atoms in the process.

The simplest conditions are those that can be well controlled. In most cases this means low temperatures rather than high, synthetic atmosphere or vacuum, and sample shapes of simple geometry.

The measurements must be simple and conducive to interpretation of results. This requirement almost eliminates tensile, hardness, and fatigue testing. It does allow tests of isolated mechanical properties such as elasticity and plasticity, electrical properties such as conductivity and Hall effect, and thermal properties such as specific heat and heat conductivity.

A powerful special tool which has recently become available is nuclear radiation. Its chief value is that nuclear particles passing through a crystal disturb its atoms in a partially predictable way with a corresponding change in properties. This change can be compared with a similar change caused, for example, by deformation and helps to pin down similarities and differences in the basic mechanisms of the two types of damage.

The experimental and theoretical approaches which are used and the type of results obtained are extremely varied. Two topics of current interest which will illustrate the approaches and results, (1) the nature of work-hardening and (2) the effect of surfaces on strength, have therefore been selected for discussion.

One of the most important phenomena in practical metallurgy is work-hardening. A piece of metal which has been held for a long time at a high temperature is said to be annealed. In this state it is soft and its strength is low. If the metal is then deformed by the application of sufficient stress, its hardness increases as does its strength. It

is said to be work-hardened. If the deformation is carried far enough, the metal cracks or breaks. Work-hardening is therefore important both as a beneficial factor in strengthening materials, if not carried too far, and as a detrimental factor, if it is carried to the point of breakage. The latter sometimes occurs in components of aircraft in use.

On an atomic scale, it is known that deformation of a single crystal increases the complexity of imperfections already present in even the most perfect crystal available and that it generates more imperfections. It is known what these individual imperfections are in a general way.

Figures 2 and 3 show what these imperfections are supposed to look like. A perfect crystal lattice is shown in figure 2. The atoms are arranged in perfectly regular order. In reality, an occasional atom is missing in the regular array, as in figure 3(a), and the missing atom is found at positions, as in figure 3(b), called interstitial positions. The larger dots (fig. 3(c)) which occasionally appear represent impurities that are always found in real materials. Figure 3(d) shows an edge dislocation, a more complicated unit of imperfection. It may be visualized as having been formed by adding an extra row of atoms above the dashed line. More complicated types of dislocation also exist and are important.

The existence of these imperfections has been well established. However, in the metal they exist in various combinations and it has not been established what these combinations are or how they are formed during the work-hardening process. The NACA Lewis laboratory (as well as many other laboratories) is working on these questions from several angles of attack.

When a piece of metal is worked, a definite amount of energy is required. The greater part of the energy goes to form heat, which is dissipated during working, but some remains in the metal as energy of formation of the imperfections and groups of imperfections. The amount of energy thus stored is of great importance for an understanding of what is going on. For example, as will be shown later, the number of imperfections can be estimated from electrical measurements. Consequently, combining the results of the energy and electrical measurements can give an idea of the energy of formation of an imperfection, a number of great value in deducing what the imperfection is.

One experiment was done by twisting a rod of annealed copper in a torsion testing machine until it contained the desired amount of work-hardening (about 10 complete turns). The rod was then electrically heated in a vacuum calorimeter in such a manner that a constant amount of heat energy was added to it per unit time. The temperature therefore rose with time, and the rate at which it rose was measured. Figure 4

shows an idealized curve for this process in which energy release at two temperatures is illustrated. The ordinate is the temperature of the sample, and the abscissa is the amount of heat which had been added at the time the temperature shown on the curve was reached. For this specimen, the temperature rises smoothly until T_1 is reached, at which point it increases rapidly then levels off until T_2 is reached. Another rapid rise occurs here, and again the curve levels off and rises smoothly. After the maximum temperature has been reached, the sample is allowed to cool and the experiment is repeated. This time the curve for temperature against time is the solid curve, which lies below that for the first run. The difference between the two curves is, of course, due to the stored energy in the worked sample which was emitted in the first run. As the difference is small, many precautions against heat leakage and other sources of error must be taken.

The energy emitted as a function of the temperature of the sample for a typical experiment is shown in figure 5. Three runs were made on each sample, the last two, of course, being on annealed material. The difference between the heat supplied in the third and second runs is shown by the squares on the curve and indicates the reproducibility of this type of determination, about 10 percent. The difference between the third and first runs is shown by the circles and is therefore the stored energy released as a function of temperature.

The following table shows the numerical results obtained for three samples containing different amounts of work-hardening:

Sample	W, cal/g	E, cal/g	E/W
3	8.2	0.23	0.028
1	9.4	.28	.030
2	11.9	.41	.034

The symbol W is the amount of mechanical energy which was exerted in working the sample, and E is the total amount of stored energy obtained in the experiment. In all three cases, E/W, the fraction of the energy which was stored, is surprisingly small, considering the severity of the deformations. Comparison of the three samples, however, indicates that the amount of stored energy is still increasing slowly with working and has not yet reached a saturation point.

When this type of experiment was performed with a fatigued specimen, an unexpected and interesting result was obtained, as shown in figure 6. When the fatigued specimen was heated in the calorimeter, energy was absorbed rather than emitted as for the cold-worked specimen. This behavior was found for three samples, so that it is well established.

It may, of course, be reversed at higher temperatures than were reached in this experiment. The over-all energy emitted may therefore be positive, but this could not be investigated because the maximum temperature attainable was limited by the apparatus. The experiment is being repeated with tin whose melting point is lower than the temperature limit.

It is also possible to attack the problem of work-hardening by a study of the electrical properties of work-hardened metals. In order to explain the application of electrical properties, it will be necessary to discuss briefly the electronic structure of a metal. The electrons in a metal behave as if they were almost free, that is, not associated with any particular atom. However, the positive ions which comprise the rest of the structure are arranged in a regular lattice, and the electrostatic field in which the electrons exist changes from ion to ion. This has the effect that the electrons preferentially exist in certain energy levels and also are preferentially found in certain regions around the ions.

If an external field is applied to the metal, some of the electrons drift in the direction of the field and a current is thereby set up. Its magnitude depends on two factors: (1) the number and energy states of the electrons and (2) the number and magnitude of the spatial fluctuations in the electrostatic field, which interfere with the moving electrons. The number of electrons is characteristic of the metal chosen. The number and magnitude of the fluctuations and the energy distribution of the electrons depend on several factors: the metal, its crystal structure, and the number and magnitude of irregularities in the structure. The last two factors make it possible to use electrical methods to study work-hardening, because the imperfections introduced by cold work provide such irregularities in the structure. If the same metal is worked or damaged in different ways, the interference with the electron motion due to the basic lattice itself does not change. What does change are the number, size, and state of aggregation of the imperfections and the distribution of the electrons among the various energy states.

Measurement of the electrical conductivity, therefore, gives information about the imperfections but is complicated by changes in electron states. The Hall effect permits these states to be studied independent of the imperfections. If a current is sent through a conductor in the direction indicated in figure 7 and a galvanometer is connected across points A and B on the conductor, no deflection of the galvanometer occurs. This shows that the potential at A and B is equal. If a magnetic field is applied perpendicular to the direction of the current, the galvanometer deflects and can be brought back to zero only by shifting the position of A or B.

On the atomic scale, an approximate description of this effect is that the paths of the moving electrons which give rise to the current are curved by the magnetic field; consequently, the line of equal potential

across the conductor rotates. The amount of rotation depends only on the number of free or higher energy electrons, not on the other quantities which complicate the interpretation of conductivity measurements.

Consequently, by measuring both the conductivity and the Hall effect it is possible to eliminate the effects due to the electrons and isolate those due to the imperfections.

Measurements of the magnetoresistivity and of the thermoelectric power when combined with measurements of resistivity also give information about the distribution and energy states of the electrons in the metal. The magnetoresistivity is the change in resistivity which occurs when a conductor carrying current is placed in a magnetic field, while thermoelectric power is the change in potential, per unit rise in temperature, between two pieces of metal which are placed in contact.

The four electrical effects described as well as others have been used to investigate the nature of work-hardening. The Hall effect has been measured on copper strips which were cold worked by rolling to a maximum of 75-percent reduction. The Hall coefficient was found to have increased by about 1 percent as a result of this amount of cold work, a rather small increase and, unfortunately, less than the probably error. If this value is accepted, however, it indicates, according to the previous discussion, that the cold work has decreased the number of free electrons by about 1 percent. If this result is combined with the resistivity measurements, it can be deduced that a decrease in average distance between imperfections of 1 or 2 percent has occurred and therefore an increase in their number.

Measurements of the resistivity and magnetoresistivity have also been made on gold-copper alloy. This is an alloy which, as previously mentioned, exists in states ranging from complete order to complete disorder. The electrical resistivity of the alloy changes with degree of order since the irregular disordered state produces larger potential fluctuations to interfere with the motion of the electrons. The process of ordering also changes the distribution of energy states for the electrons, which causes changes in the Hall effect and in the magnetoresistivity. The changes in these quantities primarily due to simple interchange of atoms in the lattice can therefore be studied.

Various degrees of order were obtained by heating wires of the alloy near their melting point, then quenching them in cold water. At the high temperature used, the equilibrium state is almost complete disorder; the quench has the effect of freezing this disorder into place because, although at room temperature the equilibrium state is ordered, diffusion is so slow that order cannot be established. The desired degree of order was then obtained by heating the wire to an intermediate temperature and requenching. Wires were also disordered by mechanical deformation.

The results of this work indicated that different types of disorder arise from thermal disordering and from mechanical disordering. The electron states corresponding to the two methods of disordering are also different.

In other work at this laboratory aimed towards an understanding of work-hardening, the possible existence and the configuration of work-hardened regions in a fatigued specimen have been investigated. This work was based on a theoretical analysis which indicated how the resistivity of a bar composed of distinct grains of two pure metals, as shown in figure 8, should depend on the proportion and configuration of the grains. The possible work-hardened regions of the fatigued metal were considered as a second metal and it was deduced from resistivity measurements at low temperature that (1) the regions were either very small (about 1000 Å or less) or that they may be larger but only in the direction perpendicular to the axis of the specimen, (2) that the regions are definitely not spherical particles larger than 1000 Å, and (3) the fraction of disordered material must be small, less than 0.5 percent. The last result also partially agrees with the calorimetric work, that is, any positive stored energy is too small to be found calorimetrically, but the negative value found in the calorimetric work remains a mystery.

The second major topic which will be discussed is the work at this laboratory on the effect of surface composition and configuration on the mechanical properties of materials. From the engineering point of view, it is known that surface condition is very important in determining creep rate, creep-rupture strength, and fatigue strength. If cracks or other stress concentrators exist, they must be sources of weakness for the material.

From the atomic point of view, the atoms on the surface should behave quite differently from those in the interior, because the forces on them are not compensated as they are in the interior. Figure 9 shows the contraction in the lattice which must occur. This contraction gives rise to a surface tension which is not obvious in a solid as in a liquid because the solid is more rigid but, nevertheless, of great importance.

One of the questions of interest was whether an intrinsic crack structure existed on the surface of a crystal because of the contraction in the surface. This question was investigated by a technique which depends on the fact that silver evaporated in a vacuum and deposited on a nonmetallic surface tends to agglomerate into deposits along irregularities in the surface. The experiment consisted of depositing silver on the surface of a single crystal of sodium chloride which had been annealed and then water polished, that is, the surface layer removed by solution. No agglomerates were seen under the microscope. However, when such a crystal had aged for a few days before it was coated, a

great many lines at a large variety of angles appeared (fig. 10). The number of lines appeared to grow with time of aging, and an analysis of the rate of growth indicated that the atomic process involved is basically the diffusion of the sodium and chlorine atoms in the surface. This is evidence that the "cracks" or faults which are delineated by the lines of silver are an intrinsic and atomic phenomenon.

The angles which the faults made with a face of the sodium chloride cube were measured, and the number of faults making a given angle with a cube face was plotted against the angle. The result is shown in figure 11 as the solid line. The dotted line that is also plotted shows the atom density as a function of angle, that is, the number of atoms per unit distance which would be seen if the lattice were viewed along a line at the given angle (fig. 12). All that can be said at present is that the correlation is too good to be overlooked but that atom density is not the only factor which determines the direction of faults.

The effect of surface composition has also been investigated by studying the creep rate of zinc single crystals with and without surface layers of oxide. Creep studies of this type are complicated by a lack of reproducibility which is very difficult to eliminate. Figure 13 is the percentage elongation against time for sections of the same single crystal with and without an oxide layer. The lower elongation of the oxide-coated specimen indicates the strengthening effect of the oxide layer. The layer in this case is about 1000 atoms thick, which is much too small for chemical analysis. It was measured by means of electron diffraction from the surface. Studies were made of the effect of increasing the load, of pre-elongation of the crystal, of sulfide rather than oxide, and of the effect of suddenly removing the surface layer with acid. This last is a dramatic demonstration of the importance of the surface layer (fig. 14). A crystal with a sulfide layer creeps slowly until hydrochloric acid is added. A sudden increase in creep rate then occurs. If the acid had not been added, the elongation-against-time curve would have followed the dotted curve.

The results of the work were compatible with the explanation that the surface layer at first actually helps to support the load even in the small thickness which is present and that it eventually breaks. The heat of reaction of the layer with the acid before the break occurs accounts for the sudden jump in elongation shown in figure 14.

Although at first sight both parts of this explanation seem implausible because of the extreme thinness of the surface layer, a closer examination makes them seem more reasonable. Because the oxide or sulfide layer is very thin, the number of imperfections it contains is also very low and it should have a strength approaching the very high theoretical strength of a perfect crystal. This would be large enough to account for the decrease in elongation.

A similar argument holds for the effect of the acid. Though the total amount of heat released is small, it is released in a very thin layer of the crystal, whose temperature is therefore instantaneously very high, and the instantaneous increase in elongation occurs.

The last experiment which is discussed is only in its beginning stages but illustrates the interrelations between various topics, in this case work-hardening and the surface. The experiment is based on the well-known skin effect. The current carried by a conductor across which a low-frequency alternating voltage is applied travels through the conductor uniformly, that is, the current per unit cross section in the center of the sample is the same as it is per unit cross section near the surface. If the frequency is increased, the current begins to decrease at the center and to increase near the surface. At the frequency of microwaves, say 8500 to 12,000 megacycles, the current flow is confined to a layer 3×10^{-3} centimeters thick in copper. The preliminary work, in which the resistance of a work-hardened copper bar to a microwave frequency current was compared with the direct-current resistance, indicates that this thin layer contains four times as much work-hardening per unit volume as the remaining material.

The information obtained thus far in the physics of solids work has contributed much more to the understanding of materials than it has to actual improvements of them. However, the next few years should begin to affect the practical developments.

ORDERED LATTICE AND DISORDERED LATTICE

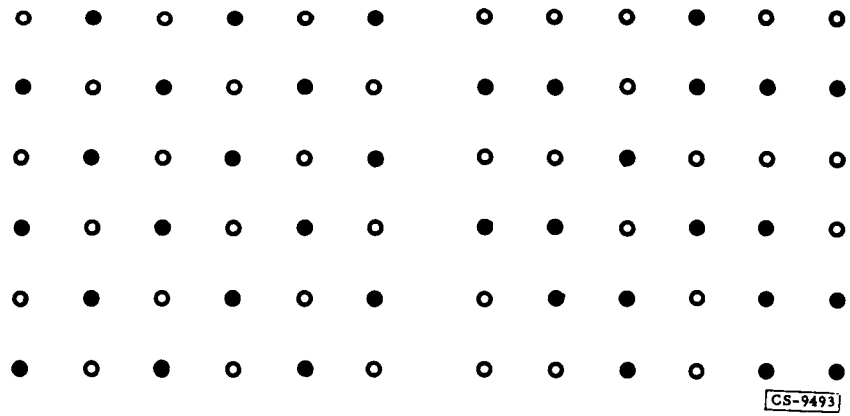

Figure 1

THE PERFECT CRYSTAL LATTICE

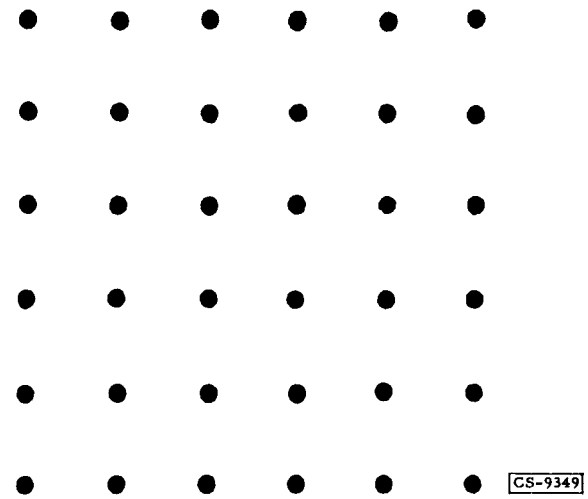

Figure 2

LATTICE IMPERFECTIONS

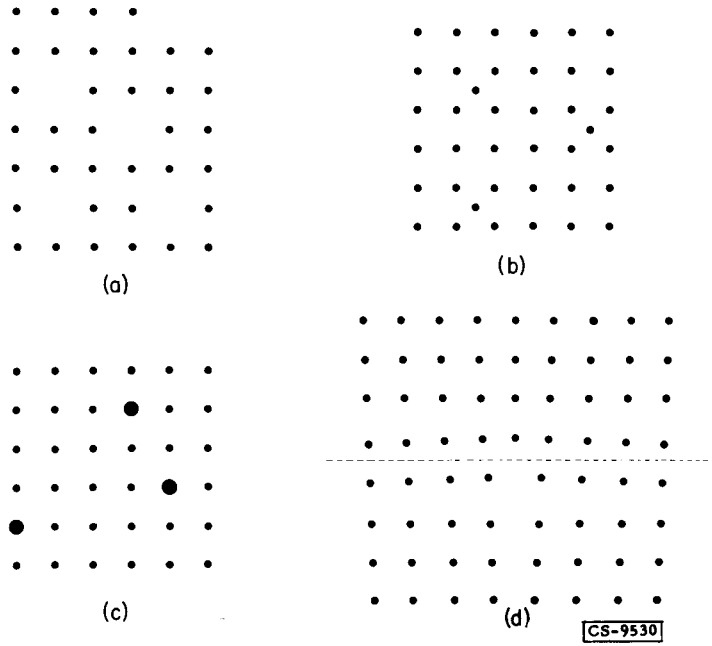

IDEALIZED TEMPERATURE VS. HEAT ADDED FOR WORK HARDENED COPPER

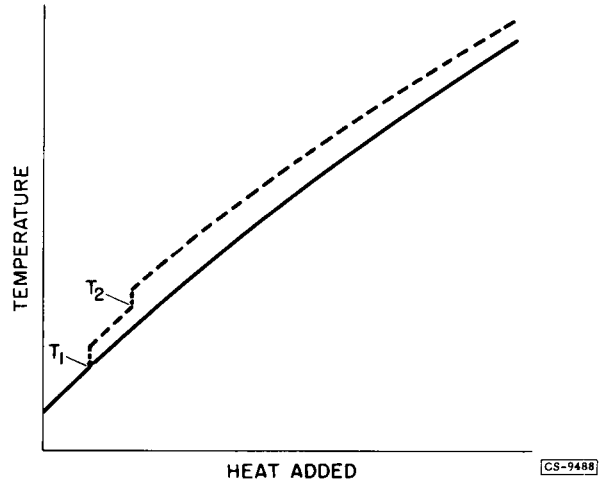

Figure 4

HEAT EMITTED VS. TEMPERATURE FOR WORK-HARDENED COPPER

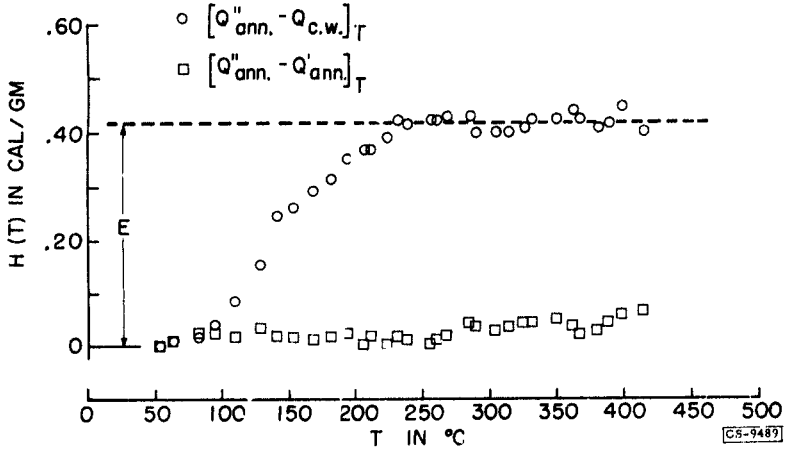

Figure 5

DEVIATION IN HEAT CONTENT OF COLD WORKED COPPER AND OF FATIGUED COPPER RELATIVE TO ANNEALED COPPER

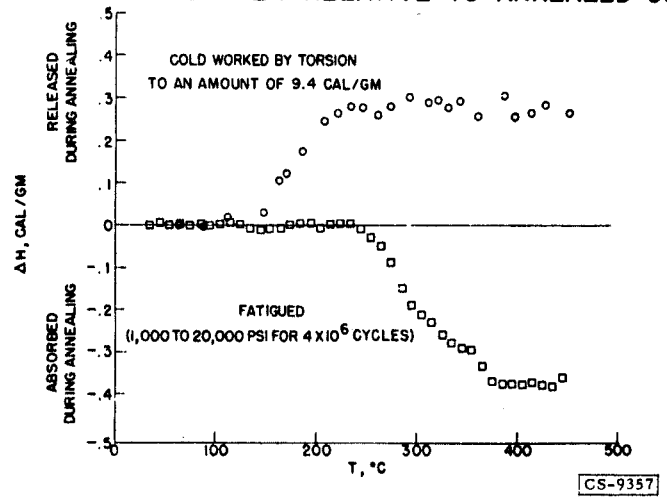

Figure 6

HALL EFFECT

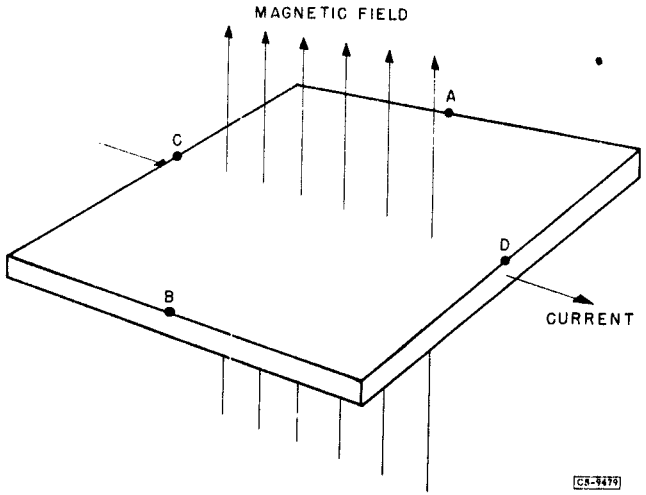

Figure 7

TWO REGION METAL

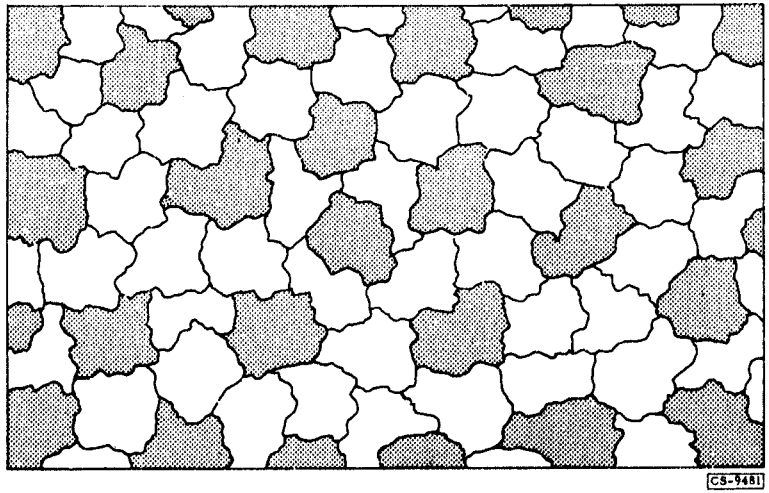

Figure 8

LATTICE CONTRACTION AT SURFACE

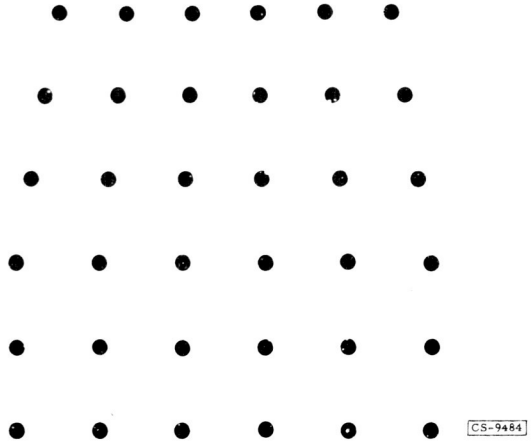

Figure 9

SILVER DEPOSITS ON A
SODIUM CHLORIDE CRYSTAL FACE

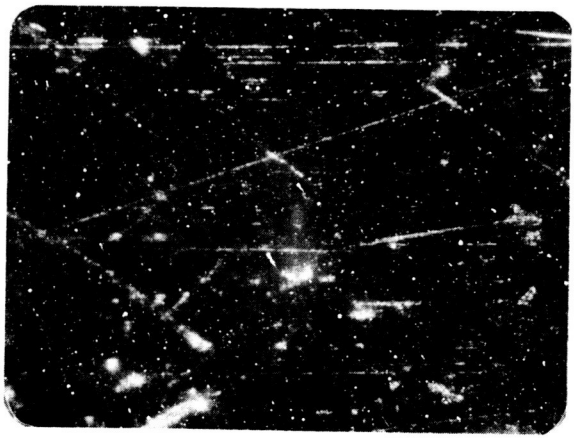

Figure 10

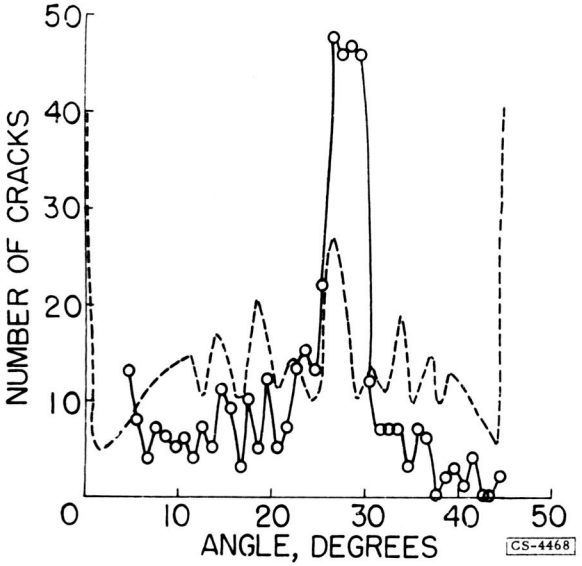

Figure 11

ATOM DENSITY IN VARIOUS DIRECTIONS

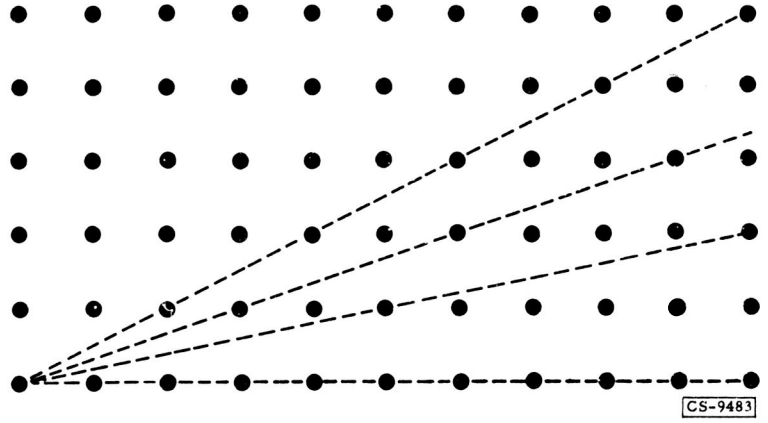

Figure 12

CREEP CURVES FOR METAL AND OXIDIZED SECTIONS OF A ZINC SINGLE CRYSTAL

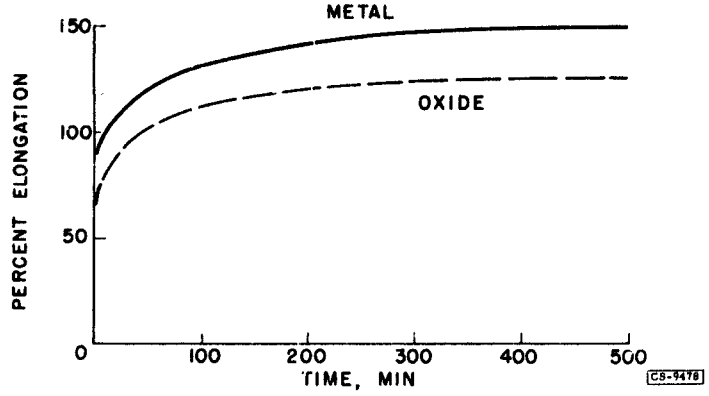

Figure 13

EFFECT OF ACID ADDITION ON ELONGATION OF SULFIDE COATED ZINC SINGLE CRYSTALS

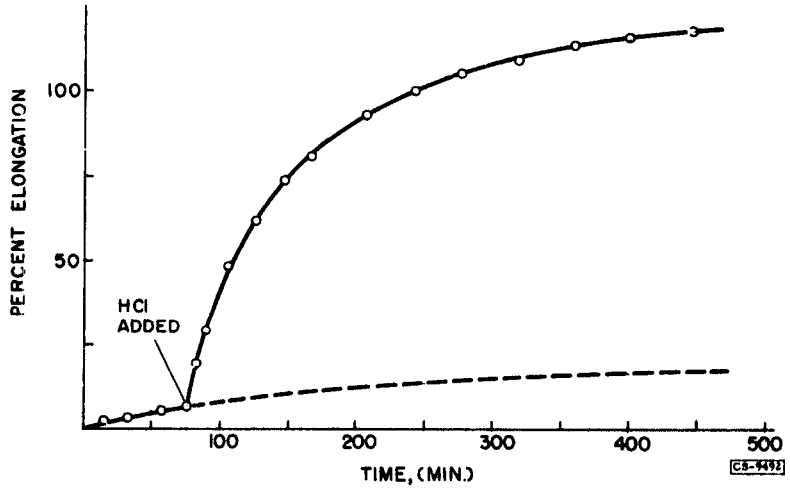

Figure 14